The Dissertation Committee for Alicia Caitlin Bloomfield Allen Certifies that this is the approved version of the following Dissertation:

Anisotropy in Cell Sheeting and Cardiac Differentiation

Committee:

Janeta Zoldan, Supervisor

Aaron B. Baker

Austin J. Cooney

Laura J. Suggs

Anisotropy in Cell Sheeting and Cardiac Differentiation

by

Alicia Caitlin Bloomfield Allen

Dissertation

Presented to the Faculty of the Graduate School of

The University of Texas at Austin

in Partial Fulfillment

of the Requirements

for the Degree of

Doctor of Philosophy

The University of Texas at Austin

May 2018

Dedication

To my friends and family, who believed in me when I didn’t

Acknowledgements

I would like to first thank my family for their love, support, and encouragement: my parents, for nurturing my interest in science and a hard work ethic, and Nate, for the perspective that there are other important things besides what you do 8-5.

I am grateful that I had the opportunity to work with many smart and generous people in the department. To my fellow current and former labmates, I don't want to think what research would have been like without you (i.e., it would have been miz-er-uh-buh l). To Chengyi, who has shared this whole Zoldan lab experience start-to-finish with me, I have always appreciated your insightful feedback and well-timed sardonic humor. Cody, I'm amazed by your unrelenting optimism and consistent hard work. To my officemates, Kevin, Shane, Kabir, and Chelsea, I have enjoyed all our science and not-so-science conversations. To Ryan and Laura (Geuss), thank you for career advice and perspectives from "the other side." To Amy Price, thank you for knowing what's-what and keeping the Zoldan lab running smoothly. To Will Goth, Nich Dana, Alex Khang, and Andrew Fowler, I am glad our research objectives aligned so that we could work together and I could learn from you. Going back to my research beginnings, I am grateful to Dr. Jennifer West and all the former West Lab members who first trained me as a researcher and continue to offer me advice and encouragement. I want to include a particular thank you to Dr. Ronke Olabisi and Dr. Jeannie Stephens, both who had confidence that I could earn a PhD before I had even started.

I had the privilege of working with talented undergraduates who assisted in this work: Andra Dugger Keierleber, Stefani Maris, Jorge Gomez Medellin, Madelyn Sziglai-Jones, Alston-Lauren Feggins, Elissa Barone, and Krista Polansky. I especially want to thank Andra, Elissa, and Krista for their patience and hard work, as Andra joined me when

I was just beginning this project, and Elissa and Krista are helping me see it through its final stage.

I would like to acknowledge core facility staff for their expertise and assistance: Dr. Dwight Romanowicz of the ICMB Imaging Core Facility and Dr. Hugo Celio of the Texas Materials Institute. I would like to also thank Dr. Amy Brock, Dr. Nicholas Peppas, and Dr. Jeanne Stachowiak for access to equipment in their laboratories. Overall, I have been grateful to the department faculty for creating a collaborative and open research environment. I thank the National Science Foundation for funding support through the Graduate Research Fellowship Program, which allowed me to dedicate more time to my research. I am also grateful to The Cockrell School of Engineering and the family of Dr. Thomas Marschall Runge for supplementary financial support.

I would like to thank Dr. Aaron Baker, Dr. Austin Cooney, and Dr. Laura Suggs for their willingness to serve as dissertation committee members and their advice towards improving this research. I especially would like to thank Dr. Suggs for letting me be part of her research group (the more labmates the merrier!) and her thoughtful research and professional advice.

Finally, I would like to thank my adviser Dr. Janet Zoldan for being confident in my abilities and challenging me to grow as a scientist. Before starting graduate school, I was wary about joining a new lab. Now that I'm nearing the conclusion of my studies, I can clearly appreciate the benefits of doing so; I've had many opportunities (and challenges) that made me a stronger, smarter researcher.

Abstract

Anisotropy in Cell Sheeting and Cardiac Differentiation

Alicia Caitlin Bloomfield Allen, Ph.D.

The University of Texas at Austin, 2018

Supervisor: Janeta Zoldan

Treatment for myocardial infarction is largely limited to alleviating symptoms and preventing recurrence rather than directly repairing or replacing the damaged myocardial tissue. Consequently, one of the overarching goals of cardiac tissue engineering is to generate myocardial tissue that could be implanted as a patch over existing cardiac tissue to improve cardiac function. Advancements in pluripotent stem cell (PSC) technology and differentiation have made PSC-derived cardiomyocytes a viable cell source for engineered cardiac tissues. Because native cardiac tissue is directional in nature (i.e., anisotropic), biomaterial systems have been designed to organize PSC-derived cardiomyocytes to recapitulate this structure. The objective of this dissertation is to use aligned electrospun fibers as anisotropic substrates to generate aligned cell sheets and to evaluate how differentiating cardiomyocytes respond to degrees of anisotropy. We demonstrate that aligned electrospun fibers containing poly(N-isopropylacrylamide), a thermo-sensitive polymer commonly used for cell sheeting, and poly(capro lactone), a hydrophobic polymer commonly used in biomaterials, can be used to generate anisotropic cell sheets. Also shown is that the structure and functional behavior of PSCs-derived cardiomyocytes varies in a gradient-based manner on degree of substrate anisotropy at relatively early timepoints. As

time progresses, cardiomyocyte alignment can be achieved on substrates that have a minimum threshold anisotropy. These electrospun, aligned fiber systems can be used in tissue engineering to generate viable cell sheets for cardiac tissue engineering or to precisely study cell sensitivity to differences in substrate anisotropy.

Table of Contents

List of Tables xiii

List of Figures xiv

Chapter 1: Introduction 1

1.1 Motivation—Engineered Cardiac Tissue to Treat Myocardial Infarction 1

1.2 Cardiac Anisotropy 2

1.2.1 Native Cardiomyocyte Structure and Function 2

1.2.2 *In vitro* Cardiomyocyte Function Assessment 2

1.3 Electrospinning of Aligned Fibers for Cardiac Tissue Engineering 3

1.3.1 Principle 4

1.3.2 Strengths and Limitations 4

1.4 Cell sheeting for Cardiac Tissue Engineering 5

1.4.1 PNIPAAm-based Cell Sheeting Systems 5

1.4.2 Non-PNIPAAm based Cell Sheeting Systems 6

1.4.3 Cardiac Cell Sheets 7

1.5 PSC-derived Cardiomyocytes 7

1.5.1 Cardiac Differentiation 8

1.5.2 Cardiac Maturation 8

1.6 Research Goals 9

1.7 References 18

Chapter 2: Electrospun Poly(N-isopropyl acrylamide)/Poly(caprolactone) Fibers for the Generation of Anisotropic Cell Sheets 26

2.0 Foreword 26

2.1 Introduction 26

2.2 Materials & Methods 28
2.2.1 Fabrication PNIPAAm/PCL fibers 28
2.2.2 Characterization of PNIPAAm/PCL fibers.....29
2.2.2.1 Fiber Orientation and Diameter 29
2.2.2.2 Fourier Transform Infrared Spectroscopy 30
2.2.2.3 PNIPAAm Mass Loss 30
2.2.2.4 Advancing Contact Angle Measurement 30
2.3.3 Cell studies.....31
2.3.3.1 PNIPAAm/PCL fiber sterilization and protein coating 31
2.3.3.2 Cell viability on PNIPAAm/PCL fibers 32
2.3.3.3 Cell alignment on PNIPAAm/PCL fibers.....32
2.3.3.4 Cell sheet detachment from PNIPAAm/PCL fibers 33
2.3.4 Statistical Methods.....33
2.4 Results and Discussion 33
2.4.1 Characterization of PNIPAAm/PCL fibers.....33
2.4.2 Cell viability and alignment on PNIPAAm/PCL fibers.....37
2.4.3 Cell sheet detachment 38
2.5 Conclusions.....39
2.6 References.....48
Chapter 3: Sensitivity of Differentiating Cardiomyocytes to Substrate Anisotropy 52
3.0 Foreword.....52
3.1 Introduction.....52
3.2 Materials and Methods.....54

3.2.1 Fabrication of Electrospun Fibers 54
3.2.2 Fiber Orientation and Diameter 55
3.2.3 Pluripotent Stem Cells 55
3.2.4 Cell Seeding and Cardiac Differentiation 55
3.2.5 Immunostaining 56
3.2.6 Quantitative Reverse Transcription-Polymerase Chain Reaction (RT-qPCR) 57
3.2.7 Cell Orientation and Overall Alignment 58
3.2.8 Intracellular Calcium Transients 58
3.2.9 Cardiomyocyte Contractility 59
3.2.10 Statistical Analysis 60
3.3 Results 60
3.3.1 Fiber Generation and Characterization 60
3.3.2 Cardiomyocyte Differentiation and Sarcomeric Protein Isoform Expression 61
3.3.3 Cardiomyocyte Orientation Relative to Fiber Orientation 61
3.3.4 Overall Cell Alignment 62
3.3.5 Cardiomyocyte Contractility 63
3.3.6 Cardiomyocyte Intracellular Calcium Transients 63
3.4 Discussion 64
3.5 Conclusions 66
3.6 References 73
Chapter 4: Conclusions and Future Directions 77
4.1 Conclusions 77

4.2 Future Directions 78
4.2.1 Mechanism of alignment 78
4.2.2 Anisotropic Cell Sheets 79
4.3 References....80
Appendix....81
A. Supplementary Information for Chapter 2....81
B. Supplementary Information for Chapter 3 86
Bibliography 88
Vita....103

List of Tables

Table 2.1 Absorption peaks and assignments for PNIPAAm and PCL.....43

Table A1 Solution and electrospinning parameters for PNIPAAm/PCL fibers 82

Table B1 Forward and reverse primers used for RT-qPCR.....86

List of Figures

Figure 1.1 Engineered cardiac tissues (A) are implanted (B) as a cardiac patch over the infarct (C). (Adapted with permission from Montgomery et al.).....11

Figure 1.2 Myocardial tissue has multi-scale organization, from cardiac muscle fibers, down to individual sarcomeres consisting of thick myosin filaments and thin actin filaments. (Adapted with permission from Golob et al.) 12

Figure 1.3 Electrospinning systems consist of a high voltage supply, a pump, and a grounded collector. Nanofibers are produced when repulsive forces cause the polymer solution to form a jet that elongates and is collected as nanofibers on the collector. (Adapted with permission from Shin et al.).....13

Figure 1.4 PNIPAAm structure and behavior. A) PNIPAAm is composed of polar and non-polar groups. B) In aqueous environments, PNIPAAm chains expand below LCST and collapse above LCST. (Adapted with permission from Lanzalcon et al.) 14

Figure 1.5 Cell sheeting using PNIPAAm-grafted plates. A) Above LCST, cell attach and can be cultured on PNIPAAm. B) When the temperature is lowered below LCST, cells detach as an intact sheet and can be layered. (Adapted with permission from Haraguchi et al.) 15

Figure 1.6 Cardiac differentiation occurs *in vitro* by modulation of the the Wnt, Activin, and BMP signaling pathways. (Adapted with permission from Jeziorowska et al.).....16

Figure 1.7 PSC-derived cardiomyocyte structure and function. A) Sarcomeres in cardiomyocytes derived from mESCs (i) mouse iPSCs (ii) and neonatal cardiomyocytes. Contractility (B) profiles and (C) output. D) Action potential, calcium transient, and tension profiles. (Adapted from Sheehy et al.) 17

Figure 2.1 Electrospun PNIPAAm/PCL fibers. A) SEM images of electrospun PNIPAAm/PCL fibers. Percentage in upper left indicates PNIPAAm content. Scalebars (black bars, bottom left) are 10 μm. B) Average fiber diameter determined using DiameterJ. C) Fiber orientation index determined using OrientationJ. *p<0.05 compared to 0% PNIPAAm fibers. 41

Figure 2.2 Chemical structures of (A) PCL and (B) PNIPAAm. C) FTIR spectra of PNIPAAm/PCL fibers. Dashed lines indicate absorption peaks. 42

Figure 2.3 PNIPAAm dissolution from PNIPAAm/PCL fibers. A) PNIPAAm/PCL mass loss in water. PNIPAAm/PCL fiber (B) area percent change and (C) axes (relative to fiber direction) length percent change following PNIPAAm dissolution. # p<0.05 compared to all other groups. 44

Figure 2.4 A) Advancing water contact angle on PNIPAAm/PCL fibers. B) Representative images of water droplet on fibers. White dashed lines indicate fiber edge. * p<0.05 compared to 0% PNIPAAm fibers. &p<0.05 compared to 100% PNIPAAm fibers. 45

Figure 2.5 Cell viability and cell alignment on PNIPAAm/PCL fibers. A) Cell viability relative to 0% PNIPAAm fibers determined by MTS assay. .*p<0.05 compared to 0% PNIPAAm fibers. B) Representative images of fibroblasts seeded on PNIPAAm/PCL fibers with actin (left) and actin/DAPI overlays (right). Scalebars are 200 μm. C) Insets from 90% PNIPAAm images, as indicated by white dashed-box in (B). Scalebar is 50 μm. 46

Figure 2.6 Cell sheet detachment. A) Cell sheets detached from 90% PNIPAAm fibers using room temperature medium; Scalebar is 1 cm. B,C) Cell sheet viability was confirmed with calcein, AM live-staining. D,E) Corresponding phase contrast images of (B,C); white arrows indicate residual PCL. Scalebars are (B,D) 400 μm and (C,E) 200 μm. 47

Figure 3.1 Fiber characterization. A) SEM images of electrospun PCL fibers. Collector speed indicated in top left corner. Scalebar is 10 μm. B) Fiber orientation index versus collector speed. C) Mean fiber diameter versus collector speed. *p<0.05. 67

Figure 3.2 Cardiac differentiation on electrospun fibers. A) Schematic of differentiation timeline. B) cTnT+ cardiomyocytes derived on electrospun fibers. Scalebar is 50 μm. C, D, E) mRNA expression ratios of sarcomeric protein isoform pairs versus fiber orientation index. 68

Figure 3.3 Cell orientation relative to fiber orientation. Images of A) Fibers and B) cardiomyocytes derived on same fibers. Fiber orientation indicated in top left corner. Green = cTnT; blue = nuclei. Scalebars are 20 μm.....69

Figure 3.4 Cardiomyocyte and cell orientation index. Representative images of A) cardiomyocytes and C) all cells differentiated on fibers over time. Scalebars = 200 μm. B) Cardiomyocyte orientation index and D) all cell orientation index over time. *p<0.05. #p<0.05 versus day 8 orientation index for same fiber alignment. +p<0.05 versus day 14 orientation index for same fiber alignment. 70

Figure 3.5 Cardiomyocyte contractility at day 14. A) Total contractile displacement. B) Displacement parallel and perpendicular to fiber direction. 71

Figure 3.6 Cardiomyocyte intracellular calcium transients. Representative Fluo-4 signals for cardiomyocytes derived on 0.23- and 0.86 fibers at A) day 8 and B) day 20. Scalebars = 50 μm. C) Beating rate and D) TPA-MAD at days 8 and 20 for cardiomyocytes derived on 0.23- and 0.86-fibers. *p<0.05. 72

Figure A1 CellCrown inserts were used to secure PNIPAAm/PCL fibers. Squares of PNIPAAm/PCL fibers and parafilm were layered onto the CellCrown bottom (middle). A fully assembled CellCrown with PNIPAAm/PCL fibers (right). 81

Figure A2 PNIPAAm/PCL fibers before and after PNIPAAm dissolution.....83

Figure A3 Advancing water contact angle of dry and wetted PNIPAAm/PCL fibers. *p<0.05 compared to corresponding 0% PNIPAAm fiber contact angle; **p< 0.05 between dry and wetted fibers. 84

Figure A4 Representative histograms of cell angles as measured from actin of cells seeded on PNIPAAm/PCL fibers. Histograms were normalized to the peak frequency. Dashed line indicates half max.....85

Figure B1 Time to peak arrival-median absolute deviation (TPA-MAD) is used to quantify synchronicity. Representative Fluo-4 signals for unsynchronized (left) and synchronized (right) intracellular calcium transients. At specified timepoints, the TPA is determined for the entire frame of view for 50 frames (transparent gray boxes). The TPA is presented as color activation maps and histograms. The mean TPA is indicated in the upper right corner. Absolute deviations from the TPA median are shown as histograms. The MAD is indicated in the upper right corner. 87

Chapter 1: Introduction

1.1 Motivation—Engineered Cardiac Tissue to Treat Myocardial Infarction

Cardiac disease is the leading cause of death across the world, and its prevalence will persist as key risk factors, including obesity and lack of physical activity, continue to rise[1]. Myocardial infarction acutely damages cardiac muscle tissue, leading to cardiomyocyte death. Because the limited regenerative capacity of the heart cannot sufficiently replace these lost cells, scarring and tissue maladaptation, such as thinning of the ventricular wall, occurs over time[2]. Cardiac function consequently decreases, which increases the risk of heart failure.

Cardiac tissue engineering aims to mitigate or even reverse impairment of cardiac function by replacing damaged tissue with functional myocardial tissue engineered *ex vivo*. Because damaged myocardial tissue cannot be safely excised, the envisioned approach calls for the engineered cardiac tissue to be patched over the infarcted area, hence the term "cardiac patch" (Figure 1)[3,4]. Approaches are typically innovative in the biomaterial design and/or in the cell source used to derive cardiomyocytes. The biomaterial design is important in that it must ideally promote or, at the very least, not impair proper cardiomyocyte electromechanical function. The cell source is a necessary consideration driven by the fact that adult cardiomyocytes are non-proliferative and cannot be safely harvested. Researchers have largely turned towards using pluripotent stem cells (PSCs) to derive cardiomyocytes as these cells can proliferate almost indefinitely and be patient-specific[5].

1.2 CARDIAC ANISOTROPY

Many tissues depend on anisotropic cellular organization for proper function. The heart's primary function—pumping blood throughout the circulatory system—relies on coordinated electrical and mechanical activity of individual cardiomyocytes. Anisotropy exists in cardiac tissue architecture and down to individual cellular organization.

1.2.1 Native Cardiomyocyte Structure and Function

Cardiac tissue is highly organized with anisotropy existing over several scales, from myofibers—bundles of cardiomyocytes—to sarcomeres—the intracellular contractile units (Figure 2)[6]. Proper electrical signal propagation and contraction of the tissue is dependent on this multi-scale, directional organization. Although cardiomyocytes make up only 30% of the heart by cell number, they comprise 75% of the heart's volume[7,8]. Cardiomyocytes are elongated, rod-shaped cells. Single cell studies have shown that the ideal aspect ratio for cardiomyocytes is 7:1, as determined by unidirectional sarcomere alignment[9]. To function as a syncytium, cardiomyocytes are connected at their transverse ends by intercalated discs, which rapidly transmit action potentials along the cells' long axis through gap junctions. Cardiomyocyte contraction is an electromechanical process, as calcium release from the sarcoplasmic reticulum enables displacement of the thick myosin filaments relative to the thin actin filaments[2].

1.2.2 *In vitro* Cardiomyocyte Function Assessment

Testing of cardiomyocyte function *in vitro* typically focuses on mechanical and electrical activity. Single cell studies allow tight control over system parameters, thus enhancing signal resolution, but are generally low throughput. Measuring collective cell behavior, on the other hand is more reminiscent of the *in vivo* function. For cardiomyocytes

seeded in or on biomaterials, the choice of analysis technique may be constrained by factors like optical clarity.

Contractility is reported as force, displacement, or contraction and relaxation velocities[10]. Measuring contractility can be done optically by computational motion detection image analysis to determine displacement or velocity[11] or by direct force measurement[12]. For materials of known stiffness, force can be determined indirectly by measuring displacement of the material via traction force microscopy[13,14] or for sufficiently thin films, material curvature[15].

Action potentials can be measured using voltage-sensitive dyes, microelectrode arrays, or via patch clamp[10]. Patch clamp, in which a micropipette with an electrode is in contact with the membrane of a single cell, records intracellular voltage. Microelectrode arrays record extracellular electrical field potentials of cardiomyocytes or cardiomyocyte monolayers[16]. Alternatively, voltage-sensitive dyes can be used to visualize action potentials and track electrical propagation in relatively large cardiac tissue constructs[17]. Similarly, calcium-sensitive fluorophores can be used to visualize intracellular calcium flux[18,19]. Depending on the recording frequency or camera frame rate, properties like beating rate, action potential duration, time to peak, and conduction velocity can be extracted[11,20]. These techniques are often used in conjunction with electrical stimulation[21].

1.3 Electrospinning of Aligned Fibers for Cardiac Tissue Engineering

Biomaterial design is often inspired by native cell microenvironments, particularly the extracellular matrix (ECM). The cardiac ECM is an organized, clearly anisotropic fibrous network that structurally supports both tissue-level contractions and cellular-level

alignment[22]. Biomaterials with comparable EMC-scale features and anisotropy can be fabricated using electrospinning.

1.3.1 Principle

Electrospinning, a technique developed and patented in the early 20th century but not popularized until the 1990s, uses electrostatic forces to generate micro- and nanoscale polymeric fibers[23]. All electrospinning systems consist of a high voltage supply, a pump, and a grounded collector[24]. Using the pump, a polymer solution is dispensed at a constant rate, typically from a syringe needle, and charged by the high voltage supply. Repulsive forces overcome the solution surface tension to form a jet. Repulsive forces within the jet causes it to whip and elongate before being collected as dry fibers on a grounded collector (Figure 1.3)[25]. Both solution properties (i.e., solvent, polymer, polymer molecular weight, polymer concentration) and working parameters (i.e., solution flow rate, applied charge, needle diameter, distance from needle to collector) affect resulting fiber properties[26,27].

Alignment of electrospun fibers can be achieved at the collection step or post-collection. Similar to textile spinning, electrospun fibers can be mechanically aligned by deposition on a rotating collector[28,29]. Alternatively, the jet can be manipulated using parallel plate electrodes to collect aligned fibers[30,31]. Electropsun fibers can also be aligned by uniaxial stretch as a post-processing step[32,33].

1.3.2 Strengths and Limitations

Electrospinning's key advantages are in its cost, ease of implementation, and versatility. The polymer solution and working parameters can be readily tuned to alter fiber properties. Protein-conjugated polymers have been electrospun to improve biocompatibility[30,34]. Blending polymers or solutions of polymers can be used to generate

core-sheath fiber architectures[35]. Although relationships between solution properties/working parameters and final fiber properties have been established, these relationships must be established empirically for each electrospinning system. Furthermore, fine control over the surface patterns is lacking, especially when compared to materials fabricated using high-resolution methods like soft or photolithography[36].

1.4 Cell sheeting for Cardiac Tissue Engineering

Although biomaterials are useful to improve cell viability, organization, and function, implantation of cell-biomaterial systems have challenges: immunogenicity, impairment of integration with host tissue, and undesirable degradation products[37]. Although clever biomaterial features have been designed to minimize these concerns, such risks cannot be completely eliminated. One alternative has the use been cell sheets—intact cell monolayers non-enzymatically detached from substrates *in vitro* to generate scaffold-less engineered tissues. This approach started more than two decades ago when Teruo Okano began using poly(N-isopropyl acrylamide) (PNIPAAm), a temperature-sensitive material, as a cell culture substrate[38]. Although cell sheets are relatively thin (approximately 50 μm/sheet), cell sheets can be stacked to produce thicker, more 3D tissues[39]. Due to the absence of a scaffolding material, cell sheets have quickly moved to testing in animal models and even clinical trials[40].

1.4.1 PNIPAAm-based Cell Sheeting Systems

PNIPAAm is a thermo-sensitive material that undergoes a rapid coil-to-globule transition in aqueous environments when the temperature is lowered past its lower critical solution temperature (LCST) of 32°C. Below 32°C, the PNIPAAm chain expands and is

water-soluble. Above 32°C, the PNIPAAm chain collapses with its hydrophobic groups at the core, causing the material to precipitate (Figure 1.4)[41]. This thermo-sensitive behavior has made PNIPAAm popular as a drug delivery vehicle[35,42,43] and as a sacrificial material[44,45].

PNIPAAm's thermo-sensitive nature was first reported in 1968[46] but PNIPAAm was not used as a cell culture substrate until 1990[38]. Cells can be cultured on short chains of PNIPAAm grafted to plates if the temperature remains above 32°C. When cells have grown into a confluent monolayer, a cell sheet can be detached by lowering the incubation temperature below PNIPAAm's LCST, typically to 4°C (Figure 1.5). The PNIPAAm chains expand, forcing cell-substrate attachments to break. PNIPAAm-grafted plates have been commercialized under the brand name UpCell™[47]. Other research groups have fabricated PNIPAAm-based materials to make cell sheets, including co- or block polymers[48–50] and conjugation of RGD[51] or ECM proteins[52–54]. Although PNIPAAm is the most popular material to generate cell sheets, it has limitations. Solubilized PNIPAAm is cytotoxic, and the polymer length must be tightly controlled. If the PNIPAAm chains are too long, cell attachment is impaired, and if the chains are too short, cell sheets will not detach[55].

1.4.2 Non-PNIPAAm based Cell Sheeting Systems

Since the emergence of PNIPAAm as a cell sheeting substrate, other materials with triggerable properties have been used to generate cell sheets. Alkanethiol materials can release cell sheets following the application of an electric field[56]. Ultra-violet (UV) light is used to cleave integrin binding peptides. For alginate-based systems, calcium chelators are used to uncrosslink alginate to release cell sheets[57]. The limitations of each system lie primarily in the materials and fabrication costs or the time and stress required to detach the

cell sheet. Detachment methods can induce cell stress through undesirable microenvironment changes (i.e., undesirably low or high temperatures, pH changes, long-wave UV light) for extended durations.

1.4.3 Cardiac Cell Sheets

Sheets of cardiac cells were first made in 2002 by Dr. Okano's group using neonatal rat cardiomyocytes. These cardiomyocyte sheets beat spontaneously and were implanted into young nude rats[58]. As PSC technology advanced, PNIPAAm plates were used to generate ESC-derived[59,60] and iPSC-derived[61,62] cardiac cell sheets, which have been tested in murine and porcine cardiomyopathy models. Notably, non-cardiomyocytes, such as fibroblasts or vascular cells, were needed to produce intact sheets as pure cardiomyocyte populations do not produce sufficient ECM. Although photolithography has been used to pattern PNIPAAm surfaces with polymer brushes, which spatially limit cell attachment to align cells[63,64], these techniques have not been used to create aligned cardiac sheets for testing in animal models.

1.5 PSC-DERIVED CARDIOMYOCYTES

Cardiomyocytes are now largely sourced from PSCs, which can theoretically provide an indefinite supply of cells, and be patient-specific[65]. Advances in cardiac differentiation first focused on improving differentiation efficiency. Now that several methods to reliably differentiate stem cells to cardiomyocytes exist, efforts have shifted towards improving cardiomyocyte maturity and function.

1.5.1 Cardiac Differentiation

Early methods to differentiate cardiomyocytes were undirected. Differentiation was initiated by the formation of embryoid bodies (EBs)—spheroid aggregations of embryonic stem cells similar to the developing embryo. Several days after EB formation, EBs were plated, and cardiomyocytes became identifiable by their beating behavior[66]. As signaling pathways for mesoderm induction and cardiac lineage specification were identified, growth factors were incorporated to chemically direct cardiac differentiation. This worked by mimicking normal cardiac development, specifically by modulating the Activin/Nodal, BMP, and Wnt/β-catenin signaling pathways[67–71] (Figure 1.6). This permitted efficient differentiation of PSCs in monolayers[72,73]. Directed differentiation methods were then refined and simplified, becoming chemically defined and significantly lower in cost while reliably hitting efficiencies of 85% and higher[74–76]. PSC-derived cardiomyocytes have consequently become widely used in cardiac tissue engineering.

Although directed differentiation heavily relies on biochemical cues, physical cues also positively affect cardiomyocyte differentiation. The "matrix sandwich method," in which PSCs are differentiated between layers of Matrigel, increased cardiac differentiation efficiency[77]. Substrate stiffness[78], geometric confinement[79], and topography[80] can modulate differentiation though the Wnt pathway. For transdifferentiation of fibroblasts to cardiomyocytes, culturing the cells on microgrooves improved cardiomyocyte yield, and this effect could only partially be reproduced chemically[81].

1.5.2 Cardiac Maturation

Despite significant improvements in the differentiation of PSCs to cardiomyocytes, the resulting cells are not appropriate for transplantation as they are immature relative to their adult counterparts. Mature adult and immature PSC-derived cardiomyocytes are

different in regards to cell shape and size, proliferative capacity, sarcomere size and alignment, cell-cell connectivity, gene expression profiles, electrophysiology, and contractility[82,83]. Because no clear definition of maturity exists, some groups have attempted to quantify maturity in terms of sarcomere structure[84], gene expression profiles[85,86], and functional behaviors[87]. Biochemical means of maturing PSC-derived cardiomyocytes, specifically the use of ascorbic acid[88] and the hormone triiodothyronine[89], have had some success.

Biophysical means to mature cardiomyocytes have also been investigated. Substrate stiffness[90], topography[91,92], cell or cell cluster geometry[93,94], uniaxial stretching[95], electrical stimulation[96], and combinations thereof[97,98] have all been used to mature PSC-derived cardiomyocytes. Many of these approaches result in sarcomere and cardiomyocyte alignment as well as improved function. There is also growing evidence that non-cardiomyocyte support cells enhance cardiomyocyte electrophysiological and contractile function[59,91,99]. Despite all these techniques, long-term culture of PSC-derived cardiomyocytes, durations longer than three months, has reliably resulted in maturation, evidenced by rarely observed ultrastructural features like transverse-tubules[100,101]. Notably, PSC-derived cardiomyocytes in long-term cultures self-align even in the absence of biophysical cues.

1.6 Research Goals

The objective of the work described herein is to develop anisotropic substrates for cell sheeting and the study of differentiating cardiomyocyte substrate sensitivity. Function is clearly linked to cell structure and organization. Although PNIPAAm-surfaces have been patterned to generate anisotropic cell sheets, incorporating substrate anisotropy into cell

sheeting systems can be costly and technically difficult. Additionally, the sensitivity of differentiating cardiomyocytes to substrate anisotropy, i.e., whether cells respond in a gradient- or threshold-based manner, is unclear. Researchers choose binary systems, consisting of only isotropic and highly anisotropic materials. Therefore, the goals of this research are to (1) develop a simple and relatively low-cost method to generate anisotropic cell sheets and (2) use a set of substrates, ranging from isotropic to semi-anisotropic to anisotropic, to investigate the sensitivity of developing cardiomyocytes to substrate anisotropy. Chapter 2 describes the fabrication and characterization of PNIPAAm and poly(caprolactone (PCL) blended fibers. These fibers have thermo-sensitive properties that are dependent on their PNIPAAm concentration. In Chapter 3, electrospinning is used to generate a set of fiber scaffolds that vary from non-aligned to semi-aligned to highly aligned. Cardiomyocytes are derived from PSCs on these fibers to study their alignment and intracellular calcium transient behavior over time. The presented work is summarized in Chapter 4 with recommendations for future applications.

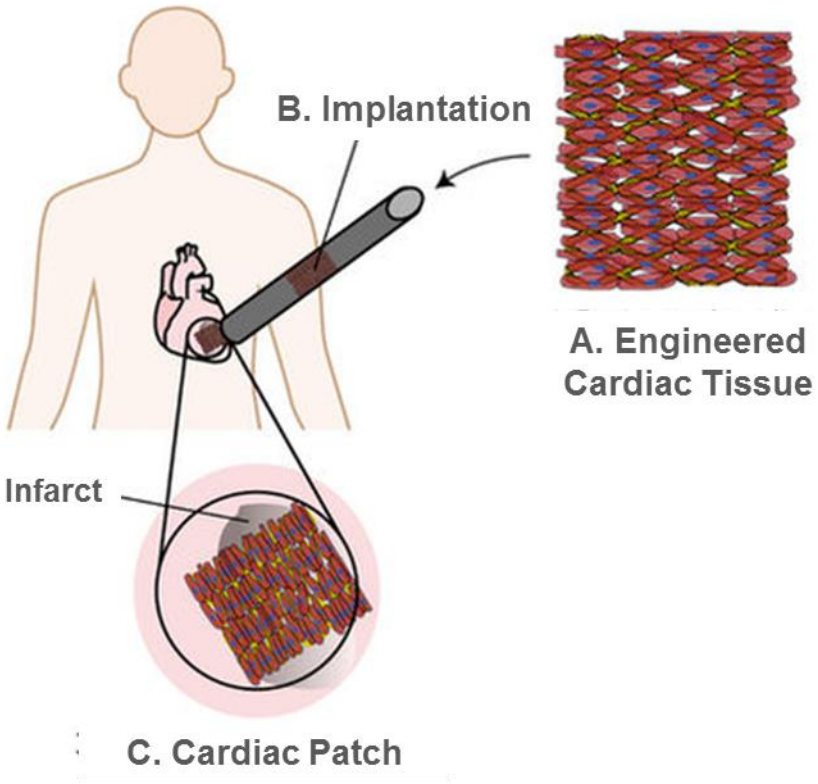

Figure 1.1 Engineered cardiac tissues (A) are implanted (B) as a cardiac patch over the infarct (C). (Adapted with permission from Montgomery et al.)

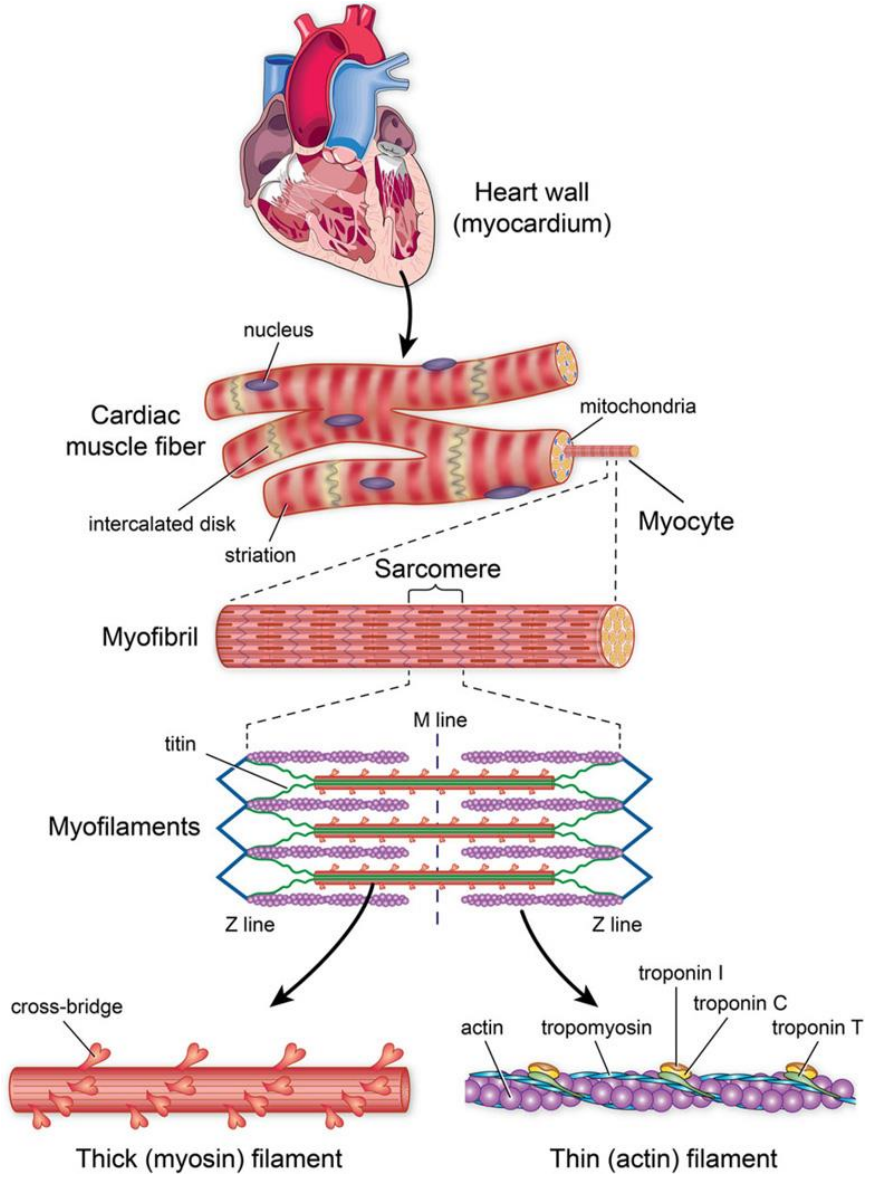

Figure 1.2 Myocardial tissue has multi-scale organization, from cardiac muscle fibers, down to individual sarcomeres consisting of thick myosin filaments and thin actin filaments. (Adapted with permission from Golob et al.)

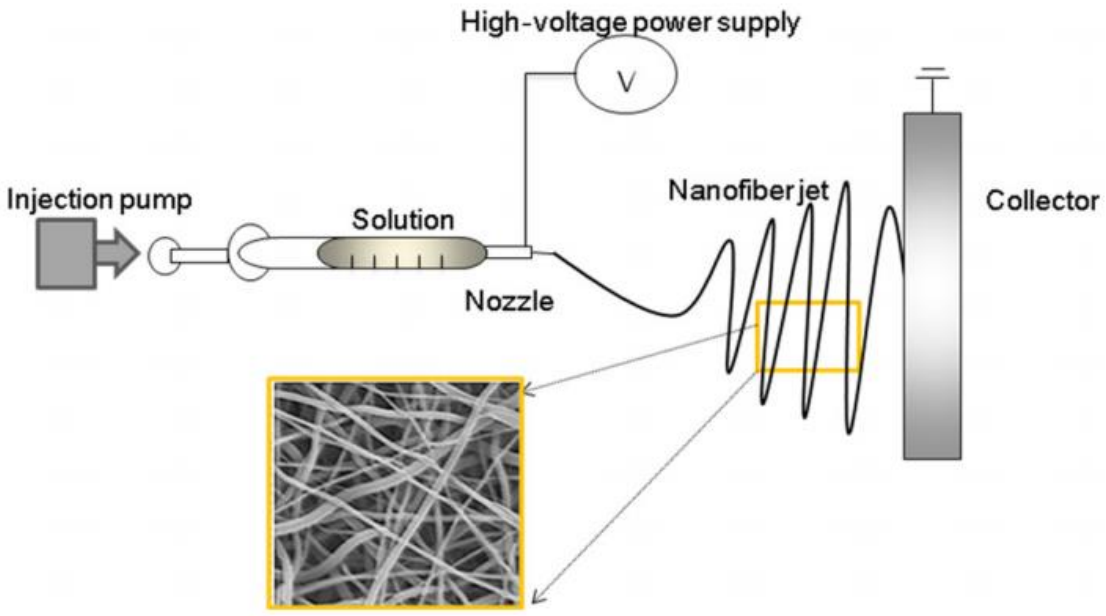

Figure 1.3 Electrospinning systems consist of a high voltage supply, a pump, and a grounded collector. Nanofibers are produced when repulsive forces cause the polymer solution to form a jet that elongates and is collected as nanofibers on the collector. (Adapted with permission from Shin et al.)

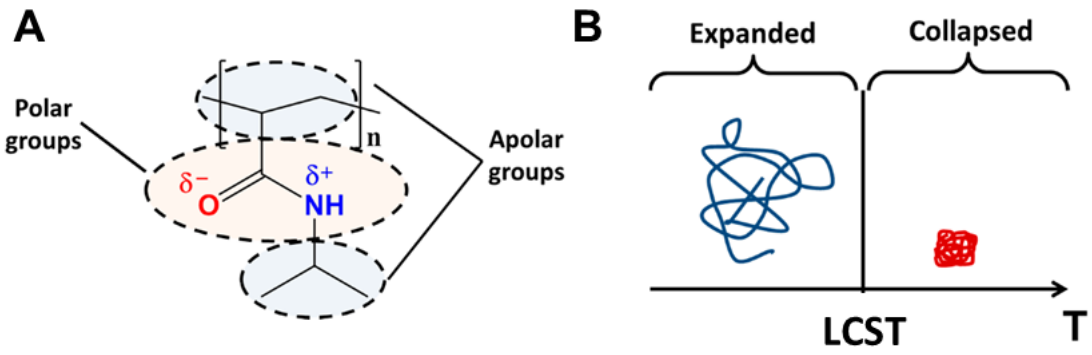

Figure 1.4 PNIPAAm structure and behavior. A) PNIPAAm is composed of polar and non-polar groups. B) In aqueous environments, PNIPAAm chains expand below LCST and collapse above LCST. (Adapted with permission from Lanzalcon et al.)

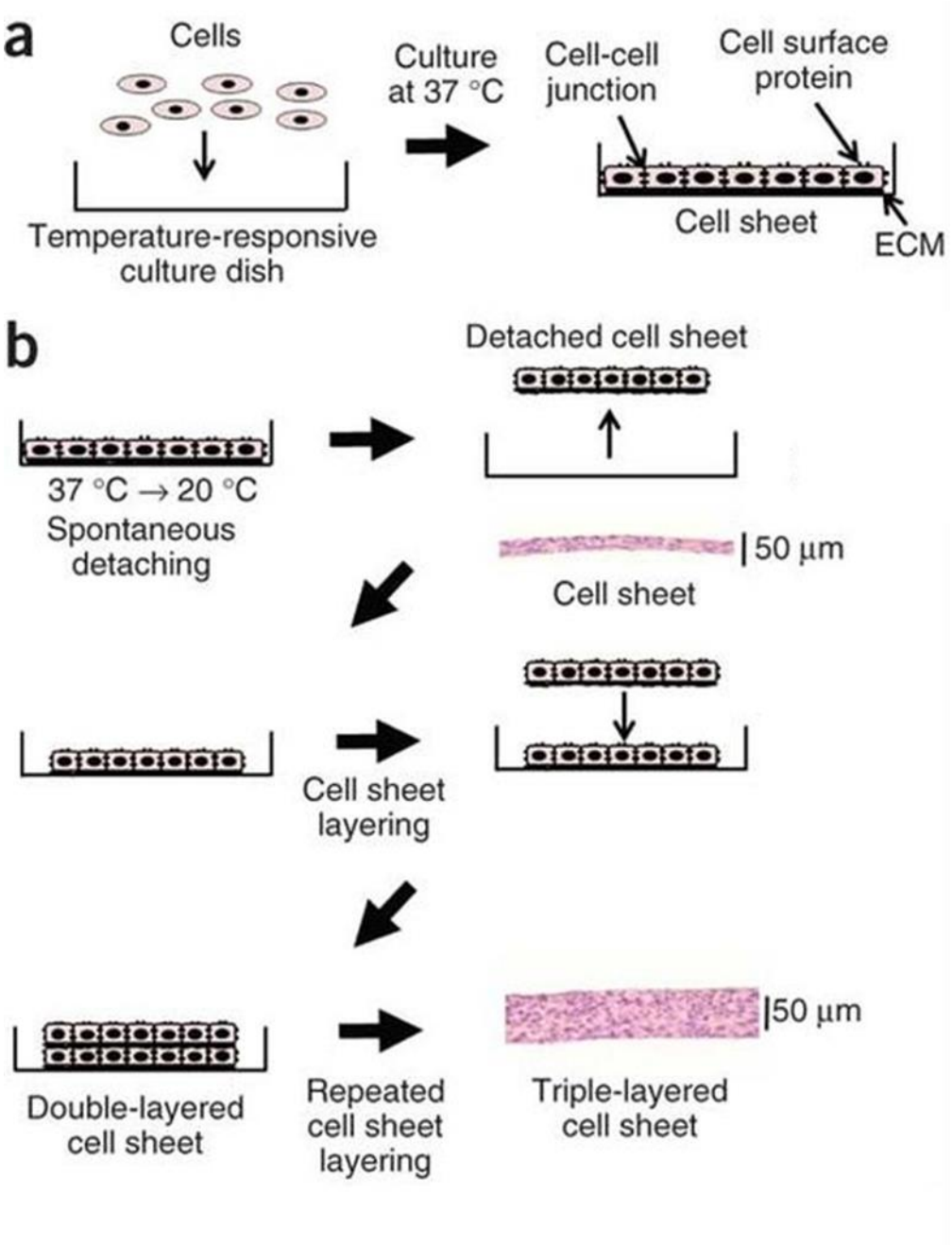

Figure 1.5 Cell sheeting using PNIPAAm-grafted plates. A) Above LCST, cell attach and can be cultured on PNIPAAm. B) When the temperature is lowered below LCST, cells detach as an intact sheet and can be layered. (Adapted with permission from Haraguchi et al.)

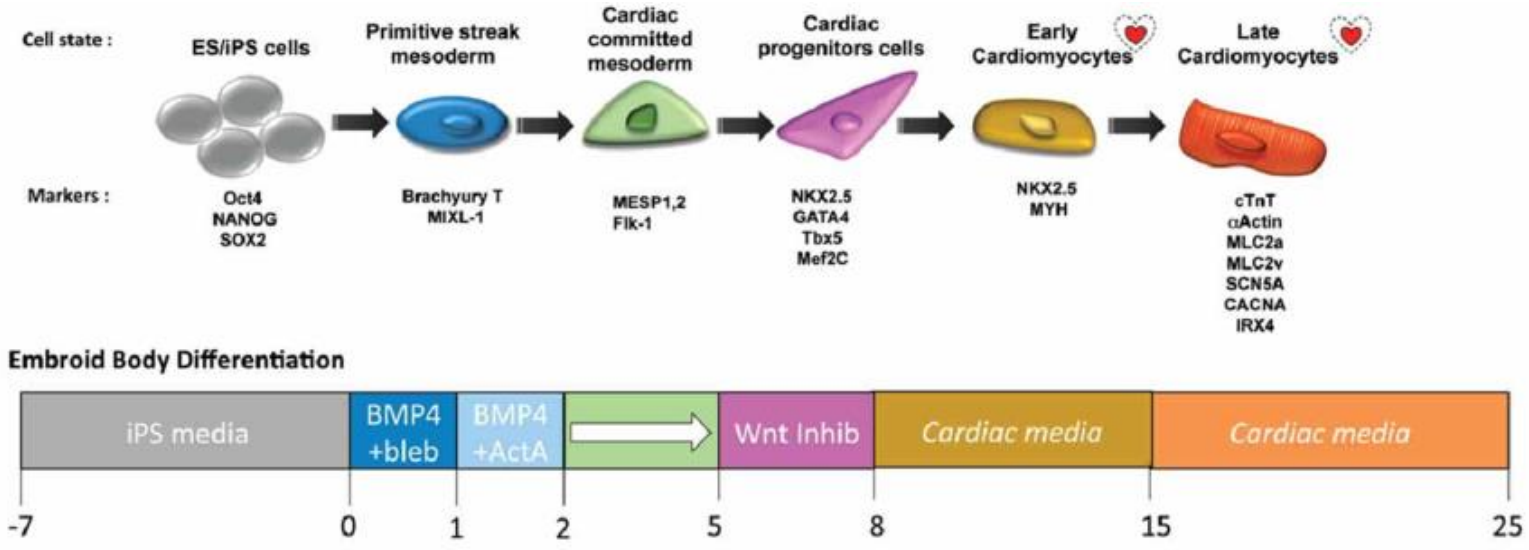

Figure 1.6 Cardiac differentiation occurs *in vitro* by modulation of the the Wnt, Activin, and BMP signaling pathways. (Adapted with permission from Jeziorowska et al.)

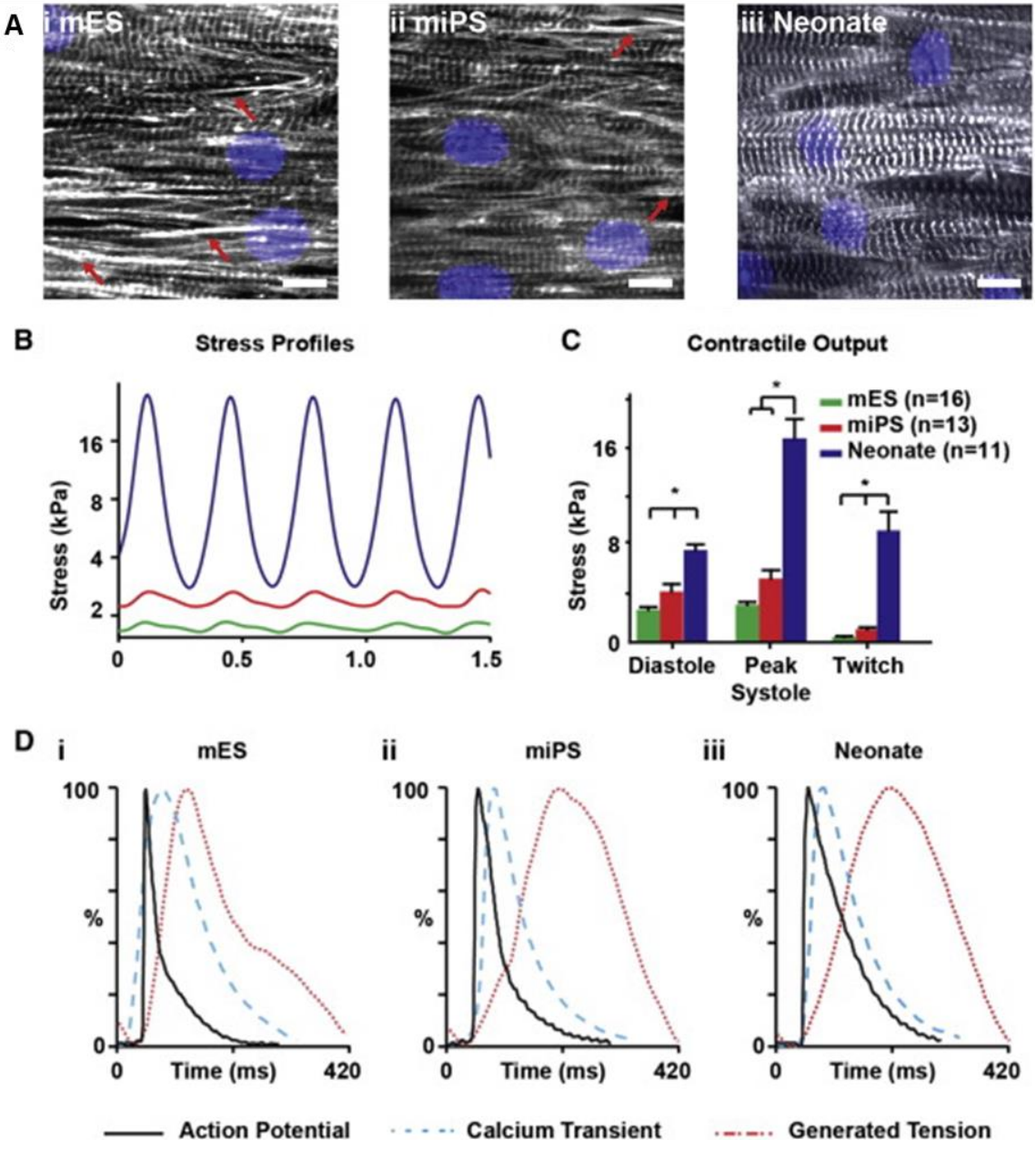

Figure 1.7 PSC-derived cardiomyocyte structure and function. A) Sarcomeres in cardiomyocytes derived from mESCs (i) mouse iPSCs (ii) and neonatal cardiomyocytes. Contractility (B) profiles and (C) output. D) Action potential, calcium transient, and tension profiles. (Adapted from Sheehy et al.)

1.7 REFERENCES

1. Benjamin, E. J. et al. Heart Disease and Stroke Statistics—2018 Update: A Report From the American Heart Association. Circulation CIR.0000000000000558 (2018). doi:10.1161/CIR.0000000000000558
2. Guyton, A. C. & Hall, J. E. Textbook of Medical Physiology. (Elsevier Science, 2000).
3. Hirt, M. N., Hansen, A. & Eschenhagen, T. Cardiac Tissue Engineering: State of the Art. Circulation Research 114, 354–367 (2014).
4. Montgomery, M. et al. Flexible shape-memory scaffold for minimally invasive delivery of functional tissues. Nat Mater 16, 1038–1046 (2017).
5. Yoshida, Y. & Yamanaka, S. Recent Stem Cell Advances: Induced Pluripotent Stem Cells for Disease Modeling and Stem Cell–Based Regeneration. Circulation 122, 80–87 (2010).
6. Golob, M., Moss, R. L. & Chesler, N. C. Cardiac Tissue Structure, Properties, and Performance: A Materials Science Perspective. Ann Biomed Eng 42, 2003–2013 (2014).
7. Tirziu, D., Giordano, F. J. & Simons, M. Cell Communications in the Heart. Circulation 122, 928–937 (2010).
8. Fan, D., Takawale, A., Lee, J. & Kassiri, Z. Cardiac fibroblasts, fibrosis and extracellular matrix remodeling in heart disease. Fibrogenesis Tissue Repair 5, 15 (2012).
9. Bray, M.-A., Sheehy, S. P. & Parker, K. K. Sarcomere Alignment is Regulated by Myocyte Shape. Cell Motil Cytoskeleton 65, 641–651 (2008).
10. Blazeski, A. et al. Electrophysiological and contractile function of cardiomyocytes derived from human embryonic stem cells. Prog Biophys Mol Biol 110, 178–195 (2012).
11. Huebsch, N. et al. Automated Video-Based Analysis of Contractility and Calcium Flux in Human-Induced Pluripotent Stem Cell-Derived Cardiomyocytes Cultured over Different Spatial Scales. Tissue Eng Part C Methods 21, 467–479 (2015).
12. Bian, W., Juhas, M., Pfeiler, T. W. & Bursac, N. Local Tissue Geometry Determines Contractile Force Generation of Engineered Muscle Networks. Tissue Engineering Part A 18, 957–967 (2011).
13. McCain, M. L., Lee, H., Aratyn-Schaus, Y., Kléber, A. G. & Parker, K. K. Cooperative coupling of cell-matrix and cell–cell adhesions in cardiac muscle. PNAS 109, 9881–9886 (2012).
14. McCain, M. L., Yuan, H., Pasqualini, F. S., Campbell, P. H. & Parker, K. K. Matrix elasticity regulates the optimal cardiac myocyte shape for contractility. American

Journal of Physiology - Heart and Circulatory Physiology 306, H1525–H1539 (2014).

15. Alford, P. W., Feinberg, A. W., Sheehy, S. P. & Parker, K. K. Biohybrid Thin Films for Measuring Contractility in Engineered Cardiovascular Muscle. Biomaterials 31, 3613–3621 (2010).

16. Natarajan, A. et al. Patterned Cardiomyocytes on Microelectrode Arrays as a Functional, High Information Content Drug Screening Platform. Biomaterials 32, 4267–4274 (2011).

17. Bursac, N., Parker, K. K., Iravanian, S. & Tung, L. Cardiomyocyte Cultures With Controlled Macroscopic Anisotropy A Model for Functional Electrophysiological Studies of Cardiac Muscle. Circulation Research 91, e45–e54 (2002).

18. Geuss, L. R., Allen, A. C. B., Ramamoorthy, D. & Suggs, L. J. Maintenance of HL-1 cardiomyocyte functional activity in PEGylated fibrin gels. Biotechnol. Bioeng. (2015). doi:10.1002/bit.25553

19. Fast, V. G. Simultaneous optical imaging of membrane potential and intracellular calcium. Journal of Electrocardiology 38, 107–112 (2005).

20. Herron, T. J., Lee, P. & Jalife, J. Optical Imaging of Voltage and Calcium in Cardiac Cells & Tissues. Circulation Research 110, 609–623 (2012).

21. Tandon, N. et al. Optimization of Electrical Stimulation Parameters for Cardiac Tissue Engineering. J Tissue Eng Regen Med 5, e115–e125 (2011).

22. Fomovsky, G. M., Thomopoulos, S. & Holmes, J. W. Contribution of Extracellular Matrix to the Mechanical Properties of the Heart. J Mol Cell Cardiol 48, 490–496 (2010).

23. Doshi, J. & Reneker, D. H. Electrospinning process and applications of electrospun fibers. in , Conference Record of the 1993 IEEE Industry Applications Society Annual Meeting, 1993 1698–1703 vol.3 (1993). doi:10.1109/IAS.1993.299067

24. Shin, S.-H., Purevdorj, O., Castano, O., Planell, J. A. & Kim, H.-W. A short review: Recent advances in electrospinning for bone tissue regeneration. Journal of Tissue Engineering 3, (2012).

25. Rutledge, G. C. & Fridrikh, S. V. Formation of fibers by electrospinning. Adv. Drug Deliv. Rev. 59, 1384–1391 (2007).

26. Fong, H., Chun, I. & Reneker, D. H. Beaded nanofibers formed during electrospinning. Polymer 40, 4585–4592 (1999).

27. Thompson, C. J., Chase, G. G., Yarin, A. L. & Reneker, D. H. Effects of parameters on nanofiber diameter determined from electrospinning model. Polymer 48, 6913–6922 (2007).

28. Li, J. et al. Human Pluripotent Stem Cell-Derived Cardiac Tissue-like Constructs for Repairing the Infarcted Myocardium. Stem Cell Reports 9, 1546–1559 (2017).

29. Kai, D. et al. Stem cell-loaded nanofibrous patch promotes the regeneration of infarcted myocardium with functional improvement in rat model. Acta Biomaterialia 10, 2727–2738 (2014).

30. Kharaziha, M. et al. PGS:Gelatin nanofibrous scaffolds with tunable mechanical and structural properties for engineering cardiac tissues. Biomaterials 34, 6355–6366 (2013).

31. Orlova, Y., Magome, N., Liu, L., Chen, Y. & Agladze, K. Electrospun nanofibers as a tool for architecture control in engineered cardiac tissue. Biomaterials 32, 5615–5624 (2011).

32. Zong, X. et al. Electrospun fine-textured scaffolds for heart tissue constructs. Biomaterials 26, 5330–5338 (2005).

33. Wanjare, M. et al. Anisotropic microfibrous scaffolds enhance the organization and function of cardiomyocytes derived from induced pluripotent stem cells. Biomaterials Science 5, 1567–1578 (2017).

34. Pham, Q. P., Sharma, U. & Mikos, A. G. Electrospinning of Polymeric Nanofibers for Tissue Engineering Applications: A Review. Tissue Engineering 12, 1197–1211 (2006).

35. Chen, M. et al. Thermo-Responsive Core−Sheath Electrospun Nanofibers from Poly (N-isopropylacrylamide)/Polycaprolactone Blends. Chem. Mater. 22, 4214–4221 (2010).

36. Qin, D., Xia, Y. & Whitesides, G. M. Soft lithography for micro- and nanoscale patterning. Nat Protoc 5, 491–502 (2010).

37. Anderson, J. M. Future challenges in the in vitro and in vivo evaluation of biomaterial biocompatibility. Regen Biomater 3, 73–77 (2016).

38. Yamada, N. et al. Thermo-responsive polymeric surfaces; control of attachment and detachment of cultured cells. Makromol. Chem., Rapid Commun. 11, 571–576 (1990).

39. Haraguchi, Y. et al. Fabrication of functional three-dimensional tissues by stacking cell sheets in vitro. Nature Protocols 7, 850–858 (2012).

40. Nagase, K., Yamato, M., Kanazawa, H. & Okano, T. Poly(N-isopropylacrylamide)-based thermoresponsive surfaces provide new types of biomedical applications. Biomaterials 153, 27–48 (2018).

41. Lanzalaco, S. & Armelin, E. Poly(N-isopropylacrylamide) and Copolymers: A Review on Recent Progresses in Biomedical Applications. Gels 3, 36 (2017).

42. Tran, T. et al. Controllable and switchable drug delivery of ibuprofen from temperature responsive composite nanofibers. Nano Convergence 2, 15 (2015).

43. Yu, H., Jia, Y., Chen, G. & Zhang, Y. Fabrication of core/sheath PCL/PEG–PNIPAAm fibers as thermosensitive release carriers by a new technique combining blend electrospinning and ultraviolet-induced graft polymerization. Materials Letters 164, 505–508 (2016).

44. Baker, B. M. et al. The potential to improve cell infiltration in composite fiber-aligned electrospun scaffolds by the selective removal of sacrificial fibers. Biomaterials 29, 2348–2358 (2008).

45. Lee, J. B. et al. Development of 3D Microvascular Networks Within Gelatin Hydrogels Using Thermoresponsive Sacrificial Microfibers. Adv. Healthcare Mater. 5, 781–785 (2016).

46. Heskins, M. & Guillet, J. E. Solution Properties of Poly(N-isopropylacrylamide). Journal of Macromolecular Science: Part A - Chemistry 2, 1441–1455 (1968).

47. Tang, Z. & Okano, T. Recent development of temperature-responsive surfaces and their application for cell sheet engineering. Regen Biomater 1, 91–102 (2014).

48. Nitschke Mirko et al. Thermo-responsive poly(NiPAAm-co-DEGMA) substrates for gentle harvest of human corneal endothelial cell sheets. Journal of Biomedical Materials Research Part A 80A, 1003–1010 (2006).

49. Moran, M. T., Carroll, W. M., Selezneva, I., Gorelov, A. & Rochev, Y. Cell growth and detachment from protein-coated PNIPAAm-based copolymers. J. Biomed. Mater. Res. 81A, 870–876 (2007).

50. Schmaljohann, D. et al. Thermo-Responsive PNiPAAm-g-PEG Films for Controlled Cell Detachment. Biomacromolecules 4, 1733–1739 (2003).

51. Pan Guoqing, Guo Qianping, Ma Yue, Yang Huilin & Li Bin. Thermo-Responsive Hydrogel Layers Imprinted with RGDS Peptide: A System for Harvesting Cell Sheets. Angewandte Chemie International Edition 52, 6907–6911 (2013).

52. Ohya, S., Kidoaki, S. & Matsuda, T. Poly(N-isopropylacrylamide) (PNIPAM)-grafted gelatin hydrogel surfaces: interrelationship between microscopic structure and mechanical property of surface regions and cell adhesiveness. Biomaterials 26, 3105–3111 (2005).

53. Wang, J., Chen, L., Zhao, Y., Guo, G. & Zhang, R. Cell adhesion and accelerated detachment on the surface of temperature-sensitive chitosan and poly(N-isopropylacrylamide) hydrogels. J Mater Sci: Mater Med 20, 583–590 (2009).

54. Zhao, X., Wang, L., Wang, P., Yang, Y. & Wang, F. Fabrication of Thermoresponsive Nanofibers for Cell Sorting and Aligned Cell Sheet Engineering. J Nanosci Nanotechnol 16, 5520–5527 (2016).

55. Akiyama, Y., Kikuchi, A., Yamato, M. & Okano, T. Ultrathin Poly(N-isopropylacrylamide) Grafted Layer on Polystyrene Surfaces for Cell Adhesion/Detachment Control. Langmuir 20, 5506–5511 (2004).

56. Inaba, R., Khademhosseini, A., Suzuki, H. & Fukuda, J. Electrochemical desorption of self-assembled monolayers for engineering cellular tissues. Biomaterials 30, 3573–3579 (2009).

57. Yan, J., Chen, F. & Amsden, B. G. Cell sheets prepared via gel–sol transition of calcium RGD–alginate. Acta Biomaterialia 30, 277–284 (2016).

58. Shimizu, T. et al. Fabrication of pulsatile cardiac tissue grafts using a novel 3-dimensional cell sheet manipulation technique and temperature-responsive cell culture surfaces. Circ. Res. 90, e40 (2002).

59. Matsuura, K. et al. Creation of mouse embryonic stem cell-derived cardiac cell sheets. Biomaterials 32, 7355–7362 (2011).

60. Matsuda, T. et al. N-cadherin-mediated cell adhesion determines the plasticity for cell alignment in response to mechanical stretch in cultured cardiomyocytes. Biochemical and Biophysical Research Communications 326, 228–232 (2004).

61. Masumoto, H. et al. Human iPS cell-engineered cardiac tissue sheets with cardiomyocytes and vascular cells for cardiac regeneration. Scientific Reports 4, 6716 (2014).

62. Kawamura, M. et al. Enhanced Therapeutic Effects of Human iPS Cell Derived-Cardiomyocyte by Combined Cell-Sheets with Omental Flap Technique in Porcine Ischemic Cardiomyopathy Model. Scientific Reports 7, 8824 (2017).

63. Takahashi, H., Nakayama, M., Shimizu, T., Yamato, M. & Okano, T. Anisotropic cell sheets for constructing three-dimensional tissue with well-organized cell orientation. Biomaterials 32, 8830–8838 (2011).

64. Lim, J. et al. Fabrication of cell sheets with anisotropically aligned myotubes using thermally expandable micropatterned hydrogels. Macromol. Res. 24, 562–572 (2016).

65. Takahashi, K. & Yamanaka, S. Induction of Pluripotent Stem Cells from Mouse Embryonic and Adult Fibroblast Cultures by Defined Factors. Cell 126, 663–676 (2006).

66. Boheler, K. R. et al. Differentiation of Pluripotent Embryonic Stem Cells Into Cardiomyocytes. Circulation Research 91, 189–201 (2002).

67. Sumi, T., Tsuneyoshi, N., Nakatsuji, N. & Suemori, H. Defining early lineage specification of human embryonic stem cells by the orchestrated balance of canonical Wnt/β-catenin, Activin/Nodal and BMP signaling. Development 135, 2969–2979 (2008).

68. Kim, M.-S. et al. Activin-A and Bmp4 levels modulate cell type specification during CHIR-induced cardiomyogenesis. PLoS ONE 10, e0118670 (2015).

69. Kattman, S. J. et al. Stage-Specific Optimization of Activin/Nodal and BMP Signaling Promotes Cardiac Differentiation of Mouse and Human Pluripotent Stem Cell Lines. Cell Stem Cell 8, 228–240 (2011).

70. Rao, J. et al. Stepwise Clearance of Repressive Roadblocks Drives Cardiac Induction in Human ESCs. Cell Stem Cell 18, 341–353 (2016).

71. Jeziorowska, D., Korniat, A., Salem, J.-E., Fish, K. & Hulot, J.-S. Generating patient-specific induced pluripotent stem cells-derived cardiomyocytes for the treatment of cardiac diseases. Expert Opin Biol Ther 15, 1399–1409 (2015).

72. Mummery, C. L. et al. Differentiation of Human Embryonic Stem Cells and Induced Pluripotent Stem Cells to Cardiomyocytes A Methods Overview. Circulation Research 111, 344–358 (2012).

73. Kokkinopoulos, I. et al. Cardiomyocyte differentiation from mouse embryonic stem cells using a simple and defined protocol. Dev. Dyn. 245, 157–165 (2016).

74. Burridge, P. W. et al. Chemically defined generation of human cardiomyocytes. Nat Meth 11, 855–860 (2014).

75. Lian, X. et al. Directed cardiomyocyte differentiation from human pluripotent stem cells by modulating Wnt/β-catenin signaling under fully defined conditions. Nat. Protocols 8, 162–175 (2013).

76. Lian, X. et al. Chemically defined, albumin-free human cardiomyocyte generation. Nat Meth 12, 595–596 (2015).

77. Zhang, J. et al. Functional Cardiomyocytes Derived from Human Induced Pluripotent Stem Cells. Circ Res 104, e30–e41 (2009).

78. Przybyla, L., Lakins, J. N. & Weaver, V. M. Tissue Mechanics Orchestrate Wnt-Dependent Human Embryonic Stem Cell Differentiation. Cell Stem Cell (2016). doi:10.1016/j.stem.2016.06.018

79. Ma, Z. et al. Self-organizing human cardiac microchambers mediated by geometric confinement. Nature Communications 6, 7413 (2015).

80. Chen, Y. et al. Three-dimensional poly-(ε-caprolactone) nanofibrous scaffolds directly promote the cardiomyocyte differentiation of murine-induced pluripotent stem cells through Wnt/β-catenin signaling. BMC Cell Biology 16, 22 (2015).

81. Sia, J., Yu, P., Srivastava, D. & Li, S. Effect of biophysical cues on reprogramming to cardiomyocytes. Biomaterials 103, 1–11 (2016).

82. Feinberg, A. W. et al. Functional Differences in Engineered Myocardium from Embryonic Stem Cell-Derived versus Neonatal Cardiomyocytes. Stem Cell Reports 1, 387–396 (2013).

83. Feric, N. T. & Radisic, M. Maturing human pluripotent stem cell-derived cardiomyocytes in human engineered cardiac tissues. Advanced Drug Delivery Reviews (2015). doi:10.1016/j.addr.2015.04.019

84. Pasqualini, F. S., Sheehy, S. P., Agarwal, A., Aratyn-Schaus, Y. & Parker, K. K. Structural Phenotyping of Stem Cell-Derived Cardiomyocytes. Stem Cell Reports 4, 340–347 (2015).

85. Bedada, F. B. et al. Acquisition of a Quantitative, Stoichiometrically Conserved Ratiometric Marker of Maturation Status in Stem Cell-Derived Cardiac Myocytes. Stem Cell Reports 3, 594–605 (2014).

86. Uosaki, H. et al. Transcriptional Landscape of Cardiomyocyte Maturation. Cell Rep 13, 1705–1716 (2015).

87. Ribeiro, M. C. et al. Functional maturation of human pluripotent stem cell derived cardiomyocytes in vitro – Correlation between contraction force and electrophysiology. Biomaterials 51, 138–150 (2015).

88. Cao, N. et al. Ascorbic acid enhances the cardiac differentiation of induced pluripotent stem cells through promoting the proliferation of cardiac progenitor cells. Cell Res 22, 219–236 (2012).

89. Parikh, S. S. et al. Thyroid and Glucocorticoid Hormones Promote Functional T-Tubule Development in Human-Induced Pluripotent Stem Cell–Derived CardiomyocytesNovelty and Significance. Circulation Research 121, 1323–1330 (2017).

90. Ribeiro, A. J. S. et al. Contractility of single cardiomyocytes differentiated from pluripotent stem cells depends on physiological shape and substrate stiffness. PNAS 112, 12705–12710 (2015).

91. Parrag, I. C., Zandstra, P. W. & Woodhouse, K. A. Fiber alignment and coculture with fibroblasts improves the differentiated phenotype of murine embryonic stem cell-derived cardiomyocytes for cardiac tissue engineering. Biotechnol. Bioeng. 109, 813–822 (2012).

92. Rao, C. et al. The effect of microgrooved culture substrates on calcium cycling of cardiac myocytes derived from human induced pluripotent stem cells. Biomaterials 34, 2399–2411 (2013).

93. Thavandiran, N. et al. Design and formulation of functional pluripotent stem cell-derived cardiac microtissues. Proc Natl Acad Sci U S A 110, E4698–E4707 (2013).

94. Zhang, D. et al. Tissue-engineered cardiac patch for advanced functional maturation of human ESC-derived cardiomyocytes. Biomaterials 34, 5813–5820 (2013).

95. Mihic, A. et al. The effect of cyclic stretch on maturation and 3D tissue formation of human embryonic stem cell-derived cardiomyocytes. Biomaterials 35, 2798–2808 (2014).

96. Nunes, S. S. et al. Biowire: a platform for maturation of human pluripotent stem cell-derived cardiomyocytes. Nat Meth 10, 781–787 (2013).

97. Au, H. T. H., Cheng, I., Chowdhury, M. F. & Radisic, M. Interactive effects of surface topography and pulsatile electrical field stimulation on orientation and elongation of fibroblasts and cardiomyocytes. Biomaterials 28, 4277–4293 (2007).

98. Thavandiran, N., Nunes, S. S., Xiao, Y. & Radisic, M. Topological and electrical control of cardiac differentiation and assembly. Stem Cell Res Ther 4, 14 (2013).

99. Liau, B., Jackman, C. P., Li, Y. & Bursac, N. Developmental stage-dependent effects of cardiac fibroblasts on function of stem cell-derived engineered cardiac tissues. Scientific Reports 7, srep42290 (2017).

100. Kerscher, P. et al. Direct hydrogel encapsulation of pluripotent stem cells enables ontomimetic differentiation and growth of engineered human heart tissues. Biomaterials 83, 383–395 (2016).

101. Lundy, S. D., Zhu, W.-Z., Regnier, M. & Laflamme, M. A. Structural and Functional Maturation of Cardiomyocytes Derived from Human Pluripotent Stem Cells. Stem Cells Dev 22, 1991–2002 (2013).

Chapter 2: Electrospun Poly(N-isopropyl acrylamide)/Poly(caprolactone) Fibers for the Generation of Anisotropic Cell Sheets

2.0 FOREWORD

This chapter is based on a research journal article published in 2017.* It describes the characterization of blended, aligned thermo-sensitive fibers and demonstrates the feasibility of using these fibers to generate anisotropic cell sheets. My contribution was in the design and execution of the experimental work as well as the writing of the manuscript. The second author, Elissa Barone, was an undergraduate research assistant who contributed the experimental work. Cody Crosby, a graduate student in the Zoldan Lab, performed the advancing water contact angle experiments and wrote the corresponding methods sub-section. Drs. Janet Zoldan and Laura Suggs conceptualized the research and aided in experimental design.

2.1 INTRODUCTION

Cell alignment, which can influence developmental and physiological processes, is driven by biophysical cues, particularly matrix nanotopography[1]. To better mimic native cell microenvironments in vitro, techniques to generate surface anisotropy, from electrospinning fibers[2,3] to micropatterning to photolithography, have been widely developed and applied to anisotropic tissues, namely muscle and nervous tissue. Both micropatterning and photolithography can be used to design surfaces with high resolution

* Allen, A.C.B., Barone, E., Crosby, C.O.K., Suggs, L.J., and Zoldan, J. (2017). Electrospun poly(N-isopropyl acrylamide)/poly(caprolactone) fibers for the generation of anisotropic cell sheets. Biomater Sci 5, 1661–1669.

but are resource-intensive, requiring microprinters and clean rooms[4]. Electrospinning, on the other hand, is a relatively simple and inexpensive technique to fabricate polymer nano- and micro-fibers that can be seeded with cells[5,6]. Electrospun fibers are extracellular matrix-mimicking in that they provide a 3-dimensional fibrous microenvironment. Aligned electrospun fibers have been successful as scaffolds for generating nervous and beating cardiac tissues that can be implanted into animal models[7,8]. These transplants, however, are rather limited in that they are only 1-2 cell layers thick, which can severely limit function depending on tissue type, and that the material component may elicit a host response upon implantation[9].

Cell sheeting is a technique to generate biomaterial-free, tissue-like constructs for transplant. Teruo Okano pioneered the re-purposing of thermosensitive poly(N-isopropylacrylamide) (PNIPAAm) as a surface coating to enable cell sheeting in vitro[10]. PNIPAAm undergoes a rapid coil-to-globule transition at its lower critical solution temperature (LCST) of 32°C that determines how the hydrophilic and hydrophobic domains interact with water. Below 32°C, PNIPAAm readily dissolves in water; above 32°C, PNIPAAm's hydrophilic domains are sequestered and PNIPAAm precipitates in aqueous solutions[11]. Thus, for cells grown on PNIPAAm-grafted tissue culture plates, cell sheet detachment is possible when the incubation temperature is lowered below the LCST: PNIPAAm expands, forcing the cell sheet to detach without perturbing cell-cell and cell-ECM adhesions. Using this technique, cells sheets have been generated for transplantation to the heart, cornea, and kidney[12,13]. Yet generating aligned cell sheets has been challenging. Although grafting hydrophilic domains to PNIPAAm-grafted spatially controls cell attachment, leading to cell alignment, this approach required chemical synthesis and photolithography patterning[14,15].

Here, we describe the use of electrospun PNIPAAm and poly(ε-caprolactone) (PCL) blended fibers (denoted PNIPAAm/PCL fibers) to generate anisotropic cell sheets. PCL is a common polymer for electrospinning, and electrospun PCL fibers have been successfully used as cell culture scaffolds[16–18]. Due to PNIPAAm's thermo-sensitive nature, we hypothesized that fibers would need to contain enough PNIPAAm to enable detachment of cell sheets yet contain a sufficient amount of PCL to ensure proper cell attachment. While PNIPAAm has been successfully electrospun[19], it has primarily been used for drug delivery[20,21] and as sacrificial fibers to negatively pattern hydrogels[22]. Only one previous report described the use of electrospun PNIPAAm fibers for cell culture, which required chemical modification of PNIPAAm to enable gelatin grafting[23]. Our method does not require chemical modification or resource-intensive techniques, thus saving time and expense, and has the potential to generate tissue-specific, aligned cell sheets for transplant studies.

2.2 Materials & Methods

2.2.1 Fabrication PNIPAAm/PCL fibers

For PNIPAAm-only fibers, PNIPAAm (300,000 Da, Scientific Polymer Products, Ontario, NY) was dissolved 20% (wt/v) in methanol (Fisher Chemical, Pittsburgh, PA), as previously described[22]. For PCL-only fibers, PCL (80,000 Da, Sigma-Aldrich, St. Louis, MO) was dissolved 10% (wt/v) in hexafluoroisopropanol (Sigma-Aldrich). For PNIPAAm/PCL fibers, PNIPAAm and PCL (at ratios of 9:1, 3:1, 1:1, and 1:3, respectively) were dissolved 12-18% (wt/v) in a 1:3 mixture of methanol and chloroform (Sigma-Aldrich). All polymer solutions were dissolved by continuous stirring until clear and homogenous. To electrospin, a syringe pump (New Era Pump Systems, Inc.) was used to

dispense the polymer solutions from a 10-mL syringe with a 25 G blunted stainless steel needle at 2.0 mL/hr for the PCL-only solution and 1.0 mL/hr for all PNIPAAm-containing solutions. A high voltage supply (Gamma High Voltage, Ormond Beach, FL) was used to apply a charge of 5-15 kV (optimal charge determined for each solution, Appendix Table A.1.1) to the needle to initiate jet formation. Fibers were deposited on a rotating grounded 7.6-cm diameter aluminum collector. To obtain aligned fibers, the collector was rotated at 2500 – 3200 rotations per minute (RPM, approximately 10.0-12.8 m/s). The working distance from the needle and to collector was set at 11 cm. PNIPAAm/PCL fibers are referred to by the percent PNIPAAm content (i.e., 75% PNIPAAm fibers consist of 75% PNIPAAm and 25% PCL). Similarly, "high PCL-content" refers to 0%, 25%, and 50% PNIPAAm and "high PNIPAAm-content" refers to 75%, 90%, and 100% PNIPAAm.

2.2.2 Characterization of PNIPAAm/PCL fibers

2.2.2.1 Fiber Orientation and Diameter

PNIPAAm/PCL fibers were sputter coated with 12 nm platinum/palladium and imaged using a Zeiss Supra 40VP scanning electron microscope (SEM, 5 kV). SEM images (n=9) were analyzed using NIH ImageJ software, specifically the OrientationJ[24,25] and DiameterJ[26] plug-ins to determine fiber orientation and diameter, respectively. The fiber orientation index, S, was calculated from angle distribution histograms using the following equation[27]: $S = 2\langle \cos 2(\alpha) \rangle - 1$; where α is the difference between an individual fiber angle and the mean angle of all fibers. S varies from 0 to 1, for perfectly random and perfectly aligned fibers, respectively.

2.2.2.2 Fourier Transform Infrared Spectroscopy

Fourier-transform infrared (FTIR) attenuated total reflectance (ATR) was used to verify fiber polymer composition. Spectra of dry PNIPAAm/PCL fibers was collected over a range of wavelengths (400 cm^{-1} to 3000 cm^{-1}) at a resolution of 2 cm^{-1} using a Thermo Scientific Nicolet iS10 FT-IR spectrometer (Waltham, MA). Background spectra was collected prior to each individual sample.

2.2.2.3 PNIPAAm Mass Loss

PNIPAAm/PCL fibers were cut (approximately 1 cm x 1 cm, n=3) and weighed before being immersed in ultrapure water. To ensure complete PNIPAAm dissolution, fibers were rinsed 3 times in 2 mL of water over 24 hours. Fibers were then dried under vacuum for 48 hours before measuring their final weight. Percent mass lost was determined by subtracting the final weight from the original weight. Fibers were imaged before and after rinsing, and original and post-dissolution areas were calculated in ImageJ. Percent contraction was determined by dividing the final area by the original area.

2.2.2.4 Advancing Contact Angle Measurement

Advancing contact angles were measured using a FTA-200 goniometer (First Ten Angstroms, Portsmouth, VA) to determine the relative hydrophobicity of dry (non-wetted) and wetted PNIPAAm/PCL fibers. Fibers were cut into squares (approximately 1.75 cm x 1.75 cm, n=3). Wetted PNIPAAm/PCL fiber squares were secured in CellCrown inserts and rinsed in water warmed to 37°C for 24 hours. Fibers were then dried in a vacuum oven at 35-55°, above the LCST of PNIPAAm and below the melting temperature. PNIPAAm/PCL fibers were placed on a heating platform to maintain the temperature between 32-60°C, as measured by an infrared thermometer. Briefly, a drop of purified water was deposited at 0.8 µL/second from a 10-mL syringe on the PNIPAAm/PCL fibers,

and high-resolution images were subsequently captured. When possible, the contact angle was determined in the sessile drop session mode in the instrument-associated software. Otherwise, advancing contact angle was calculated by manually defining the location of the fiber plane and the drop's curvature.

2.3.3 Cell studies

All cell studies were performed using NIH 3T3 fibroblasts purchased from American Type Culture Collection (Manassas, VA), passages 15-25. 3T3 fibroblasts were maintained in 10% fetal bovine serum (ThermoFisher) and 1% penicillin/streptomycin (ThermoFisher) in low glucose Dulbecco's Modified Eagle's Medium with L-glutamine (Sigma-Aldrich). 3T3 fibroblasts were passaged using trypsin/EDTA (Sigma-Aldrich).

2.3.3.1 PNIPAAm/PCL fiber sterilization and protein coating

PNIPAAm/PCL fibers and parafilm were cut into squares (1.75 cm x 1.75 cm or 2.5 cm x 2.5 cm) and sterilized by ultraviolet light, 30 minutes each side. Fibers were secured using 12-well or 24-well CellCrown inserts (Scaffdex, Tampere, Finland) and parafilm (Bemis, Oshkosh, WI)—effectively making stand-alone PNIPAAm/PCL fiber bottom wells (Appendix Figure A.1)—to improve handling and prevent PNIPAAm fiber contraction upon wetting. Prior to coating, fibers were wetted with Dulbecco's Phosphate Buffered Saline (DPBS). Fibers were then coated with a 1:50 dilution of Growth-factor Reduced (GFR)-Matrigel (Corning, Corning, NY) in DMEM. Fibers were also pre-treated with fetal bovine serum (FBS, ThermoFisher) for at least 10 minutes immediately prior to cell seeding, as recommended by Haraguchi et al.[28] All solutions were warmed to 37°C and fibers were kept on a hot plate in the tissue culture hood to ensure that PNIPAAm remained above its LCST.

2.3.3.2 Cell viability on PNIPAAm/PCL fibers

3T3 fibroblasts were seeded onto PNIPAAm/PCL fibers (n=3) at 120,000 cells/cm2. This cell density was selected to ensure that the absorbance for the colorimetric assay was in the linear range. 24 hours post-seeding, cells were rinsed and treated with the tetrazolium dye 3-(4,5-dimethylthiazol-2-yl)-5-(3-carboxymethoxyphenyl)-2-(4-sulfophenyl)-2H-tetrazolium (MTS, CellTiter 96® AQueous One Solution Cell Proliferation Assay, Promega, Madison, WI). Solution absorbance was measured at 490 nm on a Biotek Cytation 3 Cell Imaging Multi-Mode Reader. Each condition was normalized by solution absorbance of 3T3 fibroblast-seeded PCL-only controls to determine relative cell attachment.

2.3.3.3 Cell alignment on PNIPAAm/PCL fibers

3T3 fibroblasts were seeded onto PNIPAAm/PCL fibers at 240,000 cells/cm^2. 24 hours post- seeding, cells on PNIPAAm/PCL fibers were rinsed and fixed in 4% (v/v) paraformaldehyde for 15 minutes. Cells were permeabilized with 0.2% (v/v) Triton X-100 for 10 minutes and then stained with 6.6 μM rhodamine phalloidin (ThermoFisher). Following actin staining, cell nuclei were stained with 300 nM 4',6-diamidino-2-phenylindole (DAPI, ThermoFisher). All solutions were warmed to and fibers were incubated at 37°C, above PNIPAAm's LCST, as described previously[14]. Cell-seeded fibers were dissembled from CellCrown inserts, placed on slides, and imaged on a Biotek Cytation 3 Cell Imaging Multi-Mode Reader incubated to 37°C. Actin images were analyzed using NIH ImageJ software and the OrientationJ plug-in to determine cell alignment.

2.3.3.4 Cell sheet detachment from PNIPAAm/PCL fibers

3T3 fibroblasts were seeded onto PNIPAAm/PCL fibers at 630,000 cells/cm^2 and allowed to grow for 4 days. Medium was changed every day. Prior to detachment, cell were stained with 5 μM calcein, AM (ThermoFisher) and nuclear stain Hoescht 33342 (ThermoFisher) for 30 minutes. Detachment was initiated by rinsing 5 times over 10-15 minutes with cold (approximately 4°C) medium to dissolve and remove PNIPAAm. Cell sheets were rinsed from the CellCrown insert with additional medium and imaged on an Olympus IX83 fluorescent microscope.

2.3.4 Statistical Methods

All data are presented as mean ± standard deviation. Statistical significance was calculated by performing one-way ANOVA analysis followed by Tukey's multiple comparison in GraphPad, Prism Software. Differences are considered significant for $p < 0.05$.

2.4 Results and Discussion

2.4.1 Characterization of PNIPAAm/PCL fibers

To generate PNIPAAm/PCL co-fibers, a solvent combination—methanol and chloroform—that dissolves both PNIPAAm and PCL was identified by referring to previous reports on PCL solubility in electrospinning solvents[29]. SEM imaging confirmed fiber formation (Figure 2.1A). Electrospinning PCL-only and PNIPAAm-only fibers in methanol and chloroform was attempted; however, fiber formation and alignment was poor compared to the PNIPAAm/PCL blended fibers. Consequently, PCL-only and PNIPAAm-only fibers were electrospun using HFP and methanol, respectively, following previous reports[22,30]. Interestingly, only the 100% PNIPAAm fibers exhibited a flat, ribbon-like

morphology, as was previously reported for PNIPAAm fibers electrospun by Rockwood et al.[19] Average fiber diameters ranged from 1 to 3 μm, with PCL-only fibers being the smallest diameter and PNIPAAm-only fibers having the largest diameter (Figure 2.1B). Orientation analysis confirmed fiber alignment, with all conditions having an orientation index greater than 0.65, with 0% and 25% PNIPAAm fibers having significantly greater orientation indices than fibers containing 50% or more PNIPAAm (Figure 2.1C). Differences in diameter and fiber orientation between PCL-only, PNIPAAm-only, and the PNIPAAm/PCL fibers may be attributable to the solvent of choice, which affects solution viscosity—a parameter known to largely determine fiber diameter[31]. Furthermore, the solution viscosity is also influenced by the relative amounts of PNIPAAm and PCL, as their respective molecular weights, effective chain lengths, and solubility in methanol and chloroform differ. We observed that higher PCL-content fibers could be electrospun from solutions for which the combined polymer concentration of the solution was lower (Appendix Table A1). For example, 90% PNIPAAm fibers were electrospun from a solution of 18% (wt/v) of 9:1 PNIPAAm:PCL whereas 25% PNIPAAm fibers were electrospun from a solution of 12% (wt/v) of 1:3 PNIPAAm:PCL.

FTIR spectroscopy confirmed that relative polymer compositions of PNIPAAm/PCL fibers followed the starting PNIPAAm concentration (Figure 2.2), as PCL-specific peaks increased with PCL-content and PNIPAAm-specific peaks increased with PNIPAAm content. The PCL-only (0% PNIPAAm) fibers show a strong peak at 1727 cm^{-1} indicating carbonyl stretching, which is reduced as PNIPAAm content increases and is absent for the 100% PNIPAAm fibers. Similarly, PNIPAAm-only fibers (100% PNIPAAm) show strong peaks at 1626 and 1559 cm^{-1} for amide group vibrations that become less strong as PNIPAAm content decreases and are completely absent for the 0%

PNIPAAm fibers. Additional absorbance peaks for each polymer are listed in Table 2.1[32,33,34].

To further confirm relative PNIPAAm content and evaluate the potential of PNIPAAm/PCL fibers for cell sheet detachment via PNIPAAm dissolution, we immersed PNIPAAm/PCL fibers in room temperature (approximately 20°C) water to dissolve out PNIPAAm (Figure 2.3). Fibers with a considerable amount of PCL showed little mass loss (less than 5% the original weight) whereas high-content PNIPAAm fibers lost more than 50% their original mass (Figure 2.3A). Observations of PNIPAAm/PCL fiber area and axial length changes before and after wetting supported the mass loss data: high PNIPAAm-content fiber area contracted more than 55% whereas high PCL-content fibers did not contract but instead slightly swelled (Figure 2.3B). Furthermore, 75% and 90% PNIPAAm fiber contraction was uniaxial, perpendicular to fiber orientation (Figure 2.3C, Appendix Figure A.2). As expected, 100% PNIPAAm fibers completely dissolved, preventing measurements of mass loss and changes in area and axes length. For high PCL-content fibers, the percent mass lost does not match the starting percent PNIPAAm content, indicating that the PCL protects PNIPAAm from dissolving.

Relative hydrophobicity of the PNIPAAm/PCL fibers was determined by measuring advancing water contact angle above 32°C, showing that dry and wetted 100% PNIPAAm fibers (θ_{adv} = 88.0° and 55.3°, respectively) were significantly less hydrophobic than 0% PNIPAAm fibers (θ_{adv} = 120.7° and 107.1°, Figure 2.4 and Appendix Figure A.3). In fact, all dry, high PCL-content fibers (0%, 25%, 50% PNIPAAm) were significantly more hydrophobic than 100% PNIPAAm fibers with θ_{adv} > 120°. Because PNIPAAm undergoes a coil-to-globule transition at its LCST, it does not become truly hydrophobic above its LCST; rather, the hydrophobic domains are exposed to the aqueous solution, enabling protein adsorption[11]. Evaluations of relatively thick and thin layers of PNIPAAm-

grafted surfaces found that θadv decreased with thickness, meaning thicker PNIPAAm surfaces were less hydrophobic[13]. Because biomaterial hydrophobicity is an indicator of the degree of protein adsorption, low hydrophobicity may impair cell attachment and spreading.

The mass loss, area contraction, and advancing water contact angle data are largely consistent in that the high PCL-content fibers behave similarly and that significant differences are observed for high PNIPAAm-content fibers. Significant mass loss and area contraction from PNIPAAm dissolution starts to occur with 75% PNIPAAm. A possible explanation for these data is that the PNIPAAm/PCL fibers may have a core-sheath architecture, with a PNIPAAm core and PCL sheath. This has been previously observed for PNIPAAm and PCL blended fibers electrospun in dimethylformamide (DMF) and chloroform, although with a PNIPAAm sheath around a PCL core[35]. The authors proposed a thermodynamic argument: because DMF was a better solvent for PNIPAAm than for PCL and because DMF had a much lower boiling point than chloroform, the DMF evaporated first, leaving PNIPAAm on the exterior. In our case, methanol's boiling point (64.7°C) is slightly higher than chloroform's boiling point (61.2°C), and methanol is a good solvent for PNIPAAm but a bad solvent for PCL. Applying the same thermodynamic argument, the PCL should be dissolved in the chloroform portion, which would evaporate first to leaving PCL on the exterior of the fibers. For high PCL-content fibers, the PCL may form an entire sheath around the PNIPAAm; however, as PNIPAAm content increases, there would not be enough PCL to protect PNIPAAm from dissolution, as observed by the mass loss and contact angle data.

2.4.2 Cell viability and alignment on PNIPAAm/PCL fibers

After confirming the relative PNIPAAm content, we assessed the behavior of NIH 3T3 fibroblasts on PNIPAAm/PCL fibers. Given PNIPAAm's relative low hydrophobicity as indicated by advancing water contact angle, we coated PNIPAAm/PCL fibers with a 1:50 GFR-Matrigel dilution and pre-treated fibers with FBS prior to seeding, as recommended by Haraguich et al. [28]; other groups have combined PNIPAAm with gelatin[23], chitosan[36], fibronectin[14,37], collagen[38], poly-L-lysine, and laminin[39] to improve cell adhesion.

MTS assay 24-hours post-seeding demonstrated that cells attached and were viable on PNIPAAm/PCL fibers as compared to the PCL-only (0% PNIPAAm) control (Figure 2.5). However, cells were significantly less viable (60% relative to PCL-only control) on 100% PNIPAAm fibers. To visualize cytoskeletal actin, cells were stained with rhodamine phalloidin 24-hours post-seeding on PNIPAAm/PCL fibers. Fibers containing PCL (0%, 25%, 50%, 75%, and 90% PNIPAAm) showed robust spreading and significant cell alignment in a preferred direction (Figure 2.4B,C). On 100% PNIPAAm fibers, cells showed notably less spreading and grew in clusters, which is in line with the relatively poor cell viability observed on these fibers. As PNIPAAm is clearly not toxic to cells, as indicted by comparable cell viability on 0%, 25%, 50%, 75%, and 90% PNIPAAm fibers, it is likely that cell attachment was affected by poor adhesion protein adsorption due to its decreased hydrophobicity. This is consistent with our advancing water contact results and previous reports that protein adsorption onto PNIPAAm, especially thick PNIPAAm films (> 15-20 nm), is severely limited[37,39]. Understandably, coating with cell adhesion proteins[28] and grafting gelatin to PNIPAAm[23] has been used to improve cell attachment to and spreading on PNIPAAm surfaces. Representative histograms of cell angle show that cells had relatively high alignment on high-content PCL fibers (Appendix Figure A.4). Although

less aligned, cells on 75% and 90% PNIPAAm fibers had a preferred angle to which the cells aligned. The actin ridges that appeared on 75% and 90% PNIPAAm fibers is likely due to PNIPAAm contracture as the fibers had to be removed from the CellCrown inserts for imaging. This phenomenon affected the orientation analysis as these ridges, which are perpendicular to cell orientation angle, dampened the preferred cell angle peak.

2.4.3 Cell sheet detachment

We attempted detachment of aligned fibroblast cell sheets by incubating cell-seeded PNIPAAm/PCL fibers in cold medium. Following previous reports on cell sheeting[14,28], we seeded cells at an ultra-high density—630,000 cells/cm^2—to ensure sufficient cell-cell adhesion and ECM deposition. Detachment was initiated by rinsing cell-seeded PNIPAAm/PCL fibers with cold medium to dissolve the PNIPAAm. Cell sheet detachment from PNIPAAm/PCL fibers was only successful for 90% PNIPAAm fibers (Figure 2.6A), which occurred rapidly (less than 15 minutes). For lower PNIPAAm-content fibers, too much PCL remained preventing cell detachment. Cell sheet detachment from 100% PNIPAAm fibers was unsuccessful because the cells did not form a complete monolayer, as indicated by our cell morphology data (Figure 2.5B). Cell sheets exhibited slight curling at the edges, evidenced by the thickening around the edges. Calcein staining confirmed that cell sheets were viable, intact, and consisted of aligned cells (Figure 2.6B,C). Compared to previous reports of anisotropic cell sheeting from anisotropic PNIPAAm surfaces[14,23], relatively little contraction of the cell sheet was observed. This may be due to the presence of residual PCL, which can be observed in phase contrast images of the cell sheets (Figure 2.6D,E).

Our data demonstrate that electrospun PNIPAAm/PCL fibers can be used to culture aligned cells but only 90% PNIPAAm fibers can be used for cell detachment. This follows

our original hypothesis that PNIPAAm and PCL have complementary roles and must be present in sufficient amounts. PCL encourages cell attachment, but too much PCL precludes cell sheet detachment. Likewise, PNIPAAm's low hydrophobicity limits cell attachment but is necessary for cell sheet detachment. The cell sheets generated by our method did show some contraction, which is unfavorable for cell sheet stacking. Gelatin hydrogel plungers have been previously used to prevent cell sheet contracture and could easily be used in conjunction with our PNIPAAm/PCL fibers[28]. We used 3T3 fibroblasts as a proof of principle to demonstrate that PNIPAAm/PCL fibers can generate cell sheets. Our system can be used with other cell types to possibly generate more complex tissue structures, such as blood vessels with better cellular architecture of the tunica media. Thus, electrospun PNIPAAm/PCL fibers, which are simple and relatively inexpensive to produce, have the potential to be used to generate anisotropic cell sheets that can either enable analyses that are typically precluded by the use of plates or biomaterial scaffolds or be used to create tissue-like constructs for in vivo transplantation[40,41].

2.5 CONCLUSIONS

Here, we developed a simple, inexpensive, and low-resource system to generate cell sheets. PNIPAAm and PCL were successfully electrospun to generate aligned PNIPAAm/PCL blended fibers on which 3T3 fibroblasts could be cultured. Cell viability and cell alignment was observed on PCL and PNIPAAm/PCL fibers whereas cell viability and cell alignment was impaired on 100% PNIPAAm fibers. Detachment of viable cell sheets by incubation with room temperature medium was successful for 90% PNIPAAm fibers; cell sheets did not detach from fibers containing less PNIPAAm and cells did not form a contiguous monolayer on 100% PNIPAAm. In summary, our findings demonstrate

that anisotropic cell sheets can be generated simply using electrospun PNIPAAm/PCL fibers—without chemical synthesis or resource-intensive techniques.

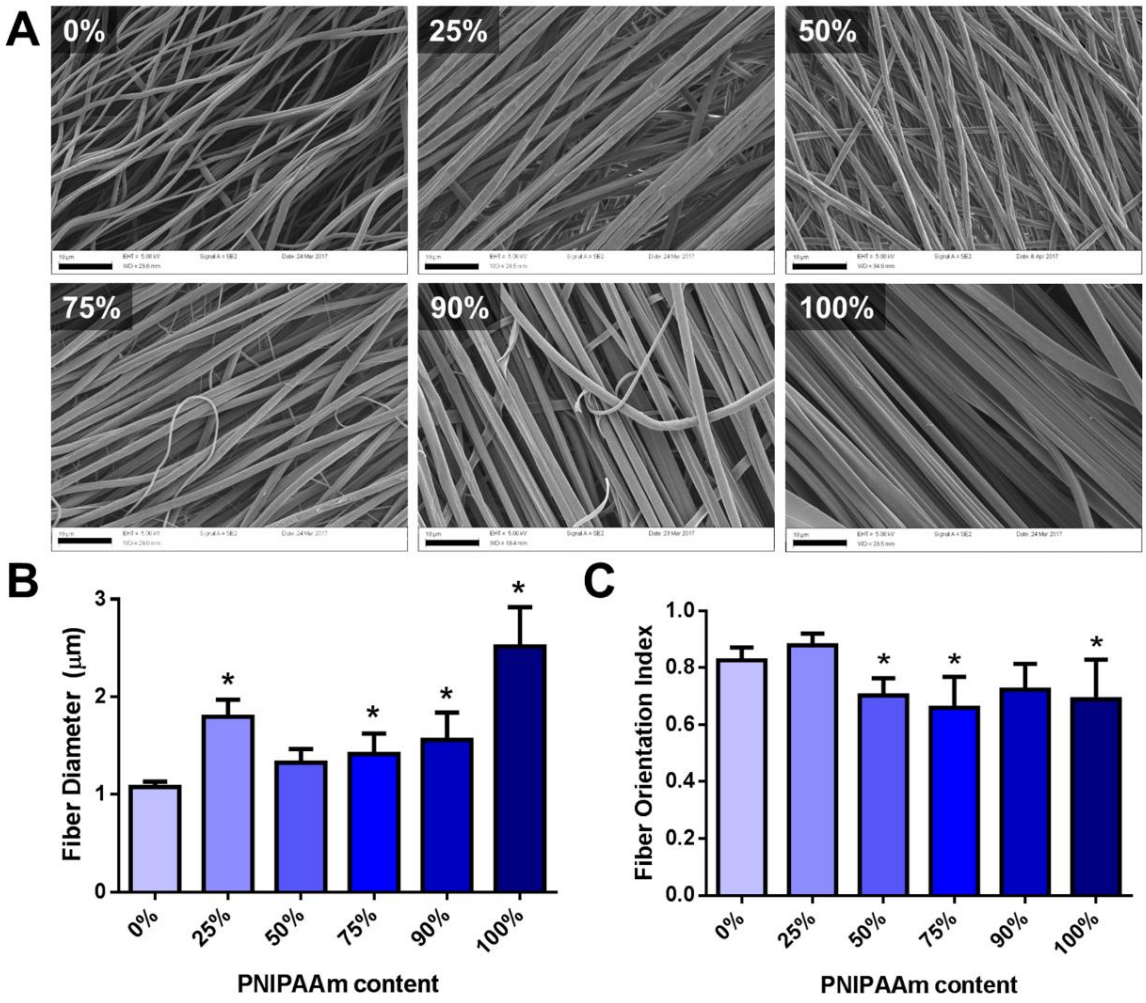

Figure 2.1 Electrospun PNIPAAm/PCL fibers. A) SEM images of electrospun PNIPAAm/PCL fibers. Percentage in upper left indicates PNIPAAm content. Scalebars (black bars, bottom left) are 10 μm. B) Average fiber diameter determined using DiameterJ. C) Fiber orientation index determined using OrientationJ. *$p<0.05$ compared to 0% PNIPAAm fibers.

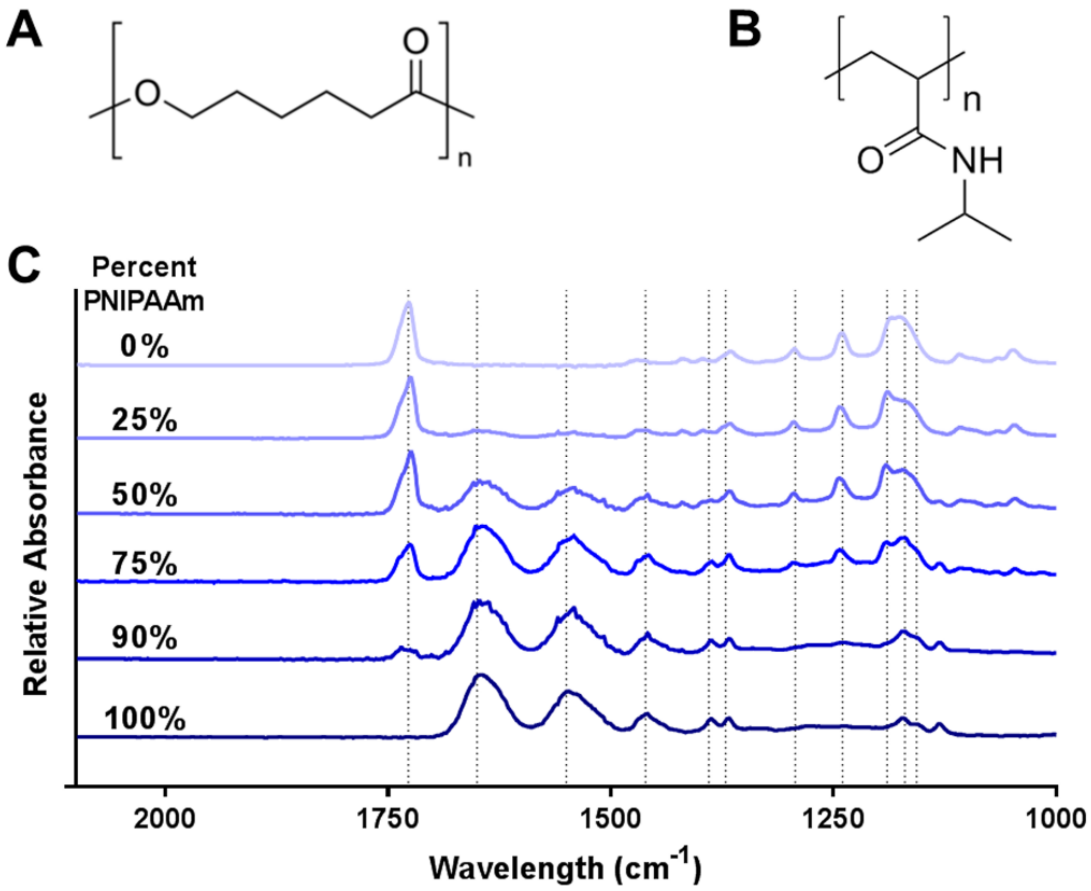

Figure 2.2 Chemical structures of (A) PCL and (B) PNIPAAm. C) FTIR spectra of PNIPAAm/PCL fibers. Dashed lines indicate absorption peaks.

Position (cm-1)	Polymer	Assignment
1727	PCL	Carbonyl Stretching
1626	PNIPAAm	Amide I
1559	PNIPAAm	Amide II
1462	PNIPAAm	CH3 asymmetrical deformation
1390, 1371	PNIPAAm	CH3 symmetrical deformation
1293	PCL	C-C, C-O stretching
1240	PCL	C-O-C asymmetric stretching
1190	PCL	OC-O stretching
1170	PCL	COC symmetric stretching
1157	PCL	C-O, C-C stretching

Table 2.1 Absorption peaks and assignments for PNIPAAm and PCL.

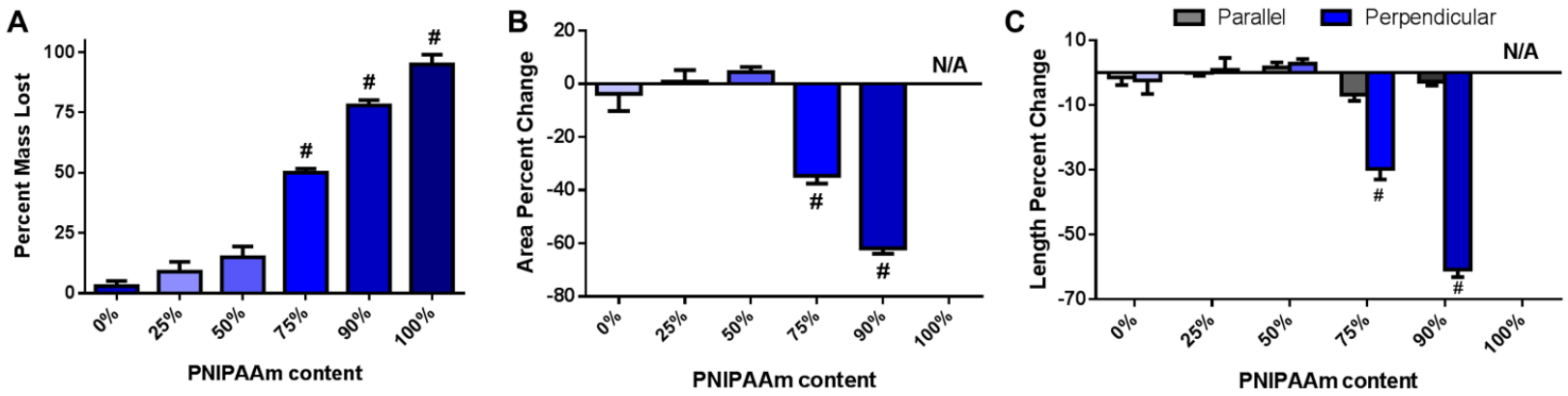

Figure 2.3 PNIPAAm dissolution from PNIPAAm/PCL fibers. A) PNIPAAm/PCL mass loss in water. PNIPAAm/PCL fiber (B) area percent change and (C) axes (relative to fiber direction) length percent change following PNIPAAm dissolution. # $p<0.05$ compared to all other groups.

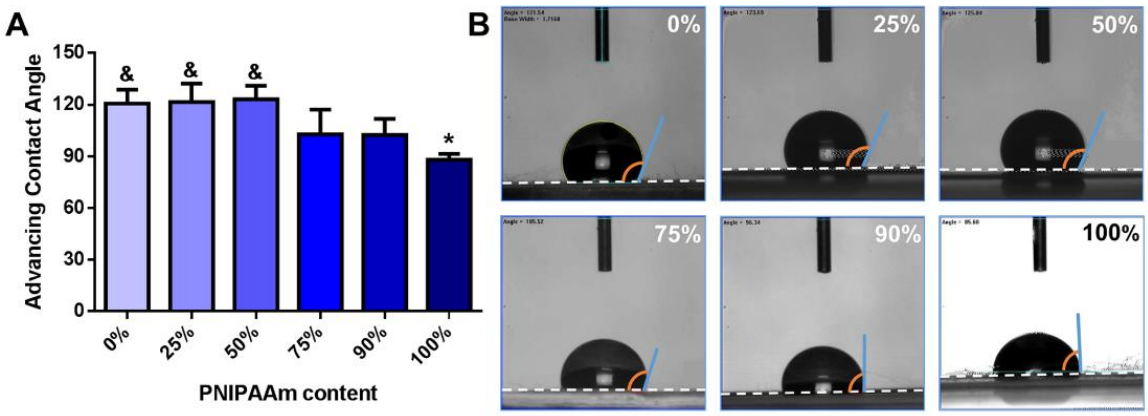

Figure 2.4 A) Advancing water contact angle on PNIPAAm/PCL fibers. B) Representative images of water droplet on fibers. White dashed lines indicate fiber edge. * $p<0.05$ compared to 0% PNIPAAm fibers. &$p<0.05$ compared to 100% PNIPAAm fibers.

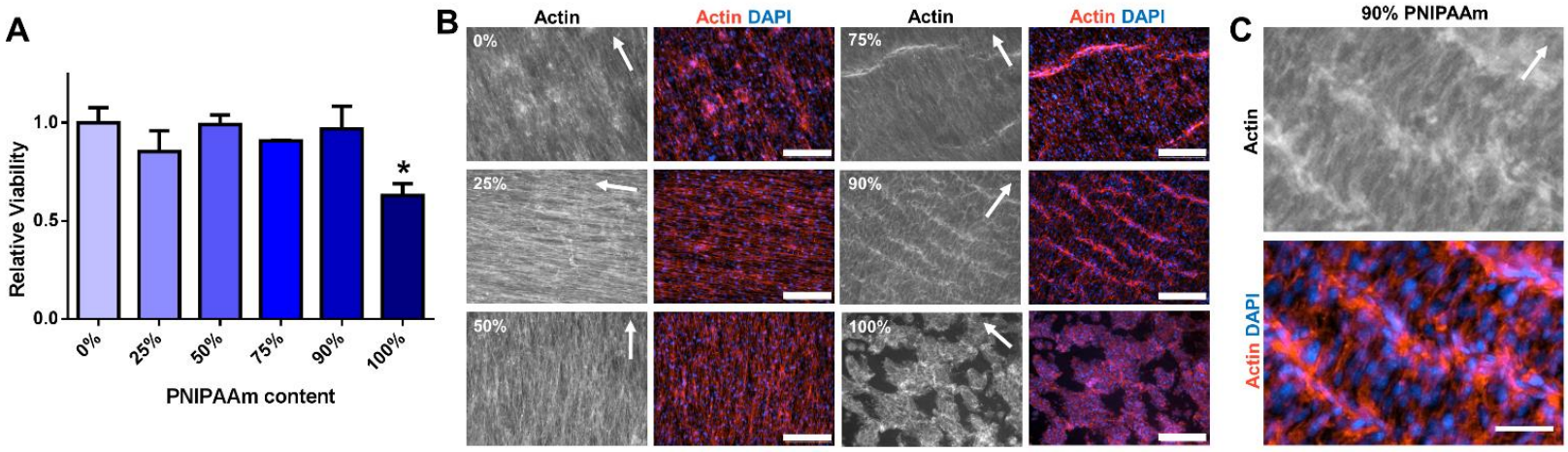

Figure 2.5 Cell viability and cell alignment on PNIPAAm/PCL fibers. A) Cell viability relative to 0% PNIPAAm fibers determined by MTS assay. .*$p<0.05$ compared to 0% PNIPAAm fibers. B) Representative images of fibroblasts seeded on PNIPAAm/PCL fibers with actin (left) and actin/DAPI overlays (right). Scalebars are 200 μm. C) Insets from 90% PNIPAAm images, as indicated by white dashed-box in (B). Scalebar is 50 μm.

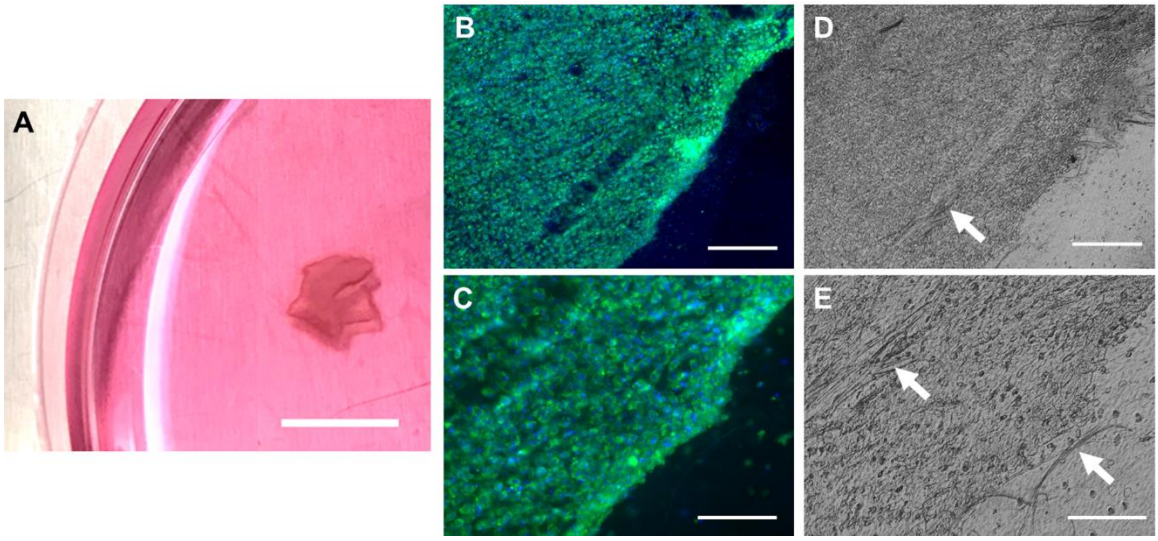

Figure 2.6 Cell sheet detachment. A) Cell sheets detached from 90% PNIPAAm fibers using room temperature medium; Scalebar is 1 cm. B,C) Cell sheet viability was confirmed with calcein, AM live-staining. D,E) Corresponding phase contrast images of (B,C); white arrows indicate residual PCL. Scalebars are (B,D) 400 μm and (C,E) 200 μm.

2.6 REFERENCES

1. Kim, D.-H., Provenzano, P. P., Smith, C. L. & Levchenko, A. Matrix nanotopography as a regulator of cell function. *J Cell Biol* **197,** 351–360 (2012).
2. Lim, S. H., Liu, X. Y., Song, H., Yarema, K. J. & Mao, H.-Q. The effect of nanofiber-guided cell alignment on the preferential differentiation of neural stem cells. *Biomaterials* **31,** 9031–9039 (2010).
3. Levorson, E. J. *et al.* Fabrication and characterization of multiscale electrospun scaffolds for cartilage regeneration. *Biomed Mater* **8,** 014103 (2013).
4. Falconnet, D., Csucs, G., Michelle Grandin, H. & Textor, M. Surface engineering approaches to micropattern surfaces for cell-based assays. *Biomaterials* **27,** 3044–3063 (2006).
5. Doshi, J. & Reneker, D. H. Electrospinning process and applications of electrospun fibers. in *, Conference Record of the 1993 IEEE Industry Applications Society Annual Meeting, 1993* 1698–1703 vol.3 (1993). doi:10.1109/IAS.1993.299067
6. Pham, Q. P., Sharma, U. & Mikos, A. G. Electrospinning of Polymeric Nanofibers for Tissue Engineering Applications: A Review. *Tissue Engineering* **12,** 1197–1211 (2006).
7. Kai, D. *et al.* Stem cell-loaded nanofibrous patch promotes the regeneration of infarcted myocardium with functional improvement in rat model. *Acta Biomaterialia* **10,** 2727–2738 (2014).
8. Wang, T.-Y., Forsythe, J. S., Nisbet, D. R. & Parish, C. L. Promoting engraftment of transplanted neural stem cells/progenitors using biofunctionalised electrospun scaffolds. *Biomaterials* **33,** 9188–9197 (2012).
9. Anderson, J. M. *et al. Biomaterials Science: an Introduction to Materials in Medicine, Host reactions to biomaterials and their evaluation.* (Academic Press, 1996).
10. Yamada, N. *et al.* Thermo-responsive polymeric surfaces; control of attachment and detachment of cultured cells. *Makromol. Chem., Rapid Commun.* **11,** 571–576 (1990).
11. Pelton, R. Poly(N-isopropylacrylamide) (PNIPAM) is never hydrophobic. *Journal of Colloid and Interface Science* **348,** 673–674 (2010).
12. Yang, J. *et al.* Cell sheet engineering: Recreating tissues without biodegradable scaffolds. *Biomaterials* **26,** 6415–6422 (2005).
13. Yamato, M. *et al.* Temperature-responsive cell culture surfaces for regenerative medicine with cell sheet engineering. *Progress in Polymer Science* **32,** 1123–1133 (2007).

14. Takahashi, H., Nakayama, M., Shimizu, T., Yamato, M. & Okano, T. Anisotropic cell sheets for constructing three-dimensional tissue with well-organized cell orientation. *Biomaterials* **32,** 8830–8838 (2011).

15. Takahashi, H., Nakayama, M., Itoga, K., Yamato, M. & Okano, T. Micropatterned Thermoresponsive Polymer Brush Surfaces for Fabricating Cell Sheets with Well-Controlled Orientational Structures. *Biomacromolecules* **12,** 1414–1418 (2011).

16. Chen, Y. *et al.* Three-dimensional poly-(ε-caprolactone) nanofibrous scaffolds directly promote the cardiomyocyte differentiation of murine-induced pluripotent stem cells through Wnt/β-catenin signaling. *BMC Cell Biology* **16,** 22 (2015).

17. Cipitria, A., Skelton, A., R. Dargaville, T., D. Dalton, P. & W. Hutmacher, D. Design, fabrication and characterization of PCL electrospun scaffolds—a review. *Journal of Materials Chemistry* **21,** 9419–9453 (2011).

18. Croisier, F. *et al.* Mechanical testing of electrospun PCL fibers. *Acta Biomaterialia* **8,** 218–224 (2012).

19. Rockwood, D. N., Chase, D. B., Akins Jr., R. E. & Rabolt, J. F. Characterization of electrospun poly(N-isopropyl acrylamide) fibers. *Polymer* **49,** 4025–4032 (2008).

20. Tran, T. *et al.* Controllable and switchable drug delivery of ibuprofen from temperature responsive composite nanofibers. *Nano Convergence* **2,** 15 (2015).

21. Yu, H., Jia, Y., Chen, G. & Zhang, Y. Fabrication of core/sheath PCL/PEG–PNIPAAm fibers as thermosensitive release carriers by a new technique combining blend electrospinning and ultraviolet-induced graft polymerization. *Materials Letters* **164,** 505–508 (2016).

22. Lee, J. B. *et al.* Development of 3D Microvascular Networks Within Gelatin Hydrogels Using Thermoresponsive Sacrificial Microfibers. *Adv. Healthcare Mater.* **5,** 781–785 (2016).

23. Zhao, X., Wang, L., Wang, P., Yang, Y. & Wang, F. Fabrication of Thermoresponsive Nanofibers for Cell Sorting and Aligned Cell Sheet Engineering. *J Nanosci Nanotechnol* **16,** 5520–5527 (2016).

24. Rezakhaniha, R. *et al.* Experimental investigation of collagen waviness and orientation in the arterial adventitia using confocal laser scanning microscopy. *Biomech Model Mechanobiol* **11,** 461–473 (2012).

25. Püspöki, Z., Storath, M., Sage, D. & Unser, M. Transforms and Operators for Directional Bioimage Analysis: A Survey. *Adv Anat Embryol Cell Biol* **219,** 69–93 (2016).

26. Hotaling, N. A., Bharti, K., Kriel, H. & Simon Jr., C. G. DiameterJ: A validated open source nanofiber diameter measurement tool. *Biomaterials* **61,** 327–338 (2015).

27. Ferdman, A. G. & Yannas, I. V. Scattering of Light from Histologic Sections: A New Method for the Analysis of Connective Tissue. *J Investig Dermatol* **100,** 710–716 (1993).

28. Haraguchi, Y. *et al.* Fabrication of functional three-dimensional tissues by stacking cell sheets in vitro. *Nature Protocols* **7,** 850–858 (2012).

29. Bordes, C. *et al.* Determination of poly(ε-caprolactone) solubility parameters: Application to solvent substitution in a microencapsulation process. *International Journal of Pharmaceutics* **383,** 236–243 (2010).

30. Nam, J., Huang, Y., Agarwal, S. & Lannutti, J. Materials selection and residual solvent retention in biodegradable electrospun fibers. *J. Appl. Polym. Sci.* **107,** 1547–1554 (2008).

31. Thompson, C. J., Chase, G. G., Yarin, A. L. & Reneker, D. H. Effects of parameters on nanofiber diameter determined from electrospinning model. *Polymer* **48,** 6913–6922 (2007).

32. A. Beattie, D., Addai-Mensah, J., Beaussart, A., V. Franks, G. & Yeap, K.-Y. In situ particle film ATR FTIR spectroscopy of poly (N -isopropyl acrylamide) (PNIPAM) adsorption onto talc. *Physical Chemistry Chemical Physics* **16,** 25143–25151 (2014).

33. Elzein, T., Nasser-Eddine, M., Delaite, C., Bistac, S. & Dumas, P. FTIR study of polycaprolactone chain organization at interfaces. *Journal of Colloid and Interface Science* **273,** 381–387 (2004).

34. Dybal, J., Trchová, M. & Schmidt, P. The role of water in structural changes of poly(N-isopropylacrylamide) and poly(N-isopropylmethacrylamide) studied by FTIR, Raman spectroscopy and quantum chemical calculations. *Vibrational Spectroscopy* **51,** 44–51 (2009).

35. Chen, M. *et al.* Thermo-Responsive Core−Sheath Electrospun Nanofibers from Poly (N-isopropylacrylamide)/Polycaprolactone Blends. *Chem. Mater.* **22,** 4214–4221 (2010).

36. Wang, J., Chen, L., Zhao, Y., Guo, G. & Zhang, R. Cell adhesion and accelerated detachment on the surface of temperature-sensitive chitosan and poly(N-isopropylacrylamide) hydrogels. *J Mater Sci: Mater Med* **20,** 583–590 (2009).

37. Akiyama, Y., Kikuchi, A., Yamato, M. & Okano, T. Ultrathin poly(N-isopropylacrylamide) grafted layer on polystyrene surfaces for cell adhesion/detachment control. *Langmuir* **20,** 5506–5511 (2004).

38. Moran, M. T., Carroll, W. M., Selezneva, I., Gorelov, A. & Rochev, Y. Cell growth and detachment from protein-coated PNIPAAm-based copolymers. *J. Biomed. Mater. Res.* **81A,** 870–876 (2007).

39. Moran, M. T., Carroll, W. M., Gorelov, A. & Rochev, Y. Intact endothelial cell sheet harvesting from thermoresponsive surfaces coated with cell adhesion promoters. *J R Soc Interface* **4,** 1151–1157 (2007).

40. Shimizu, T. *et al.* Fabrication of pulsatile cardiac tissue grafts using a novel 3-dimensional cell sheet manipulation technique and temperature-responsive cell culture surfaces. *Circ. Res.* **90,** e40 (2002).

41. Yang, J. *et al.* Reconstruction of functional tissues with cell sheet engineering. *Biomaterials* **28,** 5033–5043 (2007).

Chapter 3: Sensitivity of Differentiating Cardiomyocytes to Substrate Anisotropy

3.0 Foreword

This chapter is based on a manuscript that is in preparation. It describes the use of electrospinning to create a set of fiber substrates that includes intermediary anisotropies to study whether differentiating cardiomyocytes respond substrate anisotropy in a gradient-based or threshold-based manner. My contribution was in the design, execution, and analysis of the experimental work as well as the writing of the manuscript. The second author, Elissa Barone, an undergraduate research assistant, helped perform the experimental work. Chengyi Tu, a graduate student in the Zoldan Lab, performed mRNA isolation, reverse transcription, and qPCR. Dr. Janet Zoldan conceptualized the research and aided in experimental design.

3.1 Introduction

Over 11% of Americans have been diagnosed with heart disease[1]. This high prevalence can be partially attributed to the heart's limited regenerative capacity. When cardiac muscle tissue is acutely damaged, as in the case of myocardial infarction, the heart cannot sufficiently replace the lost cardiomyocytes[2]. Treatment for myocardial infarction alleviates symptoms but does not repair or replace the lost myocardial tissue. Over time, scarring and tissue maladaptation, like thinning of the ventricular wall, occur and further impair cardiac output[3,4]. Considerable research in the past two to three decades has focused on generating transplantable cardiac muscle tissue that can replace lost cardiomyocytes to improve overall cardiac function. Work towards engineering cardiac tissues first made major advancements in biomaterial design[5], with clear evidence that biomaterial features

can drive cellular organization to improve function of adult[6,7] and neonatal cardiomyocytes[8,9].

Advancements using pluripotent stem cells (PSCs), particularly the seminal discovery of induced pluripotency[10], created a viable human, possibly even patient-specific, source of cardiomyocytes for engineered cardiac tissues. Cardiomyocytes can now be reliably derived using chemically defined protocols[11,12]. Despite progress in differentiation, PSC-derived cardiomyocyte function, as defined by factors like morphology, contractile force, and electrophysiology, is considerably underdeveloped compared to adult cardiomyocytes and remains a hurdle to translation[13–15].

Much work has been dedicated to improving PSC-derived cardiomyocyte function, including a strong focus on biophysical stimuli[16,17]. To drive PSC-derived cardiomyocyte maturation, features like static and cyclic mechanical stretching[18,19], electrical field stimulation[20,21], material stiffness[22], and topographical or geometric features[23,24] have been incorporated into biomaterial systems. Cardiomyocytes have a clear structure-function relationship, and materials that promote an elongated cell shape and overall cardiomyocyte alignment have been successful in improving electrical and mechanical function[16]. In single cell studies, the elongated shape of PSC-derived cardiomyocytes improved myofibril alignment and force production[22]. Materials with anisotropic features, such as grooves and ridges[25,26], patterned adhesion sites[13], geometric boundary conditions[23], and aligned electrospun fibers[27–29], have been used to align PSC-derived cardiomyocytes. Myofibril alignment, however, has been observed on isotropic substrates, leading to claims that cardiomyocytes can self-align[30]. Although there are numerous studies evaluating how cardiomyocyte respond to highly anisotropic materials relative to isotropic materials, how cardiomyocytes respond to substrates with intermediary degrees of anisotropy is lacking.

The goal of this study was to assess how differentiating cardiomyocytes respond to degrees of substrate anisotropy. We predicted that cardiomyocyte alignment would depend on substrate anisotropy in a gradient-based manner, meaning that the degree of cardiomyocyte alignment would increase with the degree of substrate anisotropy, rather than in a threshold-based manner, in which a minimum threshold alignment would result in overall cardiomyocyte alignment. To test this hypothesis, we used electrospinning to control the degree of fiber alignment and thereby create a set of substrates including non-aligned, semi-aligned, and aligned fibers. Mouse embryonic stem cells (mESCs) were differentiated on these fibers for 20 days, we sought to assess structural and functional changes over time.

3.2 Materials and Methods

3.2.1 Fabrication of Electrospun Fibers

Poly(caprolactone) (PCL, 80,000 Da, Sigma-Aldrich) was dissolved 10% wt/vol in hexafluoroisopropanol (Sigma-Aldrich) with continuous stirring until homogeneous. Solutions were dispensed from a 25-gauge blunted stainless steel needle at 2 mL/hr using a syringe pump (New Era Pump Systems, Inc.). A high voltage supply (Gamma High Voltage) was used to apply a charge of 5-10 kV to the solution at the needle, which was 11 cm from the collector. Electropsun fibers were collected on a grounded copper plate or a grounded rotating aluminum drum. To vary the degree of fiber alignment, the rotational speed of the aluminum collector was varied from 500 to 3000 revolutions per minute (RPM, approximately 2-14 m/s) at 500 RPM increments.

3.2.2 Fiber Orientation and Diameter

Fiber orientation and diameter were determined as described previously[31]. Electrospun PCL fibers were sputter coated with 12 nm platinum/palladium and imaged using a Zeiss Supra 40VP scanning electron microscope (SEM, 5 kV). Images were analyzed in NIH ImageJ using the OrientationJ[32,33] and DiameterJ[34] plug-ins to measure fiber orientation and diameter, respectively. The fiber orientation index was calculated from the fiber orientation distribution using the following equation: $S = 2 < cos^2(\alpha) > -1$ where α is the angular difference between an individual fiber and the mean direction of all fibers[35]. The orientation index is 0 for perfectly random fibers and 1 for perfectly aligned fibers. At least three SEM images per sample and three independent samples were analyzed.

3.2.3 Pluripotent Stem Cells

All cell studies were performed with mESCs, a gift from Dr. Joshua Brickman of the University of Copenhagen. mESCs were maintained in serum-free N2B27 2i medium containing 1:1 DMEM/F-12 and Neurobasal mediums (Thermo Fisher), serum-free B-27 (Thermo Fisher), N-2 (Thermo Fisher), L-Glutamine (Glutamax, Thermo Fisher), leukemia inhibition factor (LIF, also a gift from Dr. Brickman), and 0.005% bovine serum albumin (BSA, Invitrogen), 3 μM CHIR99201 (Tocris), 1 μM PD0325901 (LC Laboratories), and 100 μM beta-mercaptoethanol (Sigma-Aldrich). Cells were passaged approximately every three days by dissociation with StemPro Accutase (Thermo Fisher) and seeded on plates coated with stem cell-grade 0.1% gelatin (Sigma-Aldrich).

3.2.4 Cell Seeding and Cardiac Differentiation

For cell seeding, fibers were cut into approximately 5 mm x 5 mm squares. Fibers were sterilized in 70% ethanol, rinsed twice in Dulbecco's Phosphate Buffered Saline

(DPBS, Thermo Fisher), and coated with 0.1% gelatin. mESCs were dissociated using StemPro Accutase, re-suspended in N2B27 growth medium with 0.2% dimethyl sulfoxide (DMSO) and without inhibitors, and seeded in 50-uL droplets of 15,000-30,0000 cells onto each PCL fiber square.

Monolayer directed differentiation was performed as described by Kokkinopoulos et al. with slight modification (Figure 2A)[36]. Differentiation by removal of LIF was initiated 5-6 hours after seeding by replacing the seeding medium with expansion medium containing 3:1 IMDM and Ham's F12 Nutrient Mix mediums (Thermo Fisher), L-Glutamine, serum-free B-27, N-2, 0.05% BSA, ascorbic acid (Sigma-Aldrich), and 4.5×10^{-4} M 1-thioglycerol (Sigma-Aldrich). After 24 hours, the expansion medium was replaced, and the following growth factors were added: 5 ng/mL Activin A, 0.5 ng/mL BMP4, and 5 ng/mL VEGF. After 48 additional hours (72 hours after LIF removal) and every 3 days thereafter, the medium was replaced with StemPro-34 (Thermo Fisher) supplemented with 5 ng/mL VEGF, 10 ng/mL bFGF, 50 ng/mL FGF10, L-glutamine, and ascorbic acid. All growth factors were obtained from RnD Systems.

3.2.5 Immunostaining

Cells on fibers were fixed with 4% paraformaldehyde (Polysciences), rinsed with 300 mM glycine (Sigma-Aldrich), and permeabilized with 0.2% TritonX-100 (Amresco). Cells were then incubated in blocking buffer containing 1% BSA and 0.1% Tween-20 (Fisher Scientific) for 30 minutes. Cells were incubated with mouse anti-cardiac troponin T (cTnT, Abcam) diluted 1:500 in blocking buffer overnight at 4ºC. The following day, cells were rinsed with blocking buffer and then incubated with secondary antibody goat anti-mouse Alexa-488 (Abcam) at room temperature for 60 minutes. Cells were co-stained with rhodamine-phalloidin (Thermo Fisher) and 4',6-Diamidine-2'-phenylindole

dihydrochloride (DAPI, Thermo Fisher). Stained cells were imaged on a Zeiss Apotome.2 fluorescent microscope.

3.2.6 Quantitative Reverse Transcription-Polymerase Chain Reaction (RT-qPCR)

At day 14 of differentiation, total mRNA from was isolated using RNeasy Mini Kit (QIAGEN) and then reverse transcribed using the High-Capacity cDNA Reverse Transcription Kit (Thermo Fisher) according to manufacturer instructions. RT-qPCR was performed with PowerUp SYBR green (Thermo Fisher) using the StepOne Plus system (Applied Biosystems). 25 ng of cDNA and 500 nM primers were used for each reaction. Three fiber squares were combined for mRNA isolation. Three independent biological samples with at least three technical replicates were analyzed.

Reactions were activated at 50°C for 2 minutes followed by 95°C for 2 minutes. 40 amplification cycles (95°C for 15 seconds, followed by annealing at 60°C for 60 seconds) were performed. Relative expression of mRNA was quantified using the ΔΔCT method with β-actin (ACTB) as the endogenous control and mRNA from cells on fibers with the least alignment as the reference sample: $\Delta Ct = Ct_{target} - Ct_{ACTB}$; $\Delta\Delta Ct = \Delta Ct_{sample} - \Delta Ct_{reference}$; and relative expression = $2^{-\Delta\Delta Ct}$.

The primers used (Appendix Table B1) were for cardiac troponin I (cTnI, *TNNI3*), slow skeletal troponin I (ssTnI, *TNNI1*), myosin light chain 2 atrial isoform (MLC-2a, *MYL-2a*), myosin light chain 2 ventricular isoform (MLC-2v, *MYL-2v*), myosin heavy chain α isoform (MHC-α, *MYH6*), and myosin heavy chain β isoform (MHC-β, *MYH7*). mRNA expression is presented as the following isoform ratios: *MYH6/MYH7, MYL-2V/MYL-2A*, and *TNNI3/TNNI1*, with the isoform related to cardiomyocyte maturity over the isoform related to immaturity[37].

3.2.7 Cell Orientation and Overall Alignment

To quantify cell orientation and alignment, cells were immunostained with anti-cTnT and co-stained with rhodamine-phalloidin and DAPI as described above on days 8, 14, and 20. Low magnification images (using 4x and 10x objectives) were obtained on an Olympus IX-83 fluorescent microscope. Images were analyzed in ImageJ using the Orientation J plug-in as described above to determine cell orientation index. Anti-cTnT images were used to determine cardiomyocyte-only overall alignment, and rhodamine phalloidin images were used to determine overall alignment of all cells. At least three images per sample and three independent samples were analyzed.

High magnification images (63x objective) were obtained on a Zeiss Axio Observer Z1 Spinning-disc confocal microscope to determine the direction of cell orientation relative to fiber orientation. Fibers were visualized by staining with Hoescht 33342 (Thermo Fisher). Cell and fiber images were obtained from the same samples in different locations to improve fiber visualization.

3.2.8 Intracellular Calcium Transients

Cells were stained with Fluo-4, AM (Thermo Fisher), a calcium-sensitive fluorophore, to visualize spontaneous intracellular calcium transients. Briefly, Fluo-4, AM was reconstituted 20% wt/vol in Pluronic-F127 (Sigma-Aldrich) in DMSO and diluted to 10 μM in StemPro medium for 30 minutes at 37°C. Following staining, cells were rinsed with Tyrode's Salt Solution (Sigma-Aldrich) and incubated for at least 30 minutes at room temperature prior to imaging. Videos of 30 frames per second were obtained using a Zeiss Axio Observer Z1 spinning-disc confocal microscope and 20x objective.

Videos of intracellular calcium transients were analyzed in MATLAB (Mathworks) using custom code to determine the beating rate (presented as beats per minute, BPM) and

calcium transient synchronicity. Synchronicity was quantified as the median absolute deviation (MAD, a measure of spread) of the time of peak arrival (TPA) distribution across the entire frame starting a specified timepoint. Pixels without signal flux (i.e., areas without transients) were omitted. Five timepoints per video, at least three videos per sample, and three independent samples were analyzed.

3.2.9 Cardiomyocyte Contractility

At days 8 and 20 of differentiation, cells were stained with tetramethylrhodamine (TMRM, ThermoFisher) to visualize cardiomyocytes via mitochondrial activity [38]. Briefly, cells were incubated with TMRM diluted to 100 μM in Tyrode's Salt Solution for 30 minutes at 37°C. Following staining, the cells were rinsed with Tyrode's Salt Solution and incubated for at least 30 minutes at room temperature prior to imaging. Videos of 29 frames per second were obtained using an Olympus IX-83 fluorescent microscope and 20x objective with 2x2 pixel binning.

Cardiomyocyte contractions were analyzed using MotionGUI, a publicly available MATLAB Graphics User Interface developed by Huebsch et al. to measure contraction velocity and displacement[39]. Moving foreground detection with a threshold of 5 pixels was used, and amplitude-based cleaning was applied to reduce noise. To determine the directional effect of the degree of fiber alignment on contractile displacement, displacement parallel and perpendicular to the direction of collector rotation, and therefore fiber alignment, was analyzed. Results are presented as the ratio of parallel displacement to perpendicular displacement, so that a value greater than 1 indicates greater displacement in the direction of fiber alignment. At least three videos per sample and three independent samples were analyzed.

3.2.10 Statistical Analysis

Statistical analysis was performed using one-way and two-way ANOVA tests, followed by Tukey's multiple comparison test in Prism 6 (GraphPad). Differences with $p < 0.05$ are considered statistically significant. Data are presented as mean ± standard deviation.

3.3 RESULTS

3.3.1 Fiber Generation and Characterization

To assess cardiomyocyte structure and function in response to substrate anisotropy, we electrospun PCL to generate fiber scaffolds with variable degrees of fiber alignment. A rotating collector was used to align fibers. A stationary copper plate was used to collect non-aligned fibers in the absence of rotation. SEM images show that fiber alignment increases with collector rotational speed (Figure 3.1A). Fiber orientation index starts to plateau at 0.80 for fibers collected at speeds of 2000 RPM or greater (Figure 3.1B). Notably, fibers collected at 500 RPM had a comparable orientation index ($S=0.23 \pm 0.039$) to non-aligned fibers collected on a stationary plate ($S=0.21 \pm 0.12$). Also, fibers collected on the rotating collector had smaller variation between samples than fibers collected on a stationary plate (less than ± 0.06 compared to ± 0.12). Fibers collected at 2500 RPM had the highest orientation index of 0.86 ± 0.043.

Mean fiber diameter was also quantified (Figure 3.1C) from SEM images. No trend between collector rotational speed and mean fiber diameter was observed. For all collector speeds, mean fiber diameter was approximately 1.0 μm, varying from 0.817 ± 0.105 μm for fibers collected at 1000 RPM to 1.13 ± 0.168 μm at 3000 RPM. Because fibers collected

at 3000 RPM had a significantly larger mean fiber diameter than fibers collected at 1000 RPM, 3000 RPM fibers were not included in cell studies.

As a platform to evaluate how differentiating cardiomyocytes respond to substrate anisotropy, fibers collected at 500 RPM, 1000 RPM, 1500 RPM, and 2500 RPM were selected as their orientation index varied from relatively non-aligned (S=0.23) to semi-aligned (S=0.50 and 0.72) to aligned (S=0.86), respectively. These alignment conditions will be referred to as S-fibers; for example, fibers with an orientation index of 0.23 will be referenced as 0.23-fibers.

3.3.2 Cardiomyocyte Differentiation and Sarcomeric Protein Isoform Expression

mESCs were seeded onto fibers and differentiated to cardiomyocytes using a monolayer method with slight modification (Figure 3.2A)[36]. The presence of cTnT confirmed the presence of cardiomyocytes (Figure 3.2B). Day 14 gene expression ratios of sarcomeric protein isoforms troponin I (Figure 3.2C), myosin heavy chain (Figure 3.2D), and myosin light chains (Figure 3.2E) were quantified using RT-qPCR. These isoform pairs have been used to assess relative cardiomyocyte maturity, as expression of TNNI3, MYH6, and MYL-2v increases and expression of TNNI1, MYH7, MYL-2a decrease during development. Expression of these isoform pairs was comparable (with-in 2-fold) for cardiomyocytes across all fiber alignments, indicating no differences in relative maturity.

3.3.3 Cardiomyocyte Orientation Relative to Fiber Orientation

Cardiomyocytes and fibers were stained on day 14 of differentiation to assess cell orientation relative to fiber orientation (Figure 3.3). These images show that cardiomyocytes on 0.72- and 0.86-fibers orient in the direction of fiber orientation.

Cardiomyocytes on 0.23- and 0.50-fibers show no directional preference and, consequently, appear randomly oriented.

3.3.4 Overall Cell Alignment

Cardiomyocyte orientation index, indicative of overall cardiomyocyte alignment, was quantified at days 8, 14, and 20 (Figure 3.4A,B). At day 8, shortly after beating is observed, cardiomyocyte alignment increases with fiber alignment in a gradient-based manner, from S=0.017 ± 0.012 on 0.23-fibers to S=0.11 ± 0.04 on 0.86-fibers. This relationship persists at day 14; cardiomyocytes on 0.86-fibers were significantly more aligned (S=0.20 ± 0.033) than cardiomyocytes on both 0.23- and 0.50-fibers (S=0.020 ± 0.0034 and S=0.074 ± 0.26 respectively). However, by day 20, cardiomyocyte alignment relative to fiber alignment becomes threshold-based. Cardiomyocyte alignment is relatively low on 0.23-fibers (S=0.063 ± 0.058) and relatively high on all other fiber alignments (S=0.26 ± 0.085 to S=0.33 ± 0.051). Overall, from day 8 to day 20, cardiomyocyte orientation index increases by at least 2-fold on all fiber alignments except 0.23-fibers.

The cell orientation index of all cells, including non-cardiomyocytes, was also quantified by staining for F-actin. On day 8, overall cell alignment depends on fiber alignment in a gradient-based manner. Cells on 0.86-fibers (S=0.14 ± 0.051) are significantly more aligned than cells on 0.23-fibers (S=0.025 ± 0.019). At day 14, cell alignment relative to fiber alignment starts to become less gradient-based, as cell alignment on 0.72-fibers and 0.86-fibers is comparable (S=0.29 ± 0.052 to S=0.29 ± 0.026). On day 20, as was observed with cardiomyocyte alignment, cell alignment is a threshold-based response. Cell alignment on 0.23-fibers (S=0.068 ± 0.056) is significantly less than cell

alignment on all other fiber alignment. For both cardiomyocyte and all cells, alignment switches from a gradient-based response at day 8 to a threshold-based response at day 20.

3.3.5 Cardiomyocyte Contractility

Cardiomyocyte contractile displacement was measured on day 14 on all fiber alignments. Total contractile displacement was unaffected by fiber alignment (Figure 3.5A) Contractile displacement was then separated to measure directionality, specifically displacement parallel and perpendicular to the direction of fiber alignment (Figure 3.5B). Cardiomyocytes on 0.23- and 0.50-fibers contracted equally in the perpendicular and parallel directions. Cardiomyocytes on 0.72- and 0.86-fibers contracted slightly more in the direction parallel to fiber alignment.

3.3.6 Cardiomyocyte Intracellular Calcium Transients

Spontaneous cardiomyocyte intracellular calcium transients were observed on days 8 (Figure 3.6A) and 20 (Figure 3.6B) for cardiomyocytes on 0.23-fibers and 0.86-fibers. Fluo-4,AM was used to visualize intracellular calcium flux. For both timepoints, the beating rate of cardiomyocytes on 0.23-fibers is similar to that for cardiomyocytes on 0.86-fibers (Figure 3.6C). The beating rate for both conditions increases over time, from approximately 62 BPM on day 8 to 90 BPM on day 20.

As shown in the representative images, calcium transients can markedly vary from out-of-phase (unsynchronized) to in-phase (synchronized). To quantify synchronicity, the median absolute deviation (MAD) of the time to peak arrival (TPA) was measured (Appendix Figure B.1). For calcium transients that arrive at the precisely same time, the MAD of the TPA should be 0 ms. At day 8, the TPA-MAD is significantly less for cardiomyocytes on 0.86-fibers (38.7 ms) compared to that of cardiomyocytes on 0.23-

fibers (131 ms, Figure 3.6D). By day 20, the TPA-MAD of cardiomyocytes on 0.23-fibers (41.9 ms) decreased to the same level of cardiomyocytes on 0.86-fibers (26.6 ms).

3.4 DISCUSSION

Cardiac electrical and mechanical function is directionally dependent, and consequently, biomaterial-based approaches to improve cardiomyocyte function have focused on anisotropic designs, including lithography-patterned surfaces and electrospun aligned fibers. Cardiomyocytes seeded on these materials elongate and align in the direction of the anisotropic feature. Dimensional parameters, such as channel or groove width[26,40] and fiber diameter[41], have been varied to study their effect on cardiomyocyte phenotype and behavior. Length scales from the upper nanoscale to the size of individual cells best promote cardiomyocyte structural organization[25,26,41]. The effect of the degree of substrate anisotropy, however, has not been studied.

To investigate the response of differentiating cardiomyocytes to the degree of substrate anisotropy, we used electrospinning to generate scaffolds of non-aligned, semi-aligned, or aligned fibers. Similar to previous work[42,43], we were able to derive cardiomyocytes on these fiber scaffolds. We found that the substrate anisotropy did not lead to changes in the gene expression ratios of sarcomeric protein isoforms, which are commonly used as indicators of cardiomyocyte maturity[37,44]. Bedada et al. showed that *TNNI3/TNNI1* and cTnI/ssTnI expression ratios were unaffected by alignment[44]. Similarly, the beating rate did not differ for cells on non-aligned (0.23) and aligned (0.86) fibers. The beating rate did increase over time, as is typical for murine embryonic development[45].

Overall cardiomyocyte alignment and calcium transient synchronicity was observed to vary with fiber alignment at early timepoints. At later timepoints,

cardiomyocyte alignment instead depended on a minimum threshold fiber alignment. Cardiomyocyte alignment has been observed in materials that are not highly anisotropic, like hydrogels with mesoscopic pores[46]. Myofibril alignment has been observed in PSC-derived cardiomyocytes cultured on coverslips or in hydrogels without directional cues for protracted periods of time[30,47], suggesting that cardiomyocytes may self-align over time. This may be due to cardiomyocytes contractile behavior, as models of cardiomyocyte contractility show that myofibril alignment is energetically favorable[48]. Additionally, cell confluence may have contributed to local and overall cell alignment over time. For confluent monolayers, cells were observed to locally align over length scales of 500 μm on isotropic substrates. However, overall cell alignment was not observed because the preferred direction of cell alignment within these domains were uncorrelated[49]. Local cell alignment may explain why calcium transient synchronicity, which was measured over a smaller area than overall cell alignment, was observed at day 20 for cardiomyocytes in the absence of overall cell alignment. Although cardiomyocytes may self-align over time even without directional cues, our work, along with others'[9,13,22,25–29,40,50], show that high substrate anisotropy can cause cardiomyocytes to align more quickly than on isotropic substrates.

The presence of non-cardiomyocytes is known to positively affect cardiomyocyte organization and function. Co-cultures of cardiomyocytes with fibroblasts have faster conduction velocities[51], generate more contractile force[51–53], and improve cardiomyocyte spread and organization[53,54]. Our results support the role of non-cardiomyocytes facilitating cardiomyocyte organization as overall cell alignment preceded overall cardiomyocyte alignment. One key role of cardiac fibroblasts is to remodel the extracellular matrix (ECM)[4]. Given that overall cardiomyocyte and cell alignment changed from a gradient-based response to threshold-based response over time, non-cardiomyocytes are likely

remodeling deposited ECM over time. If this case, the orientation index of deposited ECM proteins should be higher than the orientation index of the underlying fibers. Future studies should evaluate how ECM deposition, composition, and organization change over time. These studies could also be performed in the presence and absence of cardiomyocytes to determine how cardiomyocyte contraction contributes to cell alignment relative to ECM remodeling.

3.5 CONCLUSIONS

In summary, our studies show that differentiating cardiomyocytes are responsive to substrate anisotropy. Cardiomyocyte alignment initially varies with substrate anisotropy. Over time, overall cardiomyocyte alignment is dependent on a minimum threshold anisotropy of the underlying substrate. Similarly, differences in calcium transient synchronicity initially vary with fiber alignment. These findings demonstrate that the response of differentiating cardiomyocytes to substrate anisotropy is time-dependent.

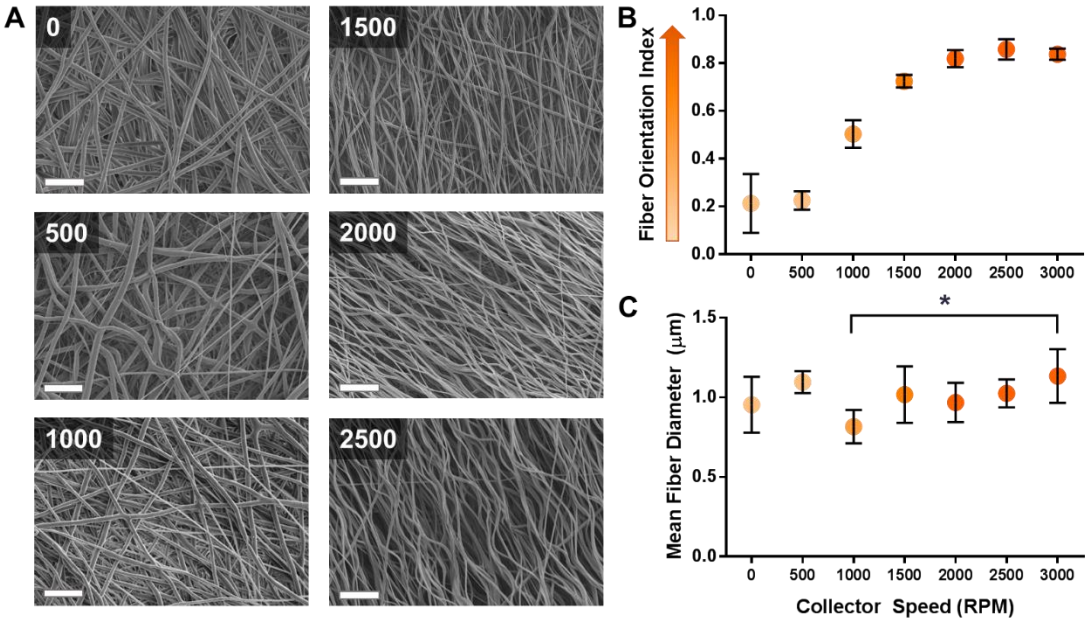

Figure 3.1 Fiber characterization. A) SEM images of electrospun PCL fibers. Collector speed indicated in top left corner. Scalebar is 10 μm. B) Fiber orientation index versus collector speed. C) Mean fiber diameter versus collector speed. *$p<0.05$.

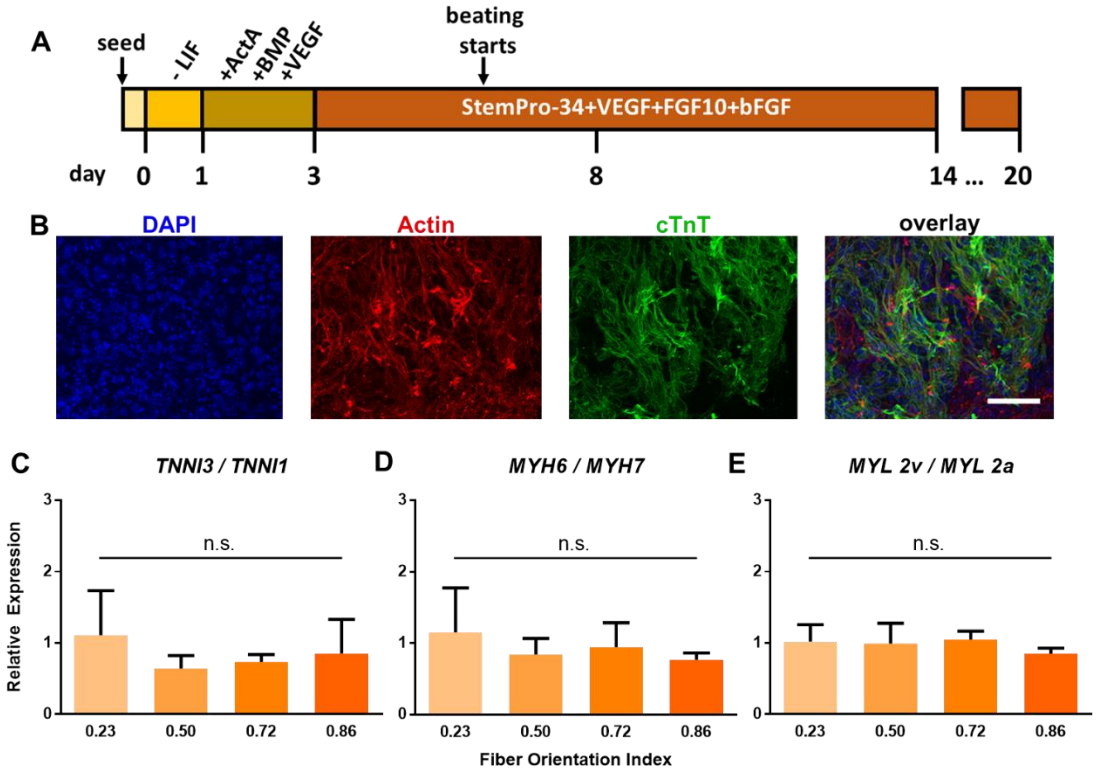

Figure 3.2 Cardiac differentiation on electrospun fibers. A) Schematic of differentiation timeline. B) cTnT+ cardiomyocytes derived on electrospun fibers. Scalebar is 50 µm. C, D, E) mRNA expression ratios of sarcomeric protein isoform pairs versus fiber orientation index.

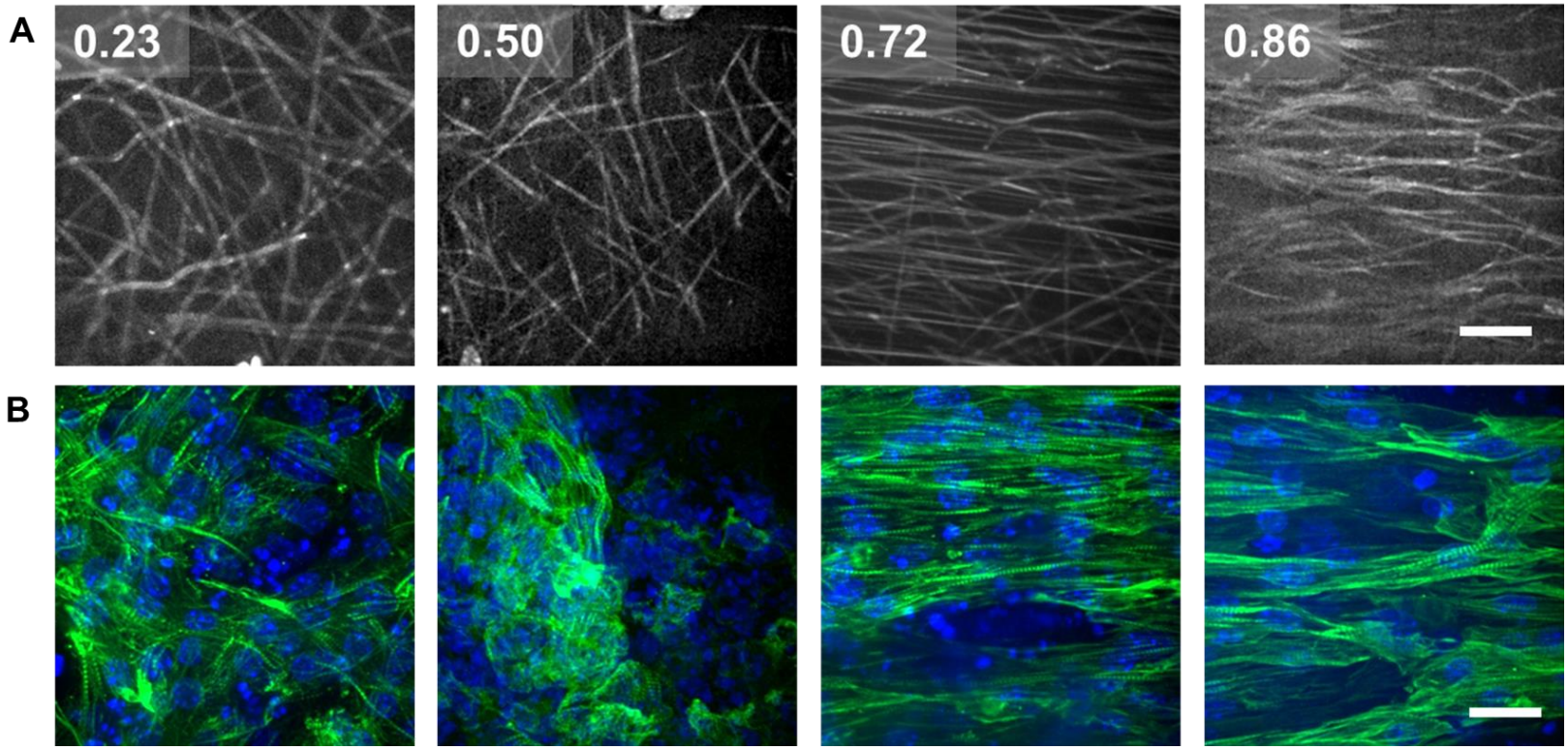

Figure 3.3 Cell orientation relative to fiber orientation. Images of A) Fibers and B) cardiomyocytes derived on same fibers. Fiber orientation indicated in top left corner. Green = cTnT; blue = nuclei. Scalebars are 20 µm.

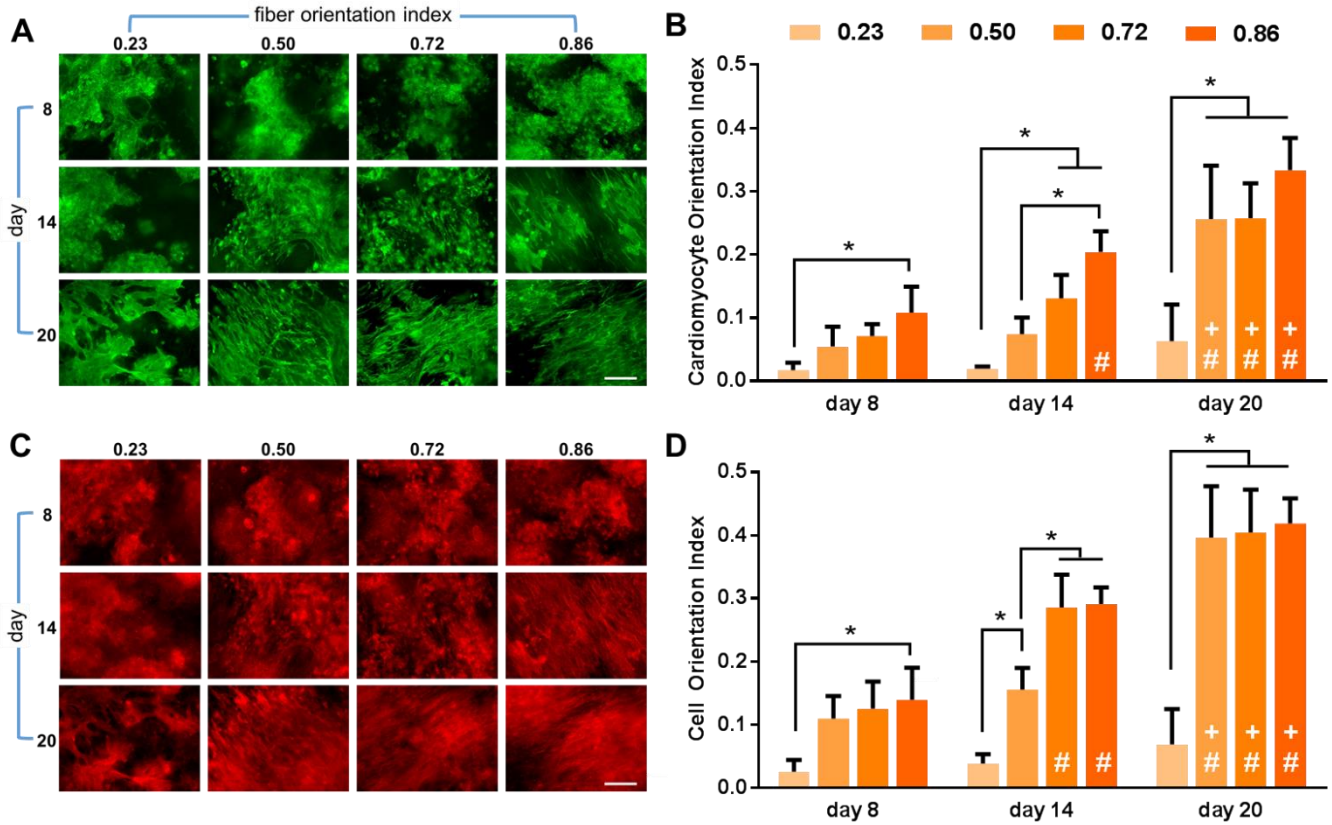

Figure 3.4 Cardiomyocyte and cell orientation index. Representative images of A) cardiomyocytes and C) all cells differentiated on fibers over time. Scalebars = 200 µm. B) Cardiomyocyte orientation index and D) all cell orientation index over time. *p<0.05. #p<0.05 versus day 8 orientation index for same fiber alignment. +p<0.05 versus day 14 orientation index for same fiber alignment.

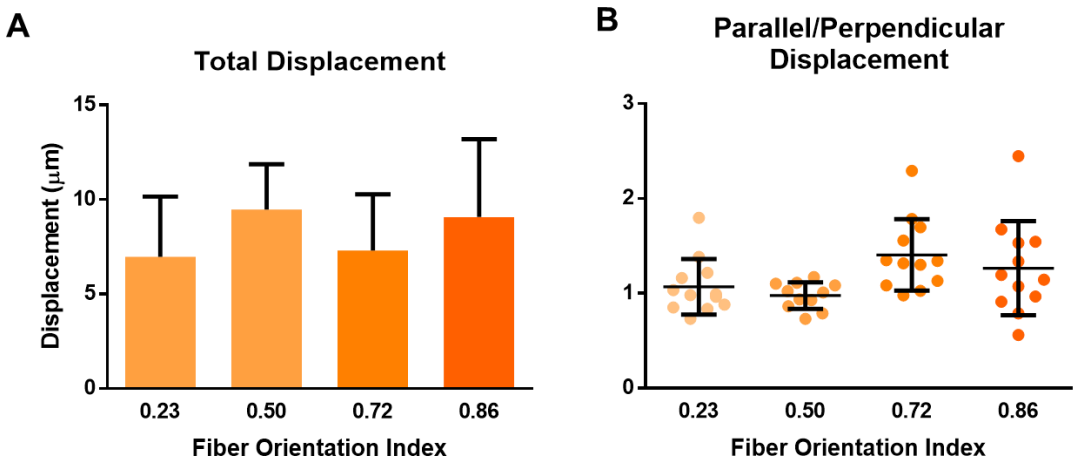

Figure 3.5 Cardiomyocyte contractility at day 14. A) Total contractile displacement. B) Displacement parallel and perpendicular to fiber direction.

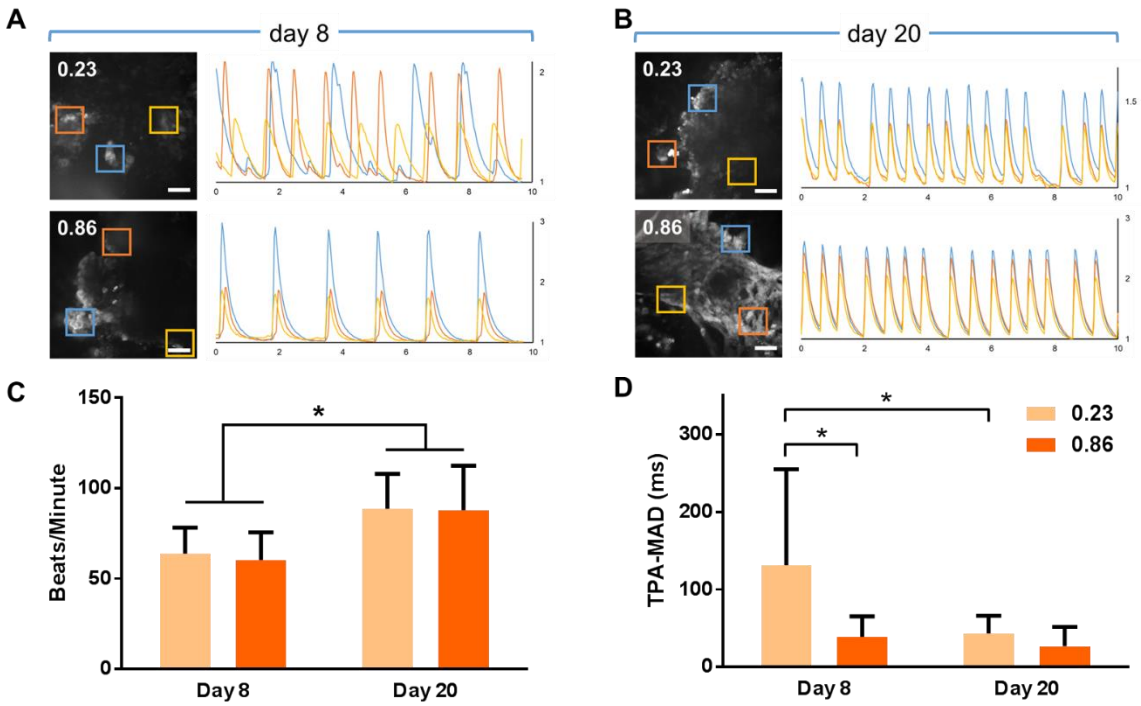

Figure 3.6 Cardiomyocyte intracellular calcium transients. Representative Fluo-4 signals for cardiomyocytes derived on 0.23- and 0.86 fibers at A) day 8 and B) day 20. Scalebars = 50 µm. C) Beating rate and D) TPA-MAD at days 8 and 20 for cardiomyocytes derived on 0.23- and 0.86-fibers. *p<0.05.

3.6 REFERENCES

1. Benjamin, E. J. *et al.* Heart Disease and Stroke Statistics—2018 Update: A Report From the American Heart Association. *Circulation* CIR.0000000000000558 (2018). doi:10.1161/CIR.0000000000000558
2. Bergmann, O. *et al.* Evidence for cardiomyocyte renewal in humans. *Science* **324,** 98–102 (2009).
3. Thygesen, K. *et al.* Third Universal Definition of Myocardial Infarction. *Circulation* **126,** 2020–2035 (2012).
4. Fan, D., Takawale, A., Lee, J. & Kassiri, Z. Cardiac fibroblasts, fibrosis and extracellular matrix remodeling in heart disease. *Fibrogenesis Tissue Repair* **5,** 15 (2012).
5. Hirt, M. N., Hansen, A. & Eschenhagen, T. Cardiac Tissue Engineering: State of the Art. *Circulation Research* **114,** 354–367 (2014).
6. Geuss, L. R., Allen, A. C. B., Ramamoorthy, D. & Suggs, L. J. Maintenance of HL-1 cardiomyocyte functional activity in PEGylated fibrin gels. *Biotechnol. Bioeng.* (2015). doi:10.1002/bit.25553
7. Gonnerman, E. A., Kelkhoff, D. O., McGregor, L. M. & Harley, B. A. C. The promotion of HL-1 cardiomyocyte beating using anisotropic collagen-GAG scaffolds. *Biomaterials* **33,** 8812–8821 (2012).
8. Alford, P. W., Feinberg, A. W., Sheehy, S. P. & Parker, K. K. Biohybrid Thin Films for Measuring Contractility in Engineered Cardiovascular Muscle. *Biomaterials* **31,** 3613–3621 (2010).
9. Kharaziha, M. *et al.* PGS:Gelatin nanofibrous scaffolds with tunable mechanical and structural properties for engineering cardiac tissues. *Biomaterials* **34,** 6355–6366 (2013).
10. Takahashi, K. & Yamanaka, S. Induction of Pluripotent Stem Cells from Mouse Embryonic and Adult Fibroblast Cultures by Defined Factors. *Cell* **126,** 663–676 (2006).
11. Burridge, P. W. *et al.* Chemically defined generation of human cardiomyocytes. *Nat Meth* **11,** 855–860 (2014).
12. Lian, X. *et al.* Chemically defined, albumin-free human cardiomyocyte generation. *Nat Meth* **12,** 595–596 (2015).
13. Feinberg, A. W. *et al.* Functional Differences in Engineered Myocardium from Embryonic Stem Cell-Derived versus Neonatal Cardiomyocytes. *Stem Cell Reports* **1,** 387–396 (2013).

14. Feric, N. T. & Radisic, M. Maturing human pluripotent stem cell-derived cardiomyocytes in human engineered cardiac tissues. *Advanced Drug Delivery Reviews* (2015). doi:10.1016/j.addr.2015.04.019

15. Ogle, B. M. *et al.* Distilling complexity to advance cardiac tissue engineering. *Science Translational Medicine* **8,** 342ps13-342ps13 (2016).

16. Stoppel, W. L., Kaplan, D. L. & Black III, L. D. Electrical and mechanical stimulation of cardiac cells and tissue constructs. *Advanced Drug Delivery Reviews* **96,** 135–155 (2016).

17. Zhu, R. *et al.* Physical developmental cues for the maturation of human pluripotent stem cell-derived cardiomyocytes. *Stem Cell Research & Therapy* **5,** 117 (2014).

18. Mihic, A. *et al.* The effect of cyclic stretch on maturation and 3D tissue formation of human embryonic stem cell-derived cardiomyocytes. *Biomaterials* **35,** 2798–2808 (2014).

19. Thavandiran, N. *et al.* Design and formulation of functional pluripotent stem cell-derived cardiac microtissues. *Proc Natl Acad Sci U S A* **110,** E4698–E4707 (2013).

20. Eng, G. *et al.* Autonomous beating rate adaptation in human stem cell-derived cardiomyocytes. *Nat Commun* **7,** 10312 (2016).

21. Nunes, S. S. *et al.* Biowire: a platform for maturation of human pluripotent stem cell-derived cardiomyocytes. *Nat Meth* **10,** 781–787 (2013).

22. Ribeiro, A. J. S. *et al.* Contractility of single cardiomyocytes differentiated from pluripotent stem cells depends on physiological shape and substrate stiffness. *PNAS* **112,** 12705–12710 (2015).

23. Liau, B., Christoforou, N., Leong, K. W. & Bursac, N. Pluripotent stem cell-derived cardiac tissue patch with advanced structure and function. *Biomaterials* **32,** 9180–9187 (2011).

24. Ma, Z. *et al.* Self-organizing human cardiac microchambers mediated by geometric confinement. *Nature Communications* **6,** 7413 (2015).

25. Salick, M. R. *et al.* Micropattern width dependent sarcomere development in human ESC-derived cardiomyocytes. *Biomaterials* **35,** 4454–4464 (2014).

26. Carson, D. *et al.* Nanotopography-Induced Structural Anisotropy and Sarcomere Development in Human Cardiomyocytes Derived from Induced Pluripotent Stem Cells. *ACS Appl. Mater. Interfaces* **8,** 21923–21932 (2016).

27. Khan, M. *et al.* Evaluation of Changes in Morphology and Function of Human Induced Pluripotent Stem Cell Derived Cardiomyocytes (HiPSC-CMs) Cultured on an Aligned-Nanofiber Cardiac Patch. *PLOS ONE* **10,** e0126338 (2015).

28. Li, J. *et al.* Human Pluripotent Stem Cell-Derived Cardiac Tissue-like Constructs for Repairing the Infarcted Myocardium. *Stem Cell Reports* **9,** 1546–1559 (2017).

29. Wanjare, M. *et al.* Anisotropic microfibrous scaffolds enhance the organization and function of cardiomyocytes derived from induced pluripotent stem cells. *Biomaterials Science* **5,** 1567–1578 (2017).

30. Kerscher, P. *et al.* Direct hydrogel encapsulation of pluripotent stem cells enables ontomimetic differentiation and growth of engineered human heart tissues. *Biomaterials* **83,** 383–395 (2016).

31. Allen, A. C. B., Barone, E., Crosby, C. O. K., Suggs, L. J. & Zoldan, J. Electrospun poly(N-isopropyl acrylamide)/poly(caprolactone) fibers for the generation of anisotropic cell sheets. *Biomater Sci* **5,** 1661–1669 (2017).

32. Püspöki, Z., Storath, M., Sage, D. & Unser, M. Transforms and Operators for Directional Bioimage Analysis: A Survey. *Adv Anat Embryol Cell Biol* **219,** 69–93 (2016).

33. Rezakhaniha, R. *et al.* Experimental investigation of collagen waviness and orientation in the arterial adventitia using confocal laser scanning microscopy. *Biomech Model Mechanobiol* **11,** 461–473 (2012).

34. Hotaling, N. A., Bharti, K., Kriel, H. & Simon Jr., C. G. DiameterJ: A validated open source nanofiber diameter measurement tool. *Biomaterials* **61,** 327–338 (2015).

35. Ferdman, A. G. & Yannas, I. V. Scattering of Light from Histologic Sections: A New Method for the Analysis of Connective Tissue. *J Investig Dermatol* **100,** 710–716 (1993).

36. Kokkinopoulos, I. *et al.* Cardiomyocyte differentiation from mouse embryonic stem cells using a simple and defined protocol. *Dev. Dyn.* **245,** 157–165 (2016).

37. Sheikh, F., Lyon, R. C. & Chen, J. Functions of Myosin Light Chain-2 (MYL2) In Cardiac Muscle and Disease. *Gene* **569,** 14–20 (2015).

38. Hattori, F. *et al.* Nongenetic method for purifying stem cell–derived cardiomyocytes. *Nature Methods* **7,** 61–66 (2010).

39. Huebsch, N. *et al.* Automated Video-Based Analysis of Contractility and Calcium Flux in Human-Induced Pluripotent Stem Cell-Derived Cardiomyocytes Cultured over Different Spatial Scales. *Tissue Eng Part C Methods* **21,** 467–479 (2015).

40. Kim, D.-H. *et al.* Nanoscale cues regulate the structure and function of macroscopic cardiac tissue constructs. *PNAS* **107,** 565–570 (2010).

41. Fleischer, S., Miller, J., Hurowitz, H., Shapira, A. & Dvir, T. Effect of fiber diameter on the assembly of functional 3D cardiac patches. *Nanotechnology* **26,** 291002 (2015).

42. Gupta, M. K. *et al.* Combinatorial Polymer Electrospun Matrices Promote Physiologically-Relevant Cardiomyogenic Stem Cell Differentiation. *PLOS ONE* **6,** e28935 (2011).

43. Prabhakaran, M. P. *et al.* Differentiation of embryonic stem cells to cardiomyocytes on electrospun nanofibrous substrates. *J. Biomed. Mater. Res.* **102,** 447–454 (2014).

44. Bedada, F. B. *et al.* Acquisition of a Quantitative, Stoichiometrically Conserved Ratiometric Marker of Maturation Status in Stem Cell-Derived Cardiac Myocytes. *Stem Cell Reports* **3,** 594–605 (2014).

45. Srinivasan, S. *et al.* Noninvasive, in utero imaging of mouse embryonic heart development with 40-MHz echocardiography. *Circulation* **98,** 912–918 (1998).

46. Bian, W., Jackman, C. P. & Bursac, N. Controlling the Structural and Functional Anisotropy of Engineered Cardiac Tissues. *Biofabrication* **6,** 024109 (2014).

47. Lundy, S. D., Zhu, W.-Z., Regnier, M. & Laflamme, M. A. Structural and Functional Maturation of Cardiomyocytes Derived from Human Pluripotent Stem Cells. *Stem Cells Dev* **22,** 1991–2002 (2013).

48. Dasbiswas, K., Majkut, S., Discher, D. E. & Safran, S. A. Substrate stiffness-modulated registry phase correlations in cardiomyocytes map structural order to coherent beating. *Nature Communications* **6,** ncomms7085 (2015).

49. Duclos, G., Garcia, S., G. Yevick, H. & Silberzan, P. Perfect nematic order in confined monolayers of spindle-shaped cells. *Soft Matter* **10,** 2346–2353 (2014).

50. Kai, D., Prabhakaran, M. P., Jin, G. & Ramakrishna, S. Guided orientation of cardiomyocytes on electrospun aligned nanofibers for cardiac tissue engineering. *J. Biomed. Mater. Res.* **98B,** 379–386 (2011).

51. Li, Y., Asfour, H. & Bursac, N. Age-dependent functional crosstalk between cardiac fibroblasts and cardiomyocytes in a 3D engineered cardiac tissue. *Acta Biomaterialia* **55,** 120–130 (2017).

52. Radisic, M. *et al.* Pre-treatment of synthetic elastomeric scaffolds by cardiac fibroblasts improves engineered heart tissue. *J. Biomed. Mater. Res.* **86A,** 713–724 (2008).

53. Liau, B., Jackman, C. P., Li, Y. & Bursac, N. Developmental stage-dependent effects of cardiac fibroblasts on function of stem cell-derived engineered cardiac tissues. *Scientific Reports* **7,** srep42290 (2017).

54. Parrag, I. C., Zandstra, P. W. & Woodhouse, K. A. Fiber alignment and coculture with fibroblasts improves the differentiated phenotype of murine embryonic stem cell-derived cardiomyocytes for cardiac tissue engineering. *Biotechnol. Bioeng.* **109,** 813–822 (2012).

Chapter 4: Conclusions and Future Directions

4.1 Conclusions

Cardiomyocyte function is directionally dependent. Biomaterial systems that force cardiomyocytes to elongate and align have been shown to improve adult and PSC-derived cardiomyocyte electrical and mechanical function. Electrospun fibers, which can be ECM-mimicking, can be aligned for this purpose. Electrospinning parameters can be easily modified to change fiber properties, like the polymer type and degree of fiber alignment, to create new systems amenable to cardiac tissue engineering purposes.

In this dissertation, we present the use of aligned fibers to generate cells sheets and to study differentiating cardiomyocyte sensitivity to substrate anisotropy. By depositing electrospun fibers on a rotating collector, we were able to control fiber alignment and use these fibers as cell culture substrates. In Chapter 2, the fabrication and characterization of electrospun PNIPAAm/PCL blended fibers was described. We demonstrated that viable, intact, and aligned cell sheets can be generated from fibers containing 90% PNIPAAm and 10% PCL. Fibers containing only PNIPAAm were a poor attachment surface for cells, and fibers containing less than 90% PNIPAAm prevented cell-substrate detachment.

In Chapter 3, we generated a set of electrospun fiber scaffolds that varied from non-aligned to semi-aligned to highly aligned. We were able to differentiate cardiomyocytes from mESCs on these scaffolds to evaluate how these cells responded to different degrees of anisotropy over time. Although we expected the cell response, especially overall cardiomyocyte alignment, to be gradient-based and increase with degree of fiber alignment, this response as a function of fiber alignment was actually time-dependent. At early timepoints, PSC-derived cardiomyocyte alignment increased with fiber alignment. However, at later timepoints, PSC-derived cardiomyocytes aligned on fibers that were only

slightly aligned, indicating that a minimum threshold alignment was sufficient to generate overall alignment. When evaluating cardiomyocyte intracellular calcium transients, a similar phenomenon was observed. Calcium transients were more synchronized on aligned fibers than on non-aligned fibers at early timepoints. This difference was lost as PSC-derived cardiomyocytes on non-aligned and aligned fibers were comparably synchronized at later timepoints.

4.2 Future Directions

4.2.1 Mechanism of alignment

In Chapter 3, we observed that cardiomyocytes on fibers that had only a slight degree of anisotropy were able to align. Other groups have observed self-alignment of cardiomyocytes in the absence of topographical cues for prolonged culture periods[1,2]. Our system of fiber scaffolds that have increasing degrees of fiber alignment could be helpful in discerning how cardiomyocytes self-align over time.

As cardiomyocytes subject to electrical and mechanical conditioning have been observed to align themselves in the direction of the stimuli[3], the cyclic electromechanical nature of contraction may allow cardiomyocytes to self-align. If this is the case, cardiomyocyte contraction could be inhibited by culturing cells with actin-myosin blockers. Similarly, gap junction blockers, like verapamil or carbenoxolone, could be used to block electrical communication between cells. Alignment would be assessed after blocking these behaviors.

Non-cardiomyocyte cells may also have a role in cardiomyocyte alignment over time. It is believed that these support cells, particularly cardiac fibroblasts, aid

cardiomyocyte structure by remodeling the surrounding matrix. Notably, support cells have also been shown to improve cardiomyocyte function, like conduction velocity[4]. An interesting experiment would be to track cardiomyocyte alignment in the presence and absence of cardiac fibroblasts. The deposition and organization of ECM proteins should also be monitored over time to assess the effects of ECM remodeling.

4.2.2 Anisotropic Cell Sheets

In Chapter 2, we described a method to fabricate blended PNIPAAm/PCL fibers that can be used to generate anisotropic cell sheets. We demonstrated proof of concept using NIH 3T3 fibroblasts. Cells were able to attach, grow, and detach on fibers consisting of 90% PNIPAAm and 10% PCL. Following the publication of the manuscript, we have optimized electrospinning parameters of 90% PNIPAAm fibers and refined the cell culture approach. In Chapter 3, we demonstrated that we were able to derive cardiomyocytes on electrospun PCL fibers.

The natural progression of these two projects is to derive cardiomyocytes on PNIPAAm/PCL fibers to later detach cardiac cell sheets. This approach would require optimization of both cardiac differentiation and cell sheeting. As this work would be more translationally-focused and could lead to *in vivo* experiments, human PSCs should be used to derive cardiac cells. Several cardiac differentiation methods have been published that rely on small molecules and common proteins, making human PSC-derived cardiomyocytes widely available to the research community[5,6]. Differentiation of human PSCs on PNIPAAm/PCL fibers should be optimized by cell density, as cell-cell contacts and nutrient availability impact differentiation efficiency.

For cell sheeting, there may be hurdles in achieving intact cardiomyocyte sheets. Pure cardiomyocytes cultured on PNIPAAm-grafted plates could not detach as cell sheets

due to the lack of deposited ECM. This was overcome by co-culturing fibroblasts with cardiomyocytes[7]. By deriving cardiomyocytes directly on fibers, enough non-cardiomyocytes may be present to permit detachment of intact cell sheets. Alternatively, a monolayer of fibroblasts could be cultured on PNIPAAm/PCL fibers prior to PSC seeding and differentiation to ensure that intact cardiac cell sheets can be detached.

Following the successful detachment of cell sheets, the functionality of the cardiac cell sheets should be assessed. These assessments should first verify that the detachment process does not negatively affect function. The detachment of cell sheets may enable assays that were not feasible on electrospun fibers due to the lack of transparency.

4.3 REFERENCES

1. Lundy, S. D., Zhu, W.-Z., Regnier, M. & Laflamme, M. A. Structural and Functional Maturation of Cardiomyocytes Derived from Human Pluripotent Stem Cells. *Stem Cells Dev* **22,** 1991–2002 (2013).
2. Kerscher, P. *et al.* Direct hydrogel encapsulation of pluripotent stem cells enables ontomimetic differentiation and growth of engineered human heart tissues. *Biomaterials* **83,** 383–395 (2016).
3. Stoppel, W. L., Kaplan, D. L. & Black III, L. D. Electrical and mechanical stimulation of cardiac cells and tissue constructs. *Advanced Drug Delivery Reviews* **96,** 135–155 (2016).
4. Liau, B., Jackman, C. P., Li, Y. & Bursac, N. Developmental stage-dependent effects of cardiac fibroblasts on function of stem cell-derived engineered cardiac tissues. *Scientific Reports* **7,** srep42290 (2017).
5. Lian, X. *et al.* Chemically defined, albumin-free human cardiomyocyte generation. *Nat Meth* **12,** 595–596 (2015).
6. Burridge, P. W. *et al.* Chemically defined generation of human cardiomyocytes. *Nat Meth* **11,** 855–860 (2014).
7. Matsuura, K. *et al.* Creation of mouse embryonic stem cell-derived cardiac cell sheets. *Biomaterials* **32,** 7355–7362 (2011).

Appendix

A. Supplementary Information for Chapter 2

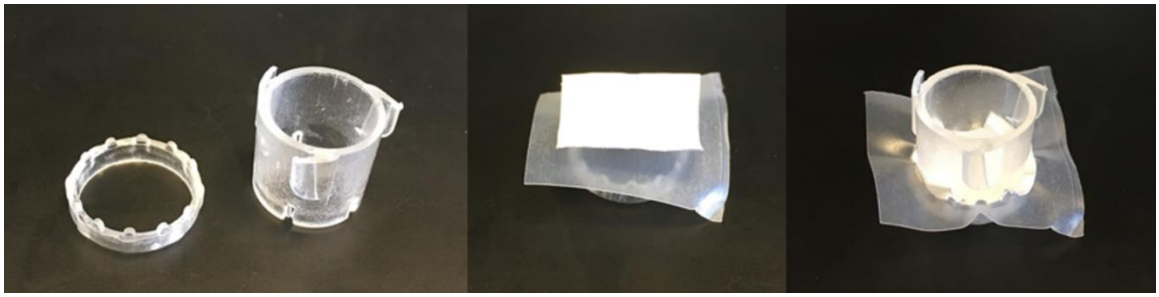

Figure A1 CellCrown inserts were used to secure PNIPAAm/PCL fibers. Squares of PNIPAAm/PCL fibers and parafilm were layered onto the CellCrown bottom (middle). A fully assembled CellCrown with PNIPAAm/PCL fibers (right).

PNIPAAm content	Total Polymer (wt/vol)	Solvent	Charge (kV)
0%	10%	HFP	4.5-6.5
25%	12%	1:3 methanol:chloroform	7.0-10.5
50%	12%	1:3 methanol:chloroform	8.5-9.5
75%	15%	1:3 methanol:chloroform	9.0-10.0
90%	18%	1:3 methanol:chloroform	13.0-15.0
100%	20%	methanol	11.0-11.5

Table A1 Solution and electrospinning parameters for PNIPAAm/PCL fibers.

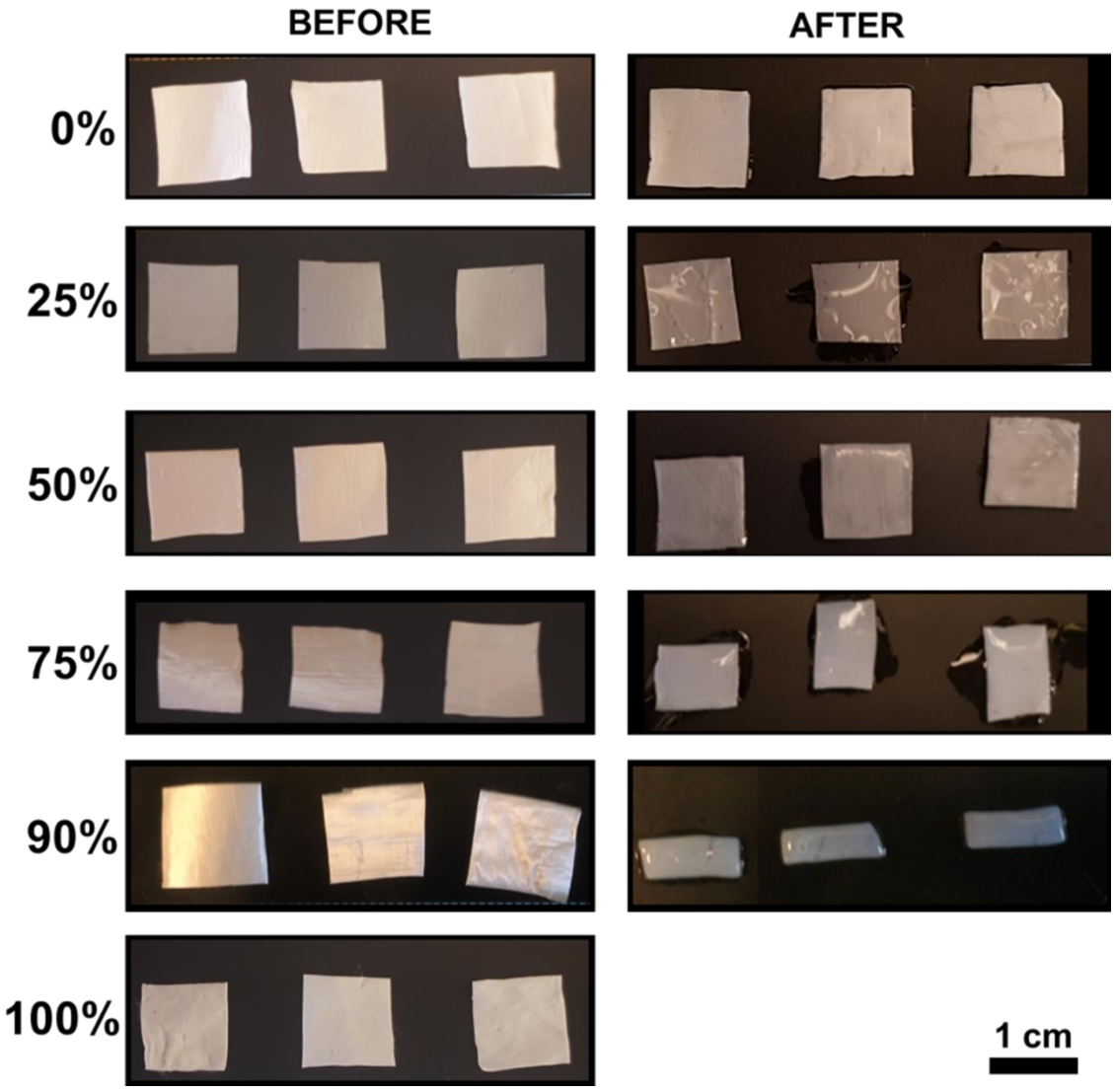

Figure A2 PNIPAAm/PCL fibers before and after PNIPAAm dissolution.

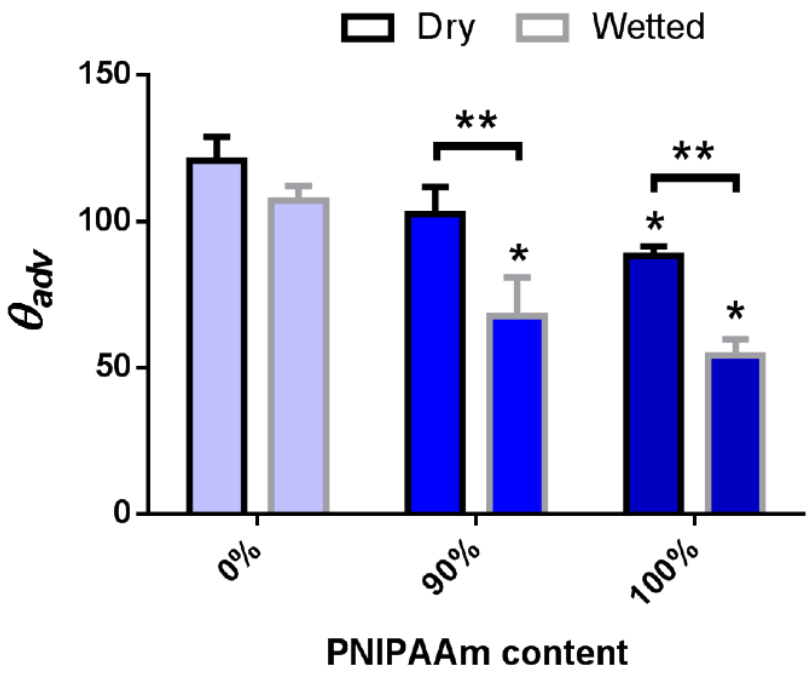

Figure A3 Advancing water contact angle of dry and wetted PNIPAAm/PCL fibers.
*p<0.05 compared to corresponding 0% PNIPAAm fiber contact angle;
**p< 0.05 between dry and wetted fibers.

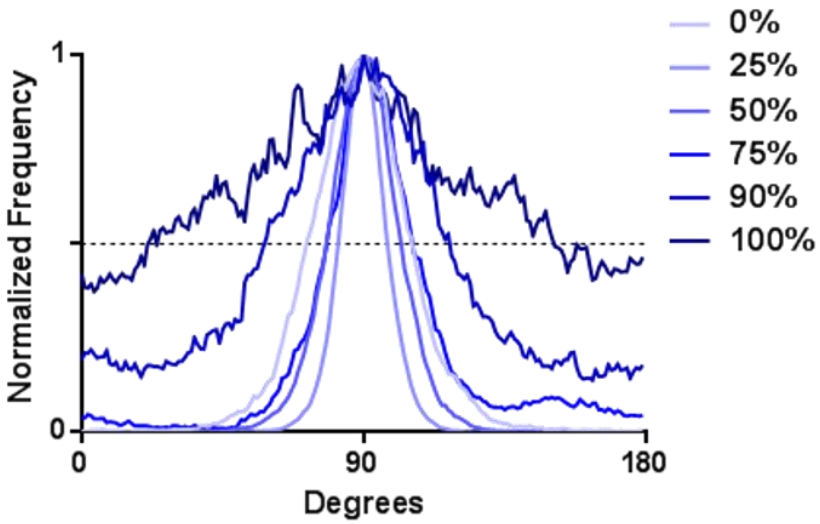

Figure A4 Representative histograms of cell angles as measured from actin of cells seeded on PNIPAAm/PCL fibers. Histograms were normalized to the peak frequency. Dashed line indicates half max.

B. SUPPLEMENTARY INFORMATION FOR CHAPTER 3

Gene name	Forward	Reverse
TNNI1	ATGCCGGAAGTTGAGAGGAAA	TCCGAGAGGTAACGCACCTT
TNNI3	TCTGCCAACTACCGAGCCTAT	CTCTTCTGCCTCTCGTTCCAT
ISL1	TAAGCATGCCTGTAGCTGGTT	GATGGATCTCAAAAAAATGGTAAAGAG
NKX2.5	ACCTTTAGGAGAAGGGCGATGACT	AAGTGGGATGGATCGGAGAAAGGT
MESP1	TTTCCTTTGGTCTTGGCACCTTCG	TCCAAGGAGGGTTGGAATGGTACA
MYH6	GCGCATTGAGTTCAAGAAGA	CTTCATCCATGGCCAATTCT
MYH7	AGCATTCTCCTGCTGTTTCC	GAGCCTTGGATTCTCAAACG
BETA ACTIN	TGAGCGCAAGTACTCTGTGTGGAT	ACTCATCGTACTCCTGCTTGCTGA
MLC2A	TCAGCTGCATTGACCAGAAC	AAGACGGTGAAGTTGATGGG
MLC2V	AAAGAGGCTCCAGGTCCAAT	CCTCTCTGCTTGTGTGGTCA

Table B1 Forward and reverse primers used for RT-qPCR.

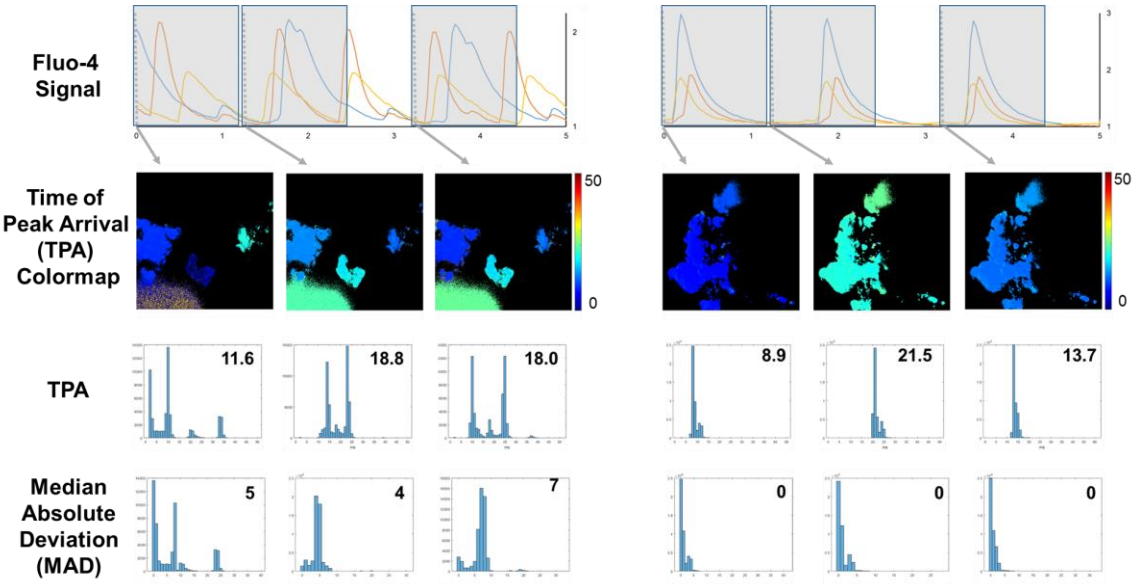

Figure B1 Time to peak arrival-median absolute deviation (TPA-MAD) is used to quantify synchronicity. Representative Fluo-4 signals for unsynchronized (left) and synchronized (right) intracellular calcium transients. At specified timepoints, the TPA is determined for the entire frame of view for 50 frames (transparent gray boxes). The TPA is presented as color activation maps and histograms. The mean TPA is indicated in the upper right corner. Absolute deviations from the TPA median are shown as histograms. The MAD is indicated in the upper right corner.

Bibliography

Akiyama, Y., Kikuchi, A., Yamato, M., & Okano, T. (2004a). Ultrathin poly(N-isopropylacrylamide) grafted layer on polystyrene surfaces for cell adhesion/detachment control. *Langmuir: The ACS Journal of Surfaces and Colloids*, *20*(13), 5506–5511.

Alford, P. W., Feinberg, A. W., Sheehy, S. P., & Parker, K. K. (2010). Biohybrid Thin Films for Measuring Contractility in Engineered Cardiovascular Muscle. *Biomaterials*, *31*(13), 3613–3621. https://doi.org/10.1016/j.biomaterials.2010.01.079

Allen, A. C. B., Barone, E., Crosby, C. O. K., Suggs, L. J., & Zoldan, J. (2017). Electrospun poly(N-isopropyl acrylamide)/poly(caprolactone) fibers for the generation of anisotropic cell sheets. *Biomaterials Science*, *5*(8), 1661–1669. https://doi.org/10.1039/c7bm00324b

Anderson, J. M. (2016). Future challenges in the in vitro and in vivo evaluation of biomaterial biocompatibility. *Regenerative Biomaterials*, *3*(2), 73–77. https://doi.org/10.1093/rb/rbw001

Anderson, J. M., Gristina, A. G., Hanson, S. R., Harker, L. A., Johnson, R. J., Merritt, K., Schoen, F. J. (1996). *Biomaterials Science: an Introduction to Materials in Medicine, Host reactions to biomaterials and their evaluation.* (B. D. Ratner, A. S. Hoffman, F. J. Schoen, & J. E. Lemons, Eds.). San Diego, CA: Academic Press.

Au, H. T. H., Cheng, I., Chowdhury, M. F., & Radisic, M. (2007). Interactive effects of surface topography and pulsatile electrical field stimulation on orientation and elongation of fibroblasts and cardiomyocytes. *Biomaterials*, *28*(29), 4277–4293. https://doi.org/10.1016/j.biomaterials.2007.06.001

Baker, B. M., Gee, A. O., Metter, R. B., Nathan, A. S., Marklein, R. A., Burdick, J. A., & Mauck, R. L. (2008). The potential to improve cell infiltration in composite fiber-aligned electrospun scaffolds by the selective removal of sacrificial fibers. *Biomaterials*, *29*(15), 2348–2358. https://doi.org/10.1016/j.biomaterials.2008.01.032

Beattie, D. A., Addai-Mensah, J., Beaussart, A., V. Franks, G., & Yeap, K.-Y. (2014). In situ particle film ATR FTIR spectroscopy of poly (N -isopropyl acrylamide) (PNIPAM) adsorption onto talc. *Physical Chemistry Chemical Physics*, *16*(45), 25143–25151. https://doi.org/10.1039/C4CP03161J

Bedada, F. B., Chan, S. S.-K., Metzger, S. K., Zhang, L., Zhang, J., Garry, D. J., … Metzger, J. M. (2014). Acquisition of a Quantitative, Stoichiometrically Conserved Ratiometric Marker of Maturation Status in Stem Cell-Derived Cardiac Myocytes. *Stem Cell Reports*, *3*(4), 594–605. https://doi.org/10.1016/j.stemcr.2014.07.012

Benjamin, E. J., Virani, S. S., Callaway, C. W., Chang, A. R., Cheng, S., Chiuve, S. E., … Muntner, P. (2018). Heart Disease and Stroke Statistics—2018 Update: A Report

From the American Heart Association. *Circulation*, CIR.0000000000000558. https://doi.org/10.1161/CIR.0000000000000558

Bergmann, O., Bhardwaj, R. D., Bernard, S., Zdunek, S., Barnabé-Heider, F., Walsh, S., … Frisén, J. (2009). Evidence for cardiomyocyte renewal in humans. *Science (New York, N.Y.)*, *324*(5923), 98–102. https://doi.org/10.1126/science.1164680

Bian, W., Jackman, C. P., & Bursac, N. (2014). Controlling the Structural and Functional Anisotropy of Engineered Cardiac Tissues. *Biofabrication*, *6*(2), 024109. https://doi.org/10.1088/1758-5082/6/2/024109

Bian, W., Juhas, M., Pfeiler, T. W., & Bursac, N. (2011). Local Tissue Geometry Determines Contractile Force Generation of Engineered Muscle Networks. *Tissue Engineering Part A*, *18*(9–10), 957–967. https://doi.org/10.1089/ten.tea.2011.0313

Blazeski, A., Zhu, R., Hunter, D. W., Weinberg, S. H., Boheler, K. R., Zambidis, E. T., & Tung, L. (2012). Electrophysiological and contractile function of cardiomyocytes derived from human embryonic stem cells. *Progress in Biophysics and Molecular Biology*, *110*(0), 178–195. https://doi.org/c

Boheler, K. R., Czyz, J., Tweedie, D., Yang, H.-T., Anisimov, S. V., & Wobus, A. M. (2002). Differentiation of Pluripotent Embryonic Stem Cells Into Cardiomyocytes. *Circulation Research*, *91*(3), 189–201. https://doi.org/10.1161/01.RES.0000027865.61704.32

Bordes, C., Fréville, V., Ruffin, E., Marote, P., Gauvrit, J. Y., Briançon, S., & Lantéri, P. (2010). Determination of poly(ε-caprolactone) solubility parameters: Application to solvent substitution in a microencapsulation process. *International Journal of Pharmaceutics*, *383*(1–2), 236–243. https://doi.org/10.1016/j.ijpharm.2009.09.023

Bray, M.-A., Sheehy, S. P., & Parker, K. K. (2008). Sarcomere Alignment is Regulated by Myocyte Shape. *Cell Motility and the Cytoskeleton*, *65*(8), 641–651. https://doi.org/10.1002/cm.20290

Burridge, P. W., Matsa, E., Shukla, P., Lin, Z. C., Churko, J. M., Ebert, A. D., … Wu, J. C. (2014). Chemically defined generation of human cardiomyocytes. *Nature Methods*, *11*(8), 855–860. https://doi.org/10.1038/nmeth.2999

Bursac, N., Parker, K. K., Iravanian, S., & Tung, L. (2002). Cardiomyocyte Cultures With Controlled Macroscopic Anisotropy A Model for Functional Electrophysiological Studies of Cardiac Muscle. *Circulation Research*, *91*(12), e45–e54. https://doi.org/10.1161/01.RES.0000047530.88338.EB

Cao, N., Liu, Z., Chen, Z., Wang, J., Chen, T., Zhao, X., … Yang, H.-T. (2012). Ascorbic acid enhances the cardiac differentiation of induced pluripotent stem cells through promoting the proliferation of cardiac progenitor cells. *Cell Research*, *22*(1), 219–236. https://doi.org/10.1038/cr.2011.195

Carson, D., Hnilova, M., Yang, X., Nemeth, C. L., Tsui, J. H., Smith, A. S. T., … Kim, D.-H. (2016). Nanotopography-Induced Structural Anisotropy and Sarcomere Development in Human Cardiomyocytes Derived from Induced Pluripotent Stem Cells. *ACS Applied Materials & Interfaces*, *8*(34), 21923–21932. https://doi.org/10.1021/acsami.5b11671

Chen, M., Dong, M., Havelund, R., Regina, V. R., Meyer, R. L., Besenbacher, F., & Kingshott, P. (2010). Thermo-Responsive Core−Sheath Electrospun Nanofibers from Poly (N-isopropylacrylamide)/Polycaprolactone Blends. *Chemistry of Materials*, *22*(14), 4214–4221. https://doi.org/10.1021/cm100753r

Chen, Y., Zeng, D., Ding, L., Li, X.-L., Liu, X.-T., Li, W.-J., … Zheng, Q.-S. (2015). Three-dimensional poly-(ε-caprolactone) nanofibrous scaffolds directly promote the cardiomyocyte differentiation of murine-induced pluripotent stem cells through Wnt/β-catenin signaling. *BMC Cell Biology*, *16*, 22. https://doi.org/10.1186/s12860-015-0067-3

Cipitria, A., Skelton, A., R. Dargaville, T., D. Dalton, P., & W. Hutmacher, D. (2011). Design, fabrication and characterization of PCL electrospun scaffolds—a review. *Journal of Materials Chemistry*, *21*(26), 9419–9453. https://doi.org/10.1039/C0JM04502K

Croisier, F., Duwez, A.-S., Jérôme, C., Léonard, A. F., van der Werf, K. O., Dijkstra, P. J., & Bennink, M. L. (2012). Mechanical testing of electrospun PCL fibers. *Acta Biomaterialia*, *8*(1), 218–224. https://doi.org/10.1016/j.actbio.2011.08.015

Dasbiswas, K., Majkut, S., Discher, D. E., & Safran, S. A. (2015). Substrate stiffness-modulated registry phase correlations in cardiomyocytes map structural order to coherent beating. *Nature Communications*, *6*, ncomms7085. https://doi.org/10.1038/ncomms7085

Doshi, J., & Reneker, D. H. (1993). Electrospinning process and applications of electrospun fibers. In *, Conference Record of the 1993 IEEE Industry Applications Society Annual Meeting, 1993* (pp. 1698–1703 vol.3). https://doi.org/10.1109/IAS.1993.299067

Duclos, G., Garcia, S., G. Yevick, H., & Silberzan, P. (2014). Perfect nematic order in confined monolayers of spindle-shaped cells. *Soft Matter*, *10*(14), 2346–2353. https://doi.org/10.1039/C3SM52323C

Dybal, J., Trchová, M., & Schmidt, P. (2009). The role of water in structural changes of poly(N-isopropylacrylamide) and poly(N-isopropylmethacrylamide) studied by FTIR, Raman spectroscopy and quantum chemical calculations. *Vibrational Spectroscopy*, *51*(1), 44–51. https://doi.org/10.1016/j.vibspec.2008.10.003

Elzein, T., Nasser-Eddine, M., Delaite, C., Bistac, S., & Dumas, P. (2004). FTIR study of polycaprolactone chain organization at interfaces. *Journal of Colloid and Interface Science*, *273*(2), 381–387. https://doi.org/10.1016/j.jcis.2004.02.001

Eng, G., Lee, B. W., Protas, L., Gagliardi, M., Brown, K., Kass, R. S., … Vunjak-Novakovic, G. (2016). Autonomous beating rate adaptation in human stem cell-derived cardiomyocytes. *Nature Communications*, *7*, 10312. https://doi.org/10.1038/ncomms10312

Falconnet, D., Csucs, G., Michelle Grandin, H., & Textor, M. (2006). Surface engineering approaches to micropattern surfaces for cell-based assays. *Biomaterials*, *27*(16), 3044–3063. https://doi.org/10.1016/j.biomaterials.2005.12.024

Fan, D., Takawale, A., Lee, J., & Kassiri, Z. (2012). Cardiac fibroblasts, fibrosis and extracellular matrix remodeling in heart disease. *Fibrogenesis & Tissue Repair*, *5*, 15. https://doi.org/10.1186/1755-1536-5-15

Fast, V. G. (2005). Simultaneous optical imaging of membrane potential and intracellular calcium. *Journal of Electrocardiology*, *38*(4), 107–112. https://doi.org/10.1016/j.jelectrocard.2005.06.023

Feinberg, A. W., Ripplinger, C. M., van der Meer, P., Sheehy, S. P., Domian, I., Chien, K. R., & Parker, K. K. (2013). Functional Differences in Engineered Myocardium from Embryonic Stem Cell-Derived versus Neonatal Cardiomyocytes. *Stem Cell Reports*, *1*(5), 387–396. https://doi.org/10.1016/j.stemcr.2013.10.004

Ferdman, A. G., & Yannas, I. V. (1993). Scattering of Light from Histologic Sections: A New Method for the Analysis of Connective Tissue. *Journal of Investigative Dermatology*, *100*(5), 710–716. https://doi.org/10.1111/1523-1747.ep12472364

Feric, N. T., & Radisic, M. (2015). Maturing human pluripotent stem cell-derived cardiomyocytes in human engineered cardiac tissues. *Advanced Drug Delivery Reviews*. https://doi.org/10.1016/j.addr.2015.04.019

Fleischer, S., Miller, J., Hurowitz, H., Shapira, A., & Dvir, T. (2015). Effect of fiber diameter on the assembly of functional 3D cardiac patches. *Nanotechnology*, *26*(29), 291002. https://doi.org/10.1088/0957-4484/26/29/291002

Fomovsky, G. M., Thomopoulos, S., & Holmes, J. W. (2010). Contribution of Extracellular Matrix to the Mechanical Properties of the Heart. *Journal of Molecular and Cellular Cardiology*, *48*(3), 490–496. https://doi.org/10.1016/j.yjmcc.2009.08.003

Fong, H., Chun, I., & Reneker, D. H. (1999). Beaded nanofibers formed during electrospinning. *Polymer*, *40*(16), 4585–4592. https://doi.org/10.1016/S0032-3861(99)00068-3

Geuss, L. R., Allen, A. C. B., Ramamoorthy, D., & Suggs, L. J. (2015). Maintenance of HL-1 cardiomyocyte functional activity in PEGylated fibrin gels. *Biotechnology and Bioengineering*. https://doi.org/10.1002/bit.25553

Golob, M., Moss, R. L., & Chesler, N. C. (2014). Cardiac Tissue Structure, Properties, and Performance: A Materials Science Perspective. *Annals of Biomedical Engineering*, *42*(10), 2003–2013. https://doi.org/10.1007/s10439-014-1071-z

Gonnerman, E. A., Kelkhoff, D. O., McGregor, L. M., & Harley, B. A. C. (2012). The promotion of HL-1 cardiomyocyte beating using anisotropic collagen-GAG scaffolds. *Biomaterials*, *33*(34), 8812–8821. https://doi.org/10.1016/j.biomaterials.2012.08.051

Gupta, M. K., Walthall, J. M., Venkataraman, R., Crowder, S. W., Jung, D. K., Yu, S. S., … Sung, H.-J. (2011). Combinatorial Polymer Electrospun Matrices Promote Physiologically-Relevant Cardiomyogenic Stem Cell Differentiation. *PLOS ONE*, *6*(12), e28935. https://doi.org/10.1371/journal.pone.0028935

Guyton, A. C., & Hall, J. E. (2000). *Textbook of Medical Physiology* (10th ed.). Philadelphia, PA: Elsevier Science.

Haraguchi, Y., Shimizu, T., Sasagawa, T., Sekine, H., Sakaguchi, K., Kikuchi, T., … Okano, T. (2012). Fabrication of functional three-dimensional tissues by stacking cell sheets in vitro. *Nature Protocols*, *7*(5), 850–858. https://doi.org/10.1038/nprot.2012.027

Herron, T. J., Lee, P., & Jalife, J. (2012). Optical Imaging of Voltage and Calcium in Cardiac Cells & Tissues. *Circulation Research*, *110*(4), 609–623. https://doi.org/10.1161/CIRCRESAHA.111.247494

Heskins, M., & Guillet, J. E. (1968). Solution Properties of Poly(N-isopropylacrylamide). *Journal of Macromolecular Science: Part A - Chemistry*, *2*(8), 1441–1455. https://doi.org/10.1080/10601326808051910

Hirschy, A., Schatzmann, F., Ehler, E., & Perriard, J.-C. (2006). Establishment of cardiac cytoarchitecture in the developing mouse heart. *Developmental Biology*, *289*(2), 430–441. https://doi.org/10.1016/j.ydbio.2005.10.046

Hirt, M. N., Hansen, A., & Eschenhagen, T. (2014). Cardiac Tissue Engineering: State of the Art. *Circulation Research*, *114*(2), 354–367. https://doi.org/10.1161/CIRCRESAHA.114.300522

Hotaling, N. A., Bharti, K., Kriel, H., & Simon Jr., C. G. (2015). DiameterJ: A validated open source nanofiber diameter measurement tool. *Biomaterials*, *61*, 327–338. https://doi.org/10.1016/j.biomaterials.2015.05.015

Huebsch, N., Loskill, P., Mandegar, M. A., Marks, N. C., Sheehan, A. S., Ma, Z., … Healy, K. E. (2015). Automated Video-Based Analysis of Contractility and Calcium Flux in Human-Induced Pluripotent Stem Cell-Derived Cardiomyocytes Cultured over Different Spatial Scales. *Tissue Engineering. Part C, Methods*, *21*(5), 467–479. https://doi.org/10.1089/ten.TEC.2014.0283

Inaba, R., Khademhosseini, A., Suzuki, H., & Fukuda, J. (2009). Electrochemical desorption of self-assembled monolayers for engineering cellular tissues. *Biomaterials*, *30*(21), 3573–3579. https://doi.org/10.1016/j.biomaterials.2009.03.045

Jeziorowska, D., Korniat, A., Salem, J.-E., Fish, K., & Hulot, J.-S. (2015). Generating patient-specific induced pluripotent stem cells-derived cardiomyocytes for the treatment of cardiac diseases. *Expert Opinion on Biological Therapy*, *15*(10), 1399–1409. https://doi.org/10.1517/14712598.2015.1064109

Kai, D., Prabhakaran, M. P., Jin, G., & Ramakrishna, S. (2011) Guided Orientation of Cardiomyocytes on Electrospun Aligned Nanofibers for Cardiac Tissue Engineering." *Journal of Biomedical Materials Research Part B: Applied Biomaterials, 98*(2), 379–86. https://doi.org/10.1002/jbm.b.31862

Kai, D., Wang, Q.-L., Wang, H.-J., Prabhakaran, M. P., Zhang, Y., Tan, Y.-Z., & Ramakrishna, S. (2014). Stem cell-loaded nanofibrous patch promotes the regeneration of infarcted myocardium with functional improvement in rat model. *Acta Biomaterialia*, *10*(6), 2727–2738. https://doi.org/10.1016/j.actbio.2014.02.030

Kattman, S. J., Witty, A. D., Gagliardi, M., Dubois, N. C., Niapour, M., Hotta, A., … Keller, G. (2011). Stage-Specific Optimization of Activin/Nodal and BMP Signaling Promotes Cardiac Differentiation of Mouse and Human Pluripotent Stem Cell Lines. *Cell Stem Cell*, *8*(2), 228–240. https://doi.org/10.1016/j.stem.2010.12.008

Kawamura, M., Miyagawa, S., Fukushima, S., Saito, A., Miki, K., Funakoshi, S., … Sawa, Y. (2017). Enhanced Therapeutic Effects of Human iPS Cell Derived-Cardiomyocyte by Combined Cell-Sheets with Omental Flap Technique in Porcine Ischemic Cardiomyopathy Model. *Scientific Reports*, *7*(1), 8824. https://doi.org/10.1038/s41598-017-08869-z

Kerscher, P., Turnbull, I. C., Hodge, A. J., Kim, J., Seliktar, D., Easley, C. J., … Lipke, E. A. (2016). Direct hydrogel encapsulation of pluripotent stem cells enables ontomimetic differentiation and growth of engineered human heart tissues. *Biomaterials*, *83*, 383–395. https://doi.org/10.1016/j.biomaterials.2015.12.011

Khan, M., Xu, Y., Hua, S., Johnson, J., Belevych, A., Janssen, P. M. L., … Angelos, M. G. (2015). Evaluation of Changes in Morphology and Function of Human Induced Pluripotent Stem Cell Derived Cardiomyocytes (HiPSC-CMs) Cultured on an Aligned-Nanofiber Cardiac Patch. *PLOS ONE*, *10*(5), e0126338. https://doi.org/10.1371/journal.pone.0126338

Kharaziha, M., Nikkhah, M., Shin, S.-R., Annabi, N., Masoumi, N., Gaharwar, A. K., … Khademhosseini, A. (2013). PGS:Gelatin nanofibrous scaffolds with tunable mechanical and structural properties for engineering cardiac tissues. *Biomaterials*, *34*(27), 6355–6366. https://doi.org/10.1016/j.biomaterials.2013.04.045

Kim, D.-H., Lipke, E. A., Kim, P., Cheong, R., Thompson, S., Delannoy, M., … Levchenko, A. (2010). Nanoscale cues regulate the structure and function of macroscopic cardiac tissue constructs. *Proceedings of the National Academy of Sciences*, *107*(2), 565–570. https://doi.org/10.1073/pnas.0906504107

Kim, D.-H., Provenzano, P. P., Smith, C. L., & Levchenko, A. (2012). Matrix nanotopography as a regulator of cell function. *The Journal of Cell Biology*, *197*(3), 351–360. https://doi.org/10.1083/jcb.201108062

Kim, M.-S., Horst, A., Blinka, S., Stamm, K., Mahnke, D., Schuman, J., … Lough, J. (2015). Activin-A and Bmp4 levels modulate cell type specification during CHIR-induced cardiomyogenesis. *PloS One*, *10*(2), e0118670. https://doi.org/10.1371/journal.pone.0118670

Kokkinopoulos, I., Ishida, H., Saba, R., Coppen, S., Suzuki, K., & Yashiro, K. (2016). Cardiomyocyte differentiation from mouse embryonic stem cells using a simple and defined protocol. *Developmental Dynamics: An Official Publication of the American Association of Anatomists*, *245*(2), 157–165. https://doi.org/10.1002/dvdy.24366

Lanzalaco, S., & Armelin, E. (2017). Poly(N-isopropylacrylamide) and Copolymers: A Review on Recent Progresses in Biomedical Applications. *Gels*, *3*(4), 36. https://doi.org/10.3390/gels3040036

Lee, J. B., Wang, X., Faley, S., Baer, B., Balikov, D. A., Sung, H.-J., & Bellan, L. M. (2016). Development of 3D Microvascular Networks Within Gelatin Hydrogels Using Thermoresponsive Sacrificial Microfibers. *Advanced Healthcare Materials*, *5*(7), 781–785. https://doi.org/10.1002/adhm.201500792

Levorson, E. J., Raman Sreerekha, P., Chennazhi, K. P., Kasper, F. K., Nair, S. V., & Mikos, A. G. (2013). Fabrication and characterization of multiscale electrospun scaffolds for cartilage regeneration. *Biomedical Materials (Bristol, England)*, *8*(1), 014103. https://doi.org/10.1088/1748-6041/8/1/014103

Li, J., Minami, I., Shiozaki, M., Yu, L., Yajima, S., Miyagawa, S., … Liu, L. (2017). Human Pluripotent Stem Cell-Derived Cardiac Tissue-like Constructs for Repairing the Infarcted Myocardium. *Stem Cell Reports*, *9*(5), 1546–1559. https://doi.org/10.1016/j.stemcr.2017.09.007

Li, Y., Asfour, H., & Bursac, N. (2017). Age-dependent functional crosstalk between cardiac fibroblasts and cardiomyocytes in a 3D engineered cardiac tissue. *Acta Biomaterialia*, *55*, 120–130. https://doi.org/10.1016/j.actbio.2017.04.027

Lian, X., Bao, X., Zilberter, M., Westman, M., Fisahn, A., Hsiao, C., … Palecek, S. P. (2015). Chemically defined, albumin-free human cardiomyocyte generation. *Nature Methods*, *12*(7), 595–596. https://doi.org/10.1038/nmeth.3448

Lian, X., Zhang, J., Azarin, S. M., Zhu, K., Hazeltine, L. B., Bao, X., … Palecek, S. P. (2013). Directed cardiomyocyte differentiation from human pluripotent stem cells by modulating Wnt/β-catenin signaling under fully defined conditions. *Nature Protocols*, *8*(1), 162–175. https://doi.org/10.1038/nprot.2012.150

Liau, B., Christoforou, N., Leong, K. W., & Bursac, N. (2011). Pluripotent stem cell-derived cardiac tissue patch with advanced structure and function. *Biomaterials*, *32*(35), 9180–9187. https://doi.org/10.1016/j.biomaterials.2011.08.050

Liau, B., Jackman, C. P., Li, Y., & Bursac, N. (2017). Developmental stage-dependent effects of cardiac fibroblasts on function of stem cell-derived engineered cardiac tissues. *Scientific Reports*, *7*, srep42290. https://doi.org/10.1038/srep42290

Lim, J., Jun, I., Lee, Y. B., Kim, E. M., Shin, D., Jeon, H., … Shin, H. (2016). Fabrication of cell sheets with anisotropically aligned myotubes using thermally expandable micropatterned hydrogels. *Macromolecular Research*, *24*(6), 562–572. https://doi.org/10.1007/s13233-016-4070-0

Lim, S. H., Liu, X. Y., Song, H., Yarema, K. J., & Mao, H.-Q. (2010). The effect of nanofiber-guided cell alignment on the preferential differentiation of neural stem cells. *Biomaterials*, *31*(34), 9031–9039. https://doi.org/10.1016/j.biomaterials.2010.08.021

Lundy, S. D., Zhu, W.-Z., Regnier, M., & Laflamme, M. A. (2013). Structural and Functional Maturation of Cardiomyocytes Derived from Human Pluripotent Stem Cells. *Stem Cells and Development*, *22*(14), 1991–2002. https://doi.org/10.1089/scd.2012.0490

Ma, Z., Wang, J., Loskill, P., Huebsch, N., Koo, S., Svedlund, F. L., … Healy, K. E. (2015). Self-organizing human cardiac microchambers mediated by geometric confinement. *Nature Communications*, *6*, 7413. https://doi.org/10.1038/ncomms8413

Masumoto, H., Ikuno, T., Takeda, M., Fukushima, H., Marui, A., Katayama, S., … Yamashita, J. K. (2014). Human iPS cell-engineered cardiac tissue sheets with cardiomyocytes and vascular cells for cardiac regeneration. *Scientific Reports*, *4*, 6716. https://doi.org/10.1038/srep06716

Matsuda, T., Takahashi, K., Nariai, T., Ito, T., Takatani, T., Fujio, Y., & Azuma, J. (2004). N-cadherin-mediated cell adhesion determines the plasticity for cell alignment in response to mechanical stretch in cultured cardiomyocytes. *Biochemical and Biophysical Research Communications*, *326*(1), 228–232. https://doi.org/10.1016/j.bbrc.2004.11.019

Matsuura, K., Masuda, S., Haraguchi, Y., Yasuda, N., Shimizu, T., Hagiwara, N., … Okano, T. (2011). Creation of mouse embryonic stem cell-derived cardiac cell sheets. *Biomaterials*, *32*(30), 7355–7362. https://doi.org/10.1016/j.biomaterials.2011.05.042

McCain, M. L., Lee, H., Aratyn-Schaus, Y., Kléber, A. G., & Parker, K. K. (2012). Cooperative coupling of cell-matrix and cell–cell adhesions in cardiac muscle. *Proceedings of the National Academy of Sciences*, *109*(25), 9881–9886. https://doi.org/10.1073/pnas.1203007109

McCain, M. L., Yuan, H., Pasqualini, F. S., Campbell, P. H., & Parker, K. K. (2014). Matrix elasticity regulates the optimal cardiac myocyte shape for contractility. *American Journal of Physiology - Heart and Circulatory Physiology*, *306*(11), H1525–H1539. https://doi.org/10.1152/ajpheart.00799.2013

Mihic, A., Li, J., Miyagi, Y., Gagliardi, M., Li, S.-H., Zu, J., … Li, R.-K. (2014). The effect of cyclic stretch on maturation and 3D tissue formation of human embryonic stem cell-derived cardiomyocytes. *Biomaterials*, *35*(9), 2798–2808. https://doi.org/10.1016/j.biomaterials.2013.12.052

Montgomery, M., Ahadian, S., Davenport Huyer, L., Lo Rito, M., Civitarese, R. A., Vanderlaan, R. D., … Radisic, M. (2017). Flexible shape-memory scaffold for minimally invasive delivery of functional tissues. *Nature Materials*, *16*(10), 1038–1046. https://doi.org/10.1038/nmat4956

Moran, M. T., Carroll, W. M., Gorelov, A., & Rochev, Y. (2007). Intact endothelial cell sheet harvesting from thermoresponsive surfaces coated with cell adhesion promoters. *Journal of the Royal Society Interface*, *4*(17), 1151–1157. https://doi.org/10.1098/rsif.2007.1023

Moran, M. T., Carroll, W. M., Selezneva, I., Gorelov, A., & Rochev, Y. (2007). Cell growth and detachment from protein-coated PNIPAAm-based copolymers. *Journal of Biomedical Materials Research Part A*, *81A*(4), 870–876. https://doi.org/10.1002/jbm.a.31089

Mummery, C. L., Zhang, J., Ng, E. S., Elliott, D. A., Elefanty, A. G., & Kamp, T. J. (2012). Differentiation of Human Embryonic Stem Cells and Induced Pluripotent Stem Cells to Cardiomyocytes A Methods Overview. Circulation Research, 111(3), 344–358. https://doi.org/10.1161/CIRCRESAHA.110.227512

Nagase, K., Yamato, M., Kanazawa, H., & Okano, T. (2018). Poly(N-Isopropylacrylamide)-Based Thermoresponsive Surfaces Provide New Types of Biomedical Applications. Biomaterials, 153: 27–48. https://doi.org/10.1016/j.biomaterials.2017.10.026

Nam, J., Huang, Y., Agarwal, S., & Lannutti, J. (2008). Materials selection and residual solvent retention in biodegradable electrospun fibers. Journal of Applied Polymer Science, 107(3), 1547–1554. https://doi.org/10.1002/app.27063

Natarajan, A., Stancescu, M., Dhir, V., Armstrong, C., Sommerhage, F., Hickman, J. J., & Molnar, P. (2011). Patterned Cardiomyocytes on Microelectrode Arrays as a Functional, High Information Content Drug Screening Platform. *Biomaterials*, *32*(18), 4267–4274. https://doi.org/10.1016/j.biomaterials.2010.12.022

Nitschke Mirko, Gramm Stefan, Götze Thomas, Valtink Monika, Drichel Juliane, Voit Brigitte, … Werner Carsten. (2006). Thermo-responsive poly(NiPAAm-co-DEGMA) substrates for gentle harvest of human corneal endothelial cell sheets.

Journal of Biomedical Materials Research Part A, *80A*(4), 1003–1010. https://doi.org/10.1002/jbm.a.31098

Nunes, S. S., Miklas, J. W., Liu, J., Aschar-Sobbi, R., Xiao, Y., Zhang, B., … Radisic, M. (2013). Biowire: a platform for maturation of human pluripotent stem cell-derived cardiomyocytes. *Nature Methods*, *10*(8), 781–787. https://doi.org/10.1038/nmeth.2524

Ogle, B. M., Bursac, N., Domian, I., Huang, N. F., Menasché, P., Murry, C. E., … Vunjak-Novakovic, G. (2016). Distilling complexity to advance cardiac tissue engineering. *Science Translational Medicine*, *8*(342), 342ps13-342ps13. https://doi.org/10.1126/scitranslmed.aad2304

Ohya, S., Kidoaki, S., & Matsuda, T. (2005). Poly(N-isopropylacrylamide) (PNIPAM)-grafted gelatin hydrogel surfaces: interrelationship between microscopic structure and mechanical property of surface regions and cell adhesiveness. *Biomaterials*, *26*(16), 3105–3111. https://doi.org/10.1016/j.biomaterials.2004.08.006

Orlova, Y., Magome, N., Liu, L., Chen, Y., & Agladze, K. (2011). Electrospun nanofibers as a tool for architecture control in engineered cardiac tissue. *Biomaterials*, *32*(24), 5615–5624. https://doi.org/10.1016/j.biomaterials.2011.04.042

Pan Guoqing, Guo Qianping, Ma Yue, Yang Huilin, & Li Bin. (2013). Thermo-Responsive Hydrogel Layers Imprinted with RGDS Peptide: A System for Harvesting Cell Sheets. *Angewandte Chemie International Edition*, *52*(27), 6907–6911. https://doi.org/10.1002/anie.201300733

Parikh, S. S., Blackwell, D. J., Gomez-Hurtado, N., Frisk, M., Wang, L., Kim, K., … Knollmann, B. C. (2017). Thyroid and Glucocorticoid Hormones Promote Functional T-Tubule Development in Human-Induced Pluripotent Stem Cell–Derived Cardiomyocytes Novelty and Significance. *Circulation Research*, *121*(12), 1323–1330. https://doi.org/10.1161/CIRCRESAHA.117.311920

Parrag, I. C., Zandstra, P. W., & Woodhouse, K. A. (2012). Fiber alignment and coculture with fibroblasts improves the differentiated phenotype of murine embryonic stem cell-derived cardiomyocytes for cardiac tissue engineering. *Biotechnology and Bioengineering*, *109*(3), 813–822. https://doi.org/10.1002/bit.23353

Pasqualini, F. S., Sheehy, S. P., Agarwal, A., Aratyn-Schaus, Y., & Parker, K. K. (2015). Structural Phenotyping of Stem Cell-Derived Cardiomyocytes. *Stem Cell Reports*, *4*(3), 340–347. https://doi.org/10.1016/j.stemcr.2015.01.020

Pelton, R. (2010). Poly(N-isopropylacrylamide) (PNIPAM) is never hydrophobic. *Journal of Colloid and Interface Science*, *348*(2), 673–674. https://doi.org/10.1016/j.jcis.2010.05.034

Pham, Q. P., Sharma, U., & Mikos, A. G. (2006). Electrospinning of Polymeric Nanofibers for Tissue Engineering Applications: A Review. *Tissue Engineering*, *12*(5), 1197–1211. https://doi.org/10.1089/ten.2006.12.1197

Prabhakaran, M. P., Mobarakeh, L. G., Kai, D., Karbalaie, K., Nasr-Esfahani, M. H., & Ramakrishna, S. (2014). Differentiation of embryonic stem cells to cardiomyocytes on electrospun nanofibrous substrates. *Journal of Biomedical Materials Research Part B: Applied Biomaterials*, *102*(3), 447–454. https://doi.org/10.1002/jbm.b.33022

Przybyla, L., Lakins, J. N., & Weaver, V. M. (2016). Tissue Mechanics Orchestrate Wnt-Dependent Human Embryonic Stem Cell Differentiation. *Cell Stem Cell*. https://doi.org/10.1016/j.stem.2016.06.018

Püspöki, Z., Storath, M., Sage, D., & Unser, M. (2016). Transforms and Operators for Directional Bioimage Analysis: A Survey. *Advances in Anatomy, Embryology, and Cell Biology*, *219*, 69–93. https://doi.org/10.1007/978-3-319-28549-8_3

Qin, D., Xia, Y., & Whitesides, G. M. (2010). Soft lithography for micro- and nanoscale patterning. *Nature Protocols*, *5*(3), 491–502. https://doi.org/10.1038/nprot.2009.234

Radisic, M., Park, H., Martens, T. P., Salazar-Lazaro, J. E., Geng, W., Wang, Y., … Vunjak-Novakovic, G. (2008). Pre-treatment of synthetic elastomeric scaffolds by cardiac fibroblasts improves engineered heart tissue. *Journal of Biomedical Materials Research Part A*, *86A*(3), 713–724. https://doi.org/10.1002/jbm.a.31578

Rao, C., Prodromakis, T., Kolker, L., Chaudhry, U. A. R., Trantidou, T., Sridhar, A., … Terracciano, C. M. (2013). The effect of microgrooved culture substrates on calcium cycling of cardiac myocytes derived from human induced pluripotent stem cells. *Biomaterials*, *34*(10), 2399–2411. https://doi.org/10.1016/j.biomaterials.2012.11.055

Rao, J., Pfeiffer, M. J., Frank, S., Adachi, K., Piccini, I., Quaranta, R., … Greber, B. (2016). Stepwise Clearance of Repressive Roadblocks Drives Cardiac Induction in Human ESCs. *Cell Stem Cell*, *18*(3), 341–353. https://doi.org/10.1016/j.stem.2015.11.019

Rezakhaniha, R., Agianniotis, A., Schrauwen, J. T. C., Griffa, A., Sage, D., Bouten, C. V. C., … Stergiopulos, N. (2012). Experimental investigation of collagen waviness and orientation in the arterial adventitia using confocal laser scanning microscopy. *Biomechanics and Modeling in Mechanobiology*, *11*(3–4), 461–473. https://doi.org/10.1007/s10237-011-0325-z

Ribeiro, A. J. S., Ang, Y.-S., Fu, J.-D., Rivas, R. N., Mohamed, T. M. A., Higgs, G. C., … Pruitt, B. L. (2015). Contractility of single cardiomyocytes differentiated from pluripotent stem cells depends on physiological shape and substrate stiffness. *Proceedings of the National Academy of Sciences*, *112*(41), 12705–12710. https://doi.org/10.1073/pnas.1508073112

Ribeiro, M. C., Tertoolen, L. G., Guadix, J. A., Bellin, M., Kosmidis, G., D'Aniello, C., … Passier, R. (2015). Functional maturation of human pluripotent stem cell derived cardiomyocytes in vitro – Correlation between contraction force

and electrophysiology. *Biomaterials*, *51*, 138–150. https://doi.org/10.1016/j.biomaterials.2015.01.067

Rockwood, D. N., Chase, D. B., Akins Jr., R. E., & Rabolt, J. F. (2008). Characterization of electrospun poly(N-isopropyl acrylamide) fibers. *Polymer*, *49*(18), 4025–4032. https://doi.org/10.1016/j.polymer.2008.06.018

Rutledge, G. C., & Fridrikh, S. V. (2007). Formation of fibers by electrospinning. *Advanced Drug Delivery Reviews*, *59*(14), 1384–1391. https://doi.org/10.1016/j.addr.2007.04.020

Salick, M. R., Napiwocki, B. N., Sha, J., Knight, G. T., Chindhy, S. A., Kamp, T. J., … Crone, W. C. (2014). Micropattern width dependent sarcomere development in human ESC-derived cardiomyocytes. *Biomaterials*, *35*(15), 4454–4464. https://doi.org/10.1016/j.biomaterials.2014.02.001

Schmaljohann, D., Oswald, J., Jørgensen, B., Nitschke, M., Beyerlein, D., & Werner, C. (2003). Thermo-Responsive PNiPAAm-g-PEG Films for Controlled Cell Detachment. *Biomacromolecules*, *4*(6), 1733–1739. https://doi.org/10.1021/bm034160p

Sheikh, F., Lyon, R. C., & Chen, J. (2015). Functions of Myosin Light Chain-2 (MYL2) In Cardiac Muscle and Disease. *Gene*, *569*(1), 14–20. https://doi.org/10.1016/j.gene.2015.06.027

Shimizu, T., Yamato, M., Isoi, Y., Akutsu, T., Setomaru, T., Abe, K., … Okano, T. (2002). Fabrication of pulsatile cardiac tissue grafts using a novel 3-dimensional cell sheet manipulation technique and temperature-responsive cell culture surfaces. *Circulation Research*, *90*(3), e40.

Shin, S.-H., Purevdorj, O., Castano, O., Planell, J. A., & Kim, H.-W. (2012). A short review: Recent advances in electrospinning for bone tissue regeneration. *Journal of Tissue Engineering*, *3*(1). https://doi.org/10.1177/2041731412443530

Sia, J., Yu, P., Srivastava, D., & Li, S. (2016). Effect of biophysical cues on reprogramming to cardiomyocytes. *Biomaterials*, *103*, 1–11. https://doi.org/10.1016/j.biomaterials.2016.06.034

Srinivasan, S., Baldwin, H. S., Aristizabal, O., Kwee, L., Labow, M., Artman, M., & Turnbull, D. H. (1998). Noninvasive, in utero imaging of mouse embryonic heart development with 40-MHz echocardiography. *Circulation*, *98*(9), 912–918.

Stoppel, W. L., Kaplan, D. L., & Black III, L. D. (2016). Electrical and mechanical stimulation of cardiac cells and tissue constructs. *Advanced Drug Delivery Reviews*, *96*, 135–155. https://doi.org/10.1016/j.addr.2015.07.009

Sumi, T., Tsuneyoshi, N., Nakatsuji, N., & Suemori, H. (2008). Defining early lineage specification of human embryonic stem cells by the orchestrated balance of

canonical Wnt/β-catenin, Activin/Nodal and BMP signaling. *Development*, *135*(17), 2969–2979. https://doi.org/10.1242/dev.021121

Takahashi, H., Nakayama, M., Itoga, K., Yamato, M., & Okano, T. (2011). Micropatterned Thermoresponsive Polymer Brush Surfaces for Fabricating Cell Sheets with Well-Controlled Orientational Structures. *Biomacromolecules*, *12*(5), 1414–1418. https://doi.org/10.1021/bm2000956

Takahashi, H., Nakayama, M., Shimizu, T., Yamato, M., & Okano, T. (2011). Anisotropic cell sheets for constructing three-dimensional tissue with well-organized cell orientation. *Biomaterials*, *32*(34), 8830–8838. https://doi.org/10.1016/j.biomaterials.2011.08.006

Takahashi, K., & Yamanaka, S. (2006). Induction of Pluripotent Stem Cells from Mouse Embryonic and Adult Fibroblast Cultures by Defined Factors. *Cell*, *126*(4), 663–676. https://doi.org/10.1016/j.cell.2006.07.024

Tandon, N., Marsano, A., Maidhof, R., Wan, L., Park, H., & Vunjak-Novakovic, G. (2011). Optimization of Electrical Stimulation Parameters for Cardiac Tissue Engineering. *Journal of Tissue Engineering and Regenerative Medicine*, *5*(6), e115–e125. https://doi.org/10.1002/term.377

Tang, Z., & Okano, T. (2014). Recent development of temperature-responsive surfaces and their application for cell sheet engineering. *Regenerative Biomaterials*, *1*(1), 91–102. https://doi.org/10.1093/rb/rbu011

Thavandiran, N., Dubois, N., Mikryukov, A., Massé, S., Beca, B., Simmons, C. A., … Zandstra, P. W. (2013). Design and formulation of functional pluripotent stem cell-derived cardiac microtissues. *Proceedings of the National Academy of Sciences of the United States of America*, *110*(49), E4698–E4707. https://doi.org/10.1073/pnas.1311120110

Thavandiran, N., Nunes, S. S., Xiao, Y., & Radisic, M. (2013). Topological and electrical control of cardiac differentiation and assembly. *Stem Cell Research & Therapy*, *4*(1), 14. https://doi.org/10.1186/scrt162

Thompson, C. J., Chase, G. G., Yarin, A. L., & Reneker, D. H. (2007). Effects of parameters on nanofiber diameter determined from electrospinning model. *Polymer*, *48*(23), 6913–6922. https://doi.org/10.1016/j.polymer.2007.09.017

Thygesen, K., Alpert, J. S., Jaffe, A. S., Simoons, M. L., Chaitman, B. R., & White, H. D. (2012). Third Universal Definition of Myocardial Infarction. *Circulation*, *126*(16), 2020–2035. https://doi.org/10.1161/CIR.0b013e31826e1058

Tirziu, D., Giordano, F. J., & Simons, M. (2010). Cell Communications in the Heart. *Circulation*, *122*(9), 928–937. https://doi.org/10.1161/CIRCULATIONAHA.108.847731

Tran, T., Hernandez, M., Patel, D., Burns, E., Peterman, V., & Wu, J. (2015). Controllable and switchable drug delivery of ibuprofen from temperature responsive composite nanofibers. *Nano Convergence*, *2*(1), 15. https://doi.org/10.1186/s40580-015-0047-5

Uosaki, H., Cahan, P., Lee, D. I., Wang, S., Miyamoto, M., Fernandez, L., … Kwon, C. (2015). Transcriptional Landscape of Cardiomyocyte Maturation. *Cell Reports*, *13*(8), 1705–1716. https://doi.org/10.1016/j.celrep.2015.10.032

Wang, J., Chen, L., Zhao, Y., Guo, G., & Zhang, R. (2009). Cell adhesion and accelerated detachment on the surface of temperature-sensitive chitosan and poly(N-isopropylacrylamide) hydrogels. *Journal of Materials Science: Materials in Medicine*, *20*(2), 583–590. https://doi.org/10.1007/s10856-008-3593-0

Wang, T.-Y., Forsythe, J. S., Nisbet, D. R., & Parish, C. L. (2012). Promoting engraftment of transplanted neural stem cells/progenitors using biofunctionalised electrospun scaffolds. *Biomaterials*, *33*(36), 9188–9197. https://doi.org/10.1016/j.biomaterials.2012.09.013

Wanjare, M., Hou, L., H. Nakayama, K., J. Kim, J., P. Mezak, N., J. Abilez, O., … F. Huang, N. (2017). Anisotropic microfibrous scaffolds enhance the organization and function of cardiomyocytes derived from induced pluripotent stem cells. *Biomaterials Science*, *5*(8), 1567–1578. https://doi.org/10.1039/C7BM00323D

Yamada, N., Okano, T., Sakai, H., Karikusa, F., Sawasaki, Y., & Sakurai, Y. (1990). Thermo-responsive polymeric surfaces; control of attachment and detachment of cultured cells. *Die Makromolekulare Chemie, Rapid Communications*, *11*(11), 571–576. https://doi.org/10.1002/marc.1990.030111109

Yamato, M., Akiyama, Y., Kobayashi, J., Yang, J., Kikuchi, A., & Okano, T. (2007). Temperature-responsive cell culture surfaces for regenerative medicine with cell sheet engineering. *Progress in Polymer Science*, *32*(8–9), 1123–1133. https://doi.org/10.1016/j.progpolymsci.2007.06.002

Yan, J., Chen, F., & Amsden, B. G. (2016). Cell sheets prepared via gel–sol transition of calcium RGD–alginate. *Acta Biomaterialia*, *30*, 277–284. https://doi.org/10.1016/j.actbio.2015.10.046

Yang, J., Yamato, M., Kohno, C., Nishimoto, A., Sekine, H., Fukai, F., & Okano, T. (2005). Cell sheet engineering: Recreating tissues without biodegradable scaffolds. *Biomaterials*, *26*(33), 6415–6422. https://doi.org/10.1016/j.biomaterials.2005.04.061

Yang, J., Yamato, M., Shimizu, T., Sekine, H., Ohashi, K., Kanzaki, M., … Okano, T. (2007). Reconstruction of functional tissues with cell sheet engineering. *Biomaterials*, *28*(34), 5033–5043. https://doi.org/10.1016/j.biomaterials.2007.07.052

Yoshida, Y., & Yamanaka, S. (2010). Recent Stem Cell Advances: Induced Pluripotent Stem Cells for Disease Modeling and Stem Cell–Based Regeneration. *Circulation*, *122*(1), 80–87. https://doi.org/10.1161/CIRCULATIONAHA.109.881433

Yu, H., Jia, Y., Chen, G., & Zhang, Y. (2016). Fabrication of core/sheath PCL/PEG–PNIPAAm fibers as thermosensitive release carriers by a new technique combining blend electrospinning and ultraviolet-induced graft polymerization. *Materials Letters*, *164*, 505–508. https://doi.org/10.1016/j.matlet.2015.11.067

Zhang, D., Shadrin, I. Y., Lam, J., Xian, H.-Q., Snodgrass, H. R., & Bursac, N. (2013). Tissue-engineered cardiac patch for advanced functional maturation of human ESC-derived cardiomyocytes. *Biomaterials*, *34*(23), 5813–5820. https://doi.org/10.1016/j.biomaterials.2013.04.026

Zhang, J., Wilson, G. F., Soerens, A. G., Koonce, C. H., Yu, J., Palecek, S. P., … Kamp, T. J. (2009). Functional Cardiomyocytes Derived from Human Induced Pluripotent Stem Cells. *Circulation Research*, *104*(4), e30–e41. https://doi.org/10.1161/CIRCRESAHA.108.192237

Zhao, X., Wang, L., Wang, P., Yang, Y., & Wang, F. (2016). Fabrication of Thermoresponsive Nanofibers for Cell Sorting and Aligned Cell Sheet Engineering. *Journal of Nanoscience and Nanotechnology*, *16*(6), 5520–5527.

Zhu, R., Blazeski, A., Poon, E., Costa, K. D., Tung, L., & Boheler, K. R. (2014). Physical developmental cues for the maturation of human pluripotent stem cell-derived cardiomyocytes. *Stem Cell Research & Therapy*, *5*, 117. https://doi.org/10.1186/scrt507

Zong, X., Bien, H., Chung, C.-Y., Yin, L., Fang, D., Hsiao, B. S., … Entcheva, E. (2005). Electrospun fine-textured scaffolds for heart tissue constructs. *Biomaterials*, *26*(26), 5330–5338. https://doi.org/10.1016/j.biomaterials.2005.01.052

Vita

Alicia Caitlin Bloomfield Allen was born in Columbus, Ohio but grew up in College Station, Texas. She graduated from A&M Consolidated High School in 2005. Alicia did not bleed maroon and pledged to go out-of-state for undergraduate studies; however, she attended Rice University in Houston, Texas where was a member of Lovett College. There, she earned a Bachelor's of Science in Bioengineering and a Bachelor's of Arts in French Literature. After graduating, Alicia finally did go out-of-state when she received a Fulbright Grant to serve as an English Teaching Assistant on Jeju-do in South Korea. In 2013, Alicia found herself back in Texas to attend the University of Texas at Austin. Alicia researched the role of biomaterials on cardiac differentiation and received a National Science Foundation Graduate Research Fellowship in 2015. Outside of research, Alicia competes in long-distance triathlons with her training partner-husband.

Permanent email: aliciacballen@gmail.com

This dissertation was typed by the author.